Lehrstuhl für Ökoklimatologie

Long-Range and Deep Convective Transport of Boreal Forest Fire Emissions

Richard Damoah

Vollständiger Abdruck der von der Fakultät Wissenschaftszentrum Weihenstephan für Ernährung, Landnutzung und Umwelt der Technischen Universität München zur Erlangung des akademischen Grades eines Doktors der Naturwissenschaft genehmigten Dissertation.

Vorsitzender: Uni-Prof. Dr. A. Fischer

Prüfer der Dissertation:

1. Univ-Prof. Dr. Dr. h. c. P. Fabian, i. R.
2. Univ-Prof. Dr. H-D. Quednau
3. apl. Prof. Dr. U. Schumann,
Ludwig-Maximilians-Universität München

Die Dissertation wurde am 23.08.2005 bei der Technischen Universität München eingereicht und durch die Fakultät Wissenschaftszentrum Weihenstephan für Ernährung, Landnutzung und Umwelt am 05.10.2005 angenommen.

ACKNOWLEDGEMENTS

I thank Prof. Dr. P. Fabian for giving me the chance of working at the Institute of Bioclimatology, Technical University of Munich. I greatly acknowledge Andreas Stohl for his tremendous motivation and supervision during my work.

For fruitful discussion and comments, I most appreciate the help of the other group members, Caroline Forster, Paul James, Nicole Spichtinger, and Sabine Eckhardt.

Finally, I thank ECMWF and the German Weather Service for permitting access to the ECMWF archives, and the provision of data via the internet by the science teams of MODIS, TOMS, POAM, SAGE, SeaWiFS and lidar groups at Leipzig and Wisconsin. My work was funded by the European Commission in the European Research Framework 5 program as part of the PARTS project, and I also thank Hans Graf for organising PARTS.

TABLE OF CONTENTS

Publications from the candidate's work

Article 1

Damoah, R., Spichtinger, N., Servranckx, R., Fromm, M., Eloranta, E. W., Razenkov, I. A., James, P., Shulski, M., Forster, C., and Stohl, A.: *Transport modelling of a pyro-convection event in Alaska*, Atmos. Chem. Phys. Discuss., 5, 6185-6214, 2005.

Article 2

Damoah, R., Spichtinger, N., Forster, C., James, P., Mattis, I., Wandinger, U., Beirle, S., Wagner, T., and Stohl, A.: *Around the world in 17 days – hemispheric-scale transport of forest fire smoke from Russia in May 2003*, Atmos. Chem. Phys., 4, 1311-1321, 2004.

Article 3

Spichtinger, N., **Damoah, R**., Eckhard, S., Forster, C., James, P.,Beirle, T., Wagner, T., Novelli, P.C., and Stohl, A.: *Boreal forest fires in 1997 and 1998: A seasonal comparison using transport model simulations and measurement data*, Atmos. Chem. Phys., 4, 1857 – 1868, 2004.

Abstract

Forest fire emissions have strong impact on the concentrations of atmospheric trace gases and aerosols on local, regional and even continental scales. This dissertation presents two case studies of the atmospheric long-range transport of emissions from severe forest fires that occurred in the summers of 1998 (**Article 3**) and 2003 (**Article 2**), and a vertical transport of fire plumes into the lower stratosphere by deep convection in 2004 (**Article 1**).

The studies combine satellite data from a variety of platforms (Moderate Resolution Imaging Spectroradiometer (MODIS), Sea-viewing Wide Field-of-view Sensor (SeaWiFS), Earth Probe Total Ozone Mapping Spectrometer (TOMS), Advanced Very High Resolution Radiometer (AVHRR) onboard NOAA-12, Polar Ozone and Aerosol Measurement (POAM III), Stratospheric Aerosol and Gas Experiment (SAGE II) and vertical aerosol profiles derived from lidar measurements with results from the Lagrangian particle dispersion model FLEXPART to understand the transport processes. The satellite data provided a unique opportunity for validating the model simulations of tropospheric transport on a truly hemispheric scale, as well as of the simulated vertical transport into the lower stratosphere.

The fire activity in the boreal region was very strong in 1998 compared to 1997, especially over Canada and Eastern Siberia. According to burned area estimates from United Nations Economic Commission for Europe (UNEC, 1999) more than 10 x 10^6 ha burned in 1998, which is more than six times the area burned in 1997. CO_2 and CO measurement data from CMDL (Climate Monitoring and Diagnostic Laboratory) taken in the entire northern hemisphere also show clearly enhanced levels during the burning seasson (May-October) of 1998

compared to that of 1997. Siberian and Canadian CO emissions from the forest fires were distinguished using the FLEXPART model to investigate the transport of both separately. Siberian fire emissions were transported towards Canada and contributed concentrations more than twice as high as those from Cananda's own CO emissions from the fires.

In 2003, severe forest fires in southeast Russia burned an area of about 19 x 10^6 ha and resulted in smoke plumes extending widely across the Northern Hemisphere. In this study it is shown that the smoke transport occurred in two directions: Smoke traveling northwestwards towards Scandinavia was lifted over the Urals and arrived over the Norwegian Sea. Smoke traveling eastwards to the Okhotsk Sea was also lifted; it then crossed the Bering Sea to Alaska from where it proceeded to Canada and was later even observed over Scandinavia and Eastern Europe on its way back to Russia. The total transport time around the northern hemisphere was about 17 days. To the author's knowledge, this is the first time that a pollution plume could be tracked across the entire northern hemisphere.

Summer 2004 also saw severe forest fires in Alaska and the Yukon Territory which were triggered by frequent lightning strikes. The registered area burned (>2.7x10^6 ha) in Alaska at the end of the season was the highest to date. Pollutant emissions from the burning in some cases lead to violation of federal standards for air quality. Deep convection in the midst of the boreal fires injected particles up to about 3 km above the tropopause. Emissions from the fires did not only perturb the upper troposphere and lower stratosphere (UT/LS) locally, but also regionally. According to satellite data, air masses that passed over the fires had enhanced UT/LS aerosol loads by a factor of 4 compared to the background UTLS load without fire influence. Furthermore, model results suggest with parameterized deep convection CO concentrations were enhanced

by approximately 9 fold over the entire region (40°-90° N, 80°-160° W) compared to when the deep convection parameterization was turned off.

1. Introduction

1.1. Fire Occurrence and Emissions

The world's total closed boreal forest covers about 1 billion ha (29% of the world's forest area), of which Russian and Scandinavia boreal forests contribute about two thirds (Kasischke et al., 2000: Stocks, 2004) and the remaining one third is located in Canada and Alaska (Stocks, 2004). Fig. 1 shows the distribution of protected boreal and temperate forests in Russia, Alaska, Canada and the Scandinavia according to the World Conservation Monitoring Centre (WCMC) (see: **http://www.unep-wcmc.org/forest/boreal/region.htm**). The boreal region consists of large almost unpopulated territories. Therefore, many fires are not actioned because they pose no threat to human property. For example, in Russia unprotected forests cover more than 40% of the total forest land (kajii et al., 2002) which are excluded in official statistics of the area burned. Canada's uncontrolled fires contribute to about 50% of the total area burned (Stocks et al., 2003). Wildfire is a natural part of the life cycle of the boreal region (Club, 1996). In Canada the contribution of lightning to fire ignition is about 15% and consume more than 85% of the total area burned (Scholes et al., 2003) while in Russia lightning-triggered fires contribute between 10-15% (Kajii et al., 2002). The boreal regions are prone to fire activity because: (1) Boreal forests are dominated by coniferous stands of high fire hazard; (2) The forests contain large amounts of accumulated organic matter due to slow decomposition of plant material; and (3) most of the boreal regions have limited amounts of precipitation and long periods of drought in the fire season. For instance, the region of northeastern China and southeastern Siberia is dominated by the Asiatic high in winter, which forms over the Lake Baikal

region and blocks the progression of winter storms (Cahoon et al., 1994), thus leading to relatively little precipitation. As the spring approaches and warming begins, the Asiatic high breaks down and storm passages occur in rapid succession from west to east. At the same time that storm frequency increases, temperature also rapidly increases and relative humidity remains low leading to the drying of forest fuels (Stocks and Jin, 1988). This combination of conditions creates a prime situation for fire development.

The annual area burned in the boreal region has increased recently, partly due to increased fire activity since the late 1990s. In 1991 and 1992 an estimated area of about 3.3 x 10^6 ha and 2.0 x 10^6 ha were burned in the boreal region, respectively (Wotawa, 2001). According to Spichtinger et al., [2004], Canada and Siberia in total recorded more than 17.9 x 10^6 ha in 1998. Biomass burning in the tropics is known for a long time to be a large source of carbon emissions into the atmosphere (Andreae, 1991). However, although fires in the boreal forest are also strong emission sources, their significance for atmospheric chemistry and the carbon budget was recognized only recently (Kajii, 2002). On a global scale, biomass burning emits 3800 to 4300 Tg C yr^{-1} (Andreae, 1991; Andreae and Merlet, 2001). Seiler and Crutzen (1980) estimated that boreal fires contribute about 23 Tg C yr^{-1} (0.6%, based on Andreae, 1991) to the global biomass emissions, while Bergamaschi et al. (2000) estimated that carbon monoxide emissions from fires in forest above 30° N latitude at 50 Tg yr^{-1} (~6% of the total from biomass burning), and that from Galanter (2000) estimated carbon monoxide emissions to be 121 Tg (Galanter, 2000) annually.

1.2. Long-range Transport

Aerosols and trace gases such as carbon monoxide, nitrogen oxides and non-methane hydrocarbons from boreal forest fires play an important role for atmospheric chemistry and radiative properties of the atmosphere. Carbon

monoxide, for instance, is involved in tropospheric ozone chemistry (Crutzen, 1973) and aerosols can be transported into the stratosphere (Fromm et al., 2000) where they may influence concentrations of stratospheric ozone through catalytic chemical reactions. Therefore, changes in the concentrations of aerosols and carbon monoxide also affect ozone, which plays an important role in the global climate system (Daniel and Solomon, 1998; Logan et al., 1981). Furthermore, aerosols by themselves can strongly influence the radiation in the atmosphere (Christopher et al., 2000; Hsu et al., 1999) and represent the largest source of uncertainty in current climate model simulations (IPCC, 2001).

Recently it was found that through long-range transport, emissions from boreal forest fires affect not only local surroundings but regional (Tanimoto et al., 2000; Kato et al., 2002) and even continental and hemispheric scales. Wotawa and Trainer (2000) found that the high CO and O_3 concentrations over the southeastern United States during a field campaign in 1995 were caused by the transport of a pollution plume from Canadian fires and photochemical ozone formation in this plume. Long-range transport events of aerosols (Hsu et al., 1999; Formenti et al., 2002; Fiebig et al., 2002; Wandinger et al., 2002), CO and O_3 (Forster et al., 2001) and NO_x (Spichtinger et al., 2001) from Canadian forest fires have also been observed over Europe. Also, long-range transport of Siberian biomass burning emissions has been observed in North America (Jaffe, 2004). In fact, Spichtinger et al., (2004) also showed that in the summer of 1998 Siberian fire emissions were transported to Canada, where they contributed more than twice the carbon monoxide concentrations caused by Canada's own emissions from fires (**see Article 3**). According to model simulations, the time scale of intercontinental transport of pollutant emissions is on the order of 3-30 days (Stohl et al., 2002). The upper range of this estimate may be a typical time scale for the mixing of pollutants into the general atmospheric background in the northern hemisphere middle latitudes. In case studies, Wotawa and Trainer

(2000) reported a duration of about 2 weeks for the transport of Canadian fire emissions to the southeastern United States, Forster et al., (2001) quoted a period of about 1 week for the transport of Canadian fire emissions to Europe, Damoah et al., (2004) reported a period of about 17 days for the transport of Russian emissions around the globe (**see Article 2**).

It is well known that volcanic eruptions can produce the explosive force to inject material from the surface deep into the stratosphere (Graf et al., 1999). Only recently, however, it was realized emissions from fires can also be transported upward in warm conveyor belts (WCBs) (Stohl, 2001). Also deep convection triggered or enhanced by forest fires (so-called pyro-convection) can also penetrate deeply into the stratosphere, leading to the deposition of gaseous and particulate products of the burning in the upper troposphere and lower stratosphere (UT/LS) (Fromm et al., 2003, 2005). The mechanisms causing this deep convection are not yet entirely clear, but it appears that normal deep convection that occurs regularly in the boreal region in summer-time under favourable meteorological conditions can be greatly enhanced by the heat released by the fire as well as by the large amounts of aerosols emitted. These aerosols reduce cloud droplet numbers, suppress precipitation formation, enhance the significance of the ice phase (thence, also increase the amount of latent heating available, especially at high altitudes) and, generally, increase the depth of the convection. Similar processes have also been observed to be effective in tropical biomass burning plumes (Andreae et al., 2004). Furthermore, the radiation absorption by black carbon particles emitted by the fires and the associated heating of the atmosphere above the cloud tops could lead to further lifting after the initial convective injection into the UT/LS region. While the relative importance of these different mechanisms is not clear, several recent papers have presented cases where pyro-convection transported forest fire emissions relatively deep into the stratosphere, using satellite (Fromm, et al.,

2003; Livesey et al., 2004), lidar (Immler et al., 2005; Fromm, et al., 2004) and aircraft (Jost et al., 2004) observations. Some of the observations (**e.g., Article 1**) even show that the emission products can be transported up to 3 km above the local tropopause

1.3. General Motion of the Atmosphere

1.3.1. Global Circulation

The global scale atmospheric circulation is driven by net radiation differences from the equator to the poles. Even though the total input and output of radiant energy to and from the earth are essentially in balance, they are not in balance at every point on the earth. The amount of energy reaching the earth's surface depends, in part, on the nature of the surface (e.g. land or sea) and the degree of cloudiness, as well as on the latitude of the point (Christopherson, 2000). For example, as shown in Fig.2 (see http://www.geog.ucsb.edu), at the equator more energy is absorbed than emitted leaving a net radiation surplus while in the polar regions there is a net radiation deficit. This uneven distribution of energy resulting from latitudinal variations creates a large temperature difference. Figures 3a and 3b taken from http://www.geog.ucsb.edu show the average surface air temperature in January and July, respectively. Higher temperature differences between the tropics and the northern Arctic region are observed in January (northern winter). Similar differences with the southern polar regions are also observed in July (southern winter). These temperature differences lead to the transport of energy from the tropics to the poles, thereby redistributing energy on the earth. The tropics would be hotter and the poles colder without poleward energy transport (Atkinson, 1981).

If the earth would not rotate, surface air (cold) flow would be directed from the poles to the equator. Upon converging at the equator, air would be lifted vertically by convection to the top of the troposphere, then beginning to flow once again horizontally from the equator to the poles. At the poles, the air in the upper atmosphere would then descend to the earth's surface to complete a one-cell global air circulation pattern known as the Hadley cell (Fig. 4). In reality, this one-cell circulation is not observed due to a force that results from the rotation of the earth, the Coriolis force. This force causes the development of three circulation cells in each hemisphere, the Hadley cell, the Ferrel cell and the polar cell. However, of these only the Hadley cell that is quasi-permanent. The others are seen only in time-averaged plots but are never observed as such in instantaneous plots.

Fig. 5 (see http://www.geog.ucsb.edu) shows the representation of the three global circulation cells, with the equatorial region still remaining the warmest region on the Earth. The equatorial region acts as zone of thermal lows known as the Intertropical Convergence Zone (ITCZ). The Intertropical Convergence Zone draws in surface air from the subtropics. When this subtropical air reaches the equator, it rises into the upper atmosphere because of convergence and convection. It attains a maximum vertical altitude of above 16 kilometers (top of the troposphere; Holton et al., 1995), and then begins to flow horizontally to the North and South Poles. The Coriolis force causes the deflection of this moving air in the upper atmosphere, and by about 30° of latitude the air begins to flow zonally from west to east. This zonal flow is known as the subtropical jet stream. The zonal flow also results in the convergence of air in the upper atmosphere as it is no longer flowing meridionally. This leads to some of the air in the upper atmosphere to sink back to the surface creating the subtropical high pressure zone. From this zone, the surface air travels in two directions. A portion of the air moves back toward the equator completing the circulation system known as

the Hadley cell. This air is also deflected by the Coriolis effect to create the Northeast Trades (right deflection in the northern hemisphere) and Southeast Trades (left deflection in the southern hemisphere).

The surface air moving towards the poles from the subtropical high zone is also deflected by Coriolis acceleration producing the Westerlies. Between the latitudes of 30 to 60° North and South, upper air winds blow generally towards the poles. Once again, the Coriolis force deflects this wind to cause it to flow west to east forming the polar jet stream at roughly 60° North and South. On the Earth's surface at 60° North and South latitude, the subtropical Westerlies converge with cold air traveling from the poles. This convergence results in frontal uplift and the creation of the subpolar lows. A small portion of this lifted air is sent back into completing the Ferrel cell after it reaches the top of the troposphere. Most of this lifted air is directed to the polar vortex where it moves downward to create the polar high.

1.3.2. Troposphere-Stratosphere Transport

Transport of chemical species between the stratosphere and troposphere is a key process for the chemical composition of both the lowermost stratosphere and the troposphere. For example, anthropogenic species transported from the troposphere into the stratosphere in the tropics (Waugh, 1996) initiate the chemistry responsible for stratospheric ozone depletion. Conversely, downward transport from the stratosphere to the troposphere in mid and high latitudes (mostly through tropopause folding) represents a significant source of ozone for the troposphere and constitutes the ultimate removal mechanism for many stratospheric species including those involved in ozone depletion. Therefore, modifications in changing climate may significantly affect stratospheric ozone depletion (Butchart and Scaife, 2001) and the oxidizing capacity of the troposphere (Lelieveld and Dentener, 2000). However, troposphere-stratosphere

transport is still poorly understood and inadequately quantified, due to the involvement of physical and dynamical processes on local to global scales (Holton et al., 1995).

The phenomenon that most distinguishes the troposphere from the stratosphere is the disparity in vertical mixing timescales. Vertical transport of air and chemical species throughout the depth of the troposphere can occur on a time scales as short as an hour via strong convective updraft associated with cumulonimbus formation, whereas vertical transport over a similar altitude range in the stratosphere takes months to a year or more. In fact, Stohl et al. [2003] present an event that occurred on 25th February 1982, where potentially polluted ABL air from the North America east coast was transported into the lowermost stratosphere within 4 days.

The global wind pattern governing the flow of stratospheric air masses is known as the Brewer-Dobson circulation. In the process, air is lofted to higher altitude in the tropics and transported poleward where it sinks again to lower altitudes. The Brewer-Dobson circulation is responsible for the high and low ozone concentrations at the tropics and higher latitudes, respectively (Plumb and Eluszkiewicz, 1999). Fig. 6 depicts dynamical aspects of stratosphere-troposphere exchange taken from Holton et al. [1995]. Transport across the tropopause occurs in both ways in the extratropics as large latitudinal displacements of the tropopause occur (Seinfeld and Pandis, 1998). The tropopause is shown by the thick line. Thin lines are isentropes of constant potential temperature labelled in Kelvin. The shaded region is the lowermost stratosphere where isentropic surfaces across the tropopause and isentropic exchange by tropopause folding occur. The region above the 380 K surface is the ``overworld´´ in which isentropes lie entirely in the stratosphere. Stratospheric air in this region can not reach the troposphere without first

descending slowly across isentropics (adiabatic cooling), as shown in Fig. 6. The broad arrows indicate transport by the global-scale circulation, which is driven by the extratropical pump. The extratropical stratosphere acts persistently on the tropical lower stratosphere as a kind of global-scale suction pump, in which air is gradually withdrawn from the tropical stratosphere and pushed poleward and ultimately downward (Holton et al., 1995).

1.4. Transport Mechanisms in the Boreal Region

There are two major meteorological mechanisms that are responsible for the redistribution of emissions in the boreal region: 1) deep convection and 2) mid-latitude cyclones.

In the boreal region, deep convective processes are important for venting pollutants from the above boundary layer (ABL) into mid- and upper troposphere, where higher wind speeds can rapidly transport the pollutants to downwind continents. Deep convection is often associated with thunderstorms, whose tops can reach tropopause or can even overshoot into the lower stratosphere (Cooper and Parrish, 2004). Recently, lightning climatologists reveal the distribution of thunderstorms and deep convection (Zajac and Rutledge, 2001; Orville et al., 2002; Christian et al., 2003). In winter, lightning activity is low across the boreal region. Due to its summertime peak, deep convection makes its greatest impact on venting the ABL during this season in North America boreal region. Research into the importance of thunderstorms for rapid vertical transport is a relatively new topic, with the first in-situ measurement study conducted in 1987 (Dickerson et al., 1987).

Mid-latitude cyclones that flow from west to east are regarded to be responsible for the bulk export of trace gas from boreal region, throughout the year, even in

summer when systems are weaker (Merrill, 1996). Over the years clouds and precipitation have been studied in terms of the component airstreams of mid-latitude cyclones (Carlson, 1998). Recently, the origin and evolution of individual airstreams have been shown to perturb mixing ratios of trace gas and their relationships in the troposphere (Bethan et al., 1998; Stohl and Trickl, 1999; Cooper et al., 2001). Fig. 7 shows a typical mid-latitude cyclone which is composed of four major airstreams, the Warm Conveyor Belt (WCB), Cold Conveyor Belt (CCB) and Dry Airstream (DA). These airstreams move approximately along sloping isentropic surfaces. The CCB originates north of the cyclone's warm front, and ascends as it heads westwards, while the WCB is located on the eastern side of the cyclone ahead of the cold front. The WCB and CCB are moist airstreams and therefore their vertical motion does not follow exactly isentropic surfaces. Instead, they rise more steeply, due to the release of latent heat from the condensation of water vapour. On the contrary, DA originates at high altitudes on the poleward side of the cyclone and descends quasi-isentropically into the mid- and lower troposphere on the polar side of the cold front. Recently Cooper et al. (2001) have used the concept of the post cold front airstream (PCFA) to explain the dry airmass that flows beneath the DA and behind the cyclone cold front. Cyclones are more important especially in Northeast Asia due to the major role they play in both continental inflow (summer) and outflow (winter) (Fig. 8) (Pochanart et al., 1999; Ogawa and Miyata, 1985; Tsuruta et al., 1989). In summertime (8a), surface high-pressure systems associated with the Pacific anticyclone cause an inflow of clean oceanic air to Northeast Asia (Pochanart et al., 1999; Pochanart et al., 2002). In winter (8b), the East Asian monsoon, also associated with a strong anticyclone over the continent and active cold surges, is the most energetic monsoon circulation system on earth. The dominant surface feature of this monsoon flow is a huge thermal anticyclone known as the Siberian High, which has a central mean-sea-level pressure of 1030 hPa or more. The Siberian High extends over large part of

northern Asia and produces north-westerly flow. On other hand, deep convection provides the route for lifting pollution into the upper troposphere, where it may be transported north-eastwards over the Pacific.

1.5. Modeling of Atmospheric Transport processes

Atmospheric models from an air-quality perspective are tools that integrate our understanding of atmospheric processes (Seinfeld and Pandis, 1998) and provide the necessary framework for addressing questions such as:

- The contribution of source A to the concentration of pollutants at site B (source-receptor relationships)?
- The effect on air quality of the addition or reduction of a specific emission source?
- Air quality in the future?

Two different types of atmospheric models can be distinguished: Physical and mathematical. Physical models are sometimes used to simulate atmospheric processes by means of a small-scale physical representation of the actual system (e.g. in the laboratory) (Seinfeld and Pandis, 1998). Problems associated with properly duplicating the actual scales of the atmospheric motion make physical models of limited usefulness in the atmospheric sciences. Mathematical models of the atmosphere can further be classified into two types: 1. models based on the fundamental description of the atmospheric physical and chemical processes and 2. models based on statistical analysis of data. In this dissertation, a mathematical model of the first type was used. This model simulates transport processes in the atmosphere and, thus, can be used to establish source-receptor relationships.

Some transport models based on atmospheric physical and chemical processes simulate changes in the chemical composition of a given air parcel as it travels through the atmosphere (so-called Lagrangian models), while others describe the

concentrations in an array of fixed computational cells (so-called Eulerian) (Seinfeld and Pandis, 1998). An Eulerian modeling framework remains fixed in space. Species enter and leave each computational cell through its walls, and the model simulates the species concentrations as a function of time.

There are different types of Lagrangian models. For example, in a Lagrangian particle dispersion, advection and turbulent diffusion are treated by calculating the trajectories of a multitude of so-called particles, while in a Lagrangian trajectory box model, turbulent diffusion is not treated. The main advantage of Lagrangian models is that there is no artificial numerical diffusion such as it occurs in Eulerian models (Stohl, 2005). Furthermore, the minimum size of a source that a Eulerian model can simulate is one grid cell. Smaller sources are smeared out over at least one grid cell.

2. FLEXPART Model Description

The model used here is called ***FLEXPART,*** a Lagrangian particle dispersion model (Stohl, 2005) that simulates the long-range transport, diffusion, dry and wet deposition, and the radioactive decay of air pollutants released from point, line, area or volume sources. It treats advection and turbulent diffusion by calculating the trajectories of a multitude of so called particles, which are released at the sources of a substance. It can also be used backward in time, in which case the particles are released at a receptor location (e.g., a measurement site of interest). It can also be used in domain-filling modes where the entire atmosphere is subdivided in particles, each representing an equal part of the atmospheric mass. Stochastic fluctuations to simulate turbulence are obtained by solving the Langevin equation

$$dV_{ti} = a_i(X, V_t, t)dt + b_{ij}(X, V_t, t)dW_j, \quad \text{.....(1)}$$

where a and b are the drift and diffusion terms, respectively, which are functions of the position, the turbulent velocity and time. dW_j are incremental components of a Wiener process with mean zero and variance dt, which are uncorrelated with the other components and in time (Thomson, 1987).

Global data sets do not resolve individual convective cells, although they reproduce the large-scale effects of convection (e.g., the strong ascent within WCBs). Therefore, FLEXPART has recently been equipped with a convection scheme (Emanuel and Zivkovic-Rothman, 1999) to account for sub-grid scale transport. The scheme relies on the grid-scale temperature and humidity fields and gives as a by-product a displacement matrix providing the necessary information for the particle redistribution. FLEXPART can be driven by meteorological analysis data either from the European Centre for Medium-Range Weather Forecasts (ECMWF, 1995) or from the Global Forecast System (GFS) of the National Center for Environmental Prediction (NCEP).

2.1. Model Setup

The ECMWF model version used has 60 hybrid model levels in the vertical except for **Article 3** where the ECMWF version used has 31 vertical levels, while the GFS output is available on 26 pressure levels. Both data sets were retrieved on a global 1°x1° latitude-longitude grid. 6-hourly analyses were supplemented by 3-hour forecast step data to provide a 3-hourly temporal resolution. An output grid with a 1°x2° latitude/longitude resolution, a vertical spacing of 1000 m and an output interval of 3 hours was employed. Due to the higher resolution of the operational ECMWF forecast model, compared to GFS model, simulations described here are mostly using ECMWF data. However, results are also compared with the results of model simulations using the GFS data. In the tracer simulations for the studies, 5 x 10^6 particles were released to

calculate the transport of CO emissions from the fires. For the Russian emission, in order to describe the regional and daily variations of the fires, the MODIS hot spot data were used to spatially and temporally disaggregate the total burned area except for **Article 3** where the ATSR (Along Track Scanning Radiometer) fire product was used. For the Alaskan emission, the MODIS hot spot data were counted daily on a 1°x1° grid. For every 3-day period the maximum daily number of hot spots in a grid cell was taken in order to minimize the effect of missing hot spot data in the presence of clouds. The daily area burned in North America on a per-province (in Canada) and per-fire-state (in the United States) basis, taken from a web page at the Center for International Disaster Information (http//www.cidi.org/wildfire), was distributed to those cells in the respective province containing the hot spots. We assumed that the hot spots detected, all burned an equal area and, CO emissions were taken to be proportional to the area burned. In addition, 4500 kg of CO were assumed to be released per hectare of forest burned, which is similar to recent estimates based on emissions from the Canadian Northwest Territories (Cofer et al., 1998).

3. Results

3.1. Seasonal Comparison of Boreal Forest Fires

Boreal forest fires peak from May to October (Lavoue et al., 2000), and are most frequent in North America and Russia. The boreal fire season in 1998 was more active, especially in Canada and Siberia compared to the previous year. In fact, according to ATSR hot spot counts, Canada recorded 974 in 1997 and 8701 in 1998 the worse in the past 5 years (Shvidenko and Goldammer, 2001), while Siberia counted 6321 in 1997 and 21721 in 1998 one of the most severe years during the last 15 years (UNECE, 1999). The intense of the fire activities were evident in CO_2 and CO anomalies from CMDL stations north of 35° N as well as FLEXPART monthly CO mixing ratios. CO_2 monthly anomaly peaked at 1.2

ppm (Fig. 9a) in September of 1998 after the strongest burning was over. The peak was sustain until April 1999, this is due to the long lifetime of CO_2 (Seinfeld and Pandis, 1998). Both CO monthly anomaly from CMDL (Fig. 9b) and FLEXPART CO mixing ratio (Fig. 9c) all peaked in the burning season of 1998 and begin to decline towards the end of the year. This in contrast to CO_2, is due to the short lifetime of CO.

In evaluating the dominating transport patterns of boreal forest fire emissions on a seasonal basis, FLEXPART model results for the Siberian and Canadian CO tracers were averaged over the burning seasons of 1997 and 1998. Fig. 10 shows the total columns of the CO tracers from the Siberian (first and third rows) and Canadian (second and last rows) emissions during the fire season of the two years. The Canadian fire plume was transported across the Atlantic to Europe, while that of Siberia travelled eastwards across the Pacific to Canada. Comparing the Siberian emissions of the two years, in 1998 more fraction of the Siberian CO tracer was transported to Canada than in 1997. This can be attributed to the abnormally high pressure system that persisted east of Siberia (Efremov and Sheshukov, 2000) during 1998 fire season. In addition, according to FLEXPART at the surface in Canada, Siberian tracer mixing ratio measured 6.8 ppb on average, while Canadian tracer was 2.4 ppb.

The boreal region suffered a strong fire activity in 1998, especially Siberia and Canada, where hot spot data and area burned were increased more than 4 and 6 times, respectively, compared to the previous year. Emissions from the fires elevated both CO_2 and CO concentrations through out the season. Transport of fire plumes were to the east. Siberian emissions travelled towards Canada, while that from Canada head towards Europe. However, the strongest transport enhanced by abnormally high pressure system occurred in Siberia, leading to

CO contribution from Siberia over Canada being as high as twice that from Canadian's own fire emissions.

3.2. Hemispheric-Scale Transport of Russian Fire Remnants

In May 2003, severe forest fires in southeast Russia resulted in smoke plumes extending widely across the Northern Hemisphere. By the end of May, tens of thousands of fires had destroyed more than 15 x 10^6 ha of land in the Russian Federation. The most affected regions were Chitinskaya Oblast (55-56°N, 114-120°E), Buryatiya Republic (55-59°N, 107-114°E) and Amurskaya Oblast (52-56°N, 120-132°E) (GFMC, 2003). At the end of the 2003 fire season, more than 19 x 10^6 ha of land had been destroyed in Russia. An estimate of the average annually burned areas for all Russian forests is 10 – 12 x 10^6 ha yr^{-1} (Conard and Ivanova, 1998; Valendik, 1996). The year 1987, when 14.5 x 10^6 ha of forest and other lands were reported to have been destroyed, was considered to be an extreme fire year in Russia, (Cahoon et al., 1994). The year 2003 clearly exceeded this number and, furthermore, the intense burning in May caused a unique emission pulse to the atmosphere. (Nedelec, 2005: Jaffe, 2004: Yurganov et al., 2004)

In the following, the results obtained by Damoah et al. (2004) on the hemispheric-scale transport of emissions from these fires are described. This study combines satellite data from a variety of platforms (Moderate Resolution Imaging Spectroradiometer (MODIS) (Kaufman et al. 1998), Sea-viewing Wide Field-of-view Sensor (SeaWiFS) (Hook et al., 1993), Earth Probe Total Ozone Mapping Spectrometer (TOMS) (Hsu et al., 1999) and Global Ozone Monitoring Experiment (GOME) (Beirle et al., 2003) and vertical aerosol profiles derived with Raman lidar measurements (Mattis et al., 2003) with

results from a Lagrangian particle dispersion model to understand the transport processes that led to the large haze plumes observed over North America and Europe.

Transport of the smoke emitted by the fires in May occurred mostly in two directions: Smoke travelling northwestwards towards Scandinavia was lifted over the Urals and arrived over the Norwegian Sea. Smoke travelling eastwards to the Okhotsk Sea was also lifted; it then crossed the Bering Sea to Alaska from where it proceeded to Canada and was later even observed over Scandinavia and Eastern Europe on its way back to Russia. The total transport time around the northern hemisphere was about 17 days.

During the period 19-22 May 2003, the north Pacific jet was split into two components: a southern component near 40°N associated with the north Pacific storm track, and a zonally elongated polar jet component stretching from north-east Siberia across the Bering Sea into Alaska. A large amount of forest fire emissions were advected out of Siberia by this strong westerly flow which was further intensified by the growth of two synoptic waves on the jet, which crossed the Bering Strait within 36 hours of each other (Figs. 11a and 11b). The main body of the plume was pushed by the second wave over Alaska and has been very well simulated by the FLEXPART CO tracer (Fig. 11b) as a comparison with available satellite images. On 21 May 2003, Sea WiFS captured an aerosol plume (Fig. 11c) over Alaska that was presumably transported from the intense forest fire burning in Russia. When comparing this available satellite image with the simulated FLEXPART tracer, in particular, the sharp edges of the plume in the image over the Gulf of Alaska, westwards to the Aleutians and then northwards over the Bering Sea, coincide well with the edges of the CO tracer plume. A vertical section through the FLEXPART CO tracer at 64°N indicates that the main plume over Alaska is concentrated between 2 and 5 km altitude

while the leading plume over northwestern Canada is somewhat higher, lying primarily between 4 and 7 km.

On 24 May 2003 simulated FLEXPART CO tracer (Fig. 12c) showed an elongated plume stretching from the north-western edge of Lake Superior up towards James Bay and reaching Quebec and the St. Lawrence River. The simulated plume coincides well with an image of the MODIS instrument aboard the Terra satellite which also showed an elongated smoke plume (Figs. 12a,b) on 23 and 24 May. On 23 May a smoke maximum is indicated over part of Manitoba in the upper left corner of Fig. 12a. This is the edge of the main plume body which was seen previously over Alaska on 22 May (Fig. 11b) and moved into Canada about 48 hours behind the leading plume above. This large main part of the plume is advected in the strong westerly flow and arrives over the Hudson Bay on 25 May, where much of it slows down as it comes under the influence of diffluent flow ahead of a developing ridge. Fig. 12f shows the TOMS aerosol index on 24 May. It also shows a maximum over Hudson Bay and a filament stretching from south-east of James Bay to the St. Lawrence River, in fairly good agreement with the FLEXPART tracer simulation. However, no significant aerosols registered in TOMS near Lake Superior. This can be partly attributed to the dissipation of the smoke in this region later on 24 May (note that local midday, when the TOMS measurements were made, was after 18 UTC).

The plume was subsequently advected rapidly across the Atlantic due to the development of a small but intense and mobile synoptic wave and associated strong winds near Iceland on 25 May. The FLEXPART simulation (Fig. 13a) showed CO tracer over parts of the North Atlantic, Scandinavia and the Baltic Sea. The tracer plume formed a curve from just to the south of Iceland to southern Norway and south-central Sweden and from there to western and central Finland. Further filaments are in evidence across the Skagerrak Strait

near Denmark and over parts of the Baltic Sea, while further parts of the tracer plume are over parts of the European mainland, notably over Latvia, Lithuania and Poland. The location and shape of the primary plume is very well confirmed by an image from the SeaWiFS sensor on 27 May 2003, (Fig. 13b). The positions of the maxima over southern Norway and western Finland have been well captured by the model simulation, although the leading edge of the smoke appears in the satellite image to have reached slightly further east over Finland than in the simulation. The smoke thus arriving over Europe on 27 May had almost completed a loop around the globe and was heading back towards the source region in Russia. It also began to merge with smoke that had been transported eastwards directly from Russia.

During the two days following 27 May, the smoke maximum over southern Norway was dissipated by diffluent flow on the edge of a strong ridge building to the south-west. Parts of the plume encroached on eastern Germany and continued to merge with the remnants of the eastern European plume which had been advected directly out of Russia. Observations from the Raman lidar at Leipzig, Germany on 29 May (51.35°N, 12.43°E, 92m) recorded unusually high aerosol levels which have never been observed before since the start of the measurements in 1997 (Mattis et al., 2003). Fig. 14a shows a strong lidar backscatter ratio of aerosol at 1064 nm without any separation between the boundary layer and the free tropospheric aerosol layers. Nevertheless, according to radiosonde profiles of potential temperature the boundary layer height was below 2 km (Mattis et al., 2003). One can easily see two maxima, one below 4 km and the other one above 5km. These lidar results are in good agreement with the FLEXPART forest fire CO simulations with ECMWF (dotted line) and GFS (solid line) data (Fig. 14b), which also show double maxima at similar altitudes over Leipzig between 18-21 UTC on 29 May 2003. Backward calculations suggest that the lower and larger maximum corresponds to parts of the smoke

plume that had been over southern Norway two days earlier. The upper and smaller maximum is associated with the remnants of a thin filament which stretched southwards across Ireland and western France on 25 May and was subsequently advected eastwards, reaching western Germany on 27 May (Fig. 13a).

The transport of the Russian smoke plumes in May 2003 was unique in the sense that, within 17 days, smoke had circumnavigated the globe. The study by Damoah et al. (2004) is perhaps the first to document so clearly such a hemispheric-scale transport event. The fact that haze plumes from boreal forest fires can circumnavigate the globe and can persist for longer than two weeks has large implications for the radiative heating of the atmosphere (Fiebig et al., 2002) as well as the air quality (Jaffe, 2004). Not accounting for such plumes in climate model simulations or numerical weather predictions may possibly lead to large errors.

3.3. Pyro-Convective Transport of Alaskan Fire Emissions

In June, 2004, dry conditions, above normal temperatures and strong lightning activity caused severe forest fires in Alaska and the Canadian Yukon Territory. Being the third driest summer on record (Rozell, 2004), the fires, also fanned by surface winds of about 32 km/h (Rozell, 2004) on average in June, consumed large areas in Alaska and its surroundings. Infact, 707 fires burned a new record of about 2.7×10^6 ha. The old record of 2×10^6 ha was registered in 1957. For the Yukon Territory, a total of 282 fires destroy more than 1.7×10^6 ha at the end of the year. The annual burned area according to the Yukon History MetaData (see **http://www.community.gov.yk.ca/pdf/yukon_fire_history2004_metadata.pdf**) is 120,000 ha. Air quality was significantly degraded in large regions by these fires. For instance, particulate matter smaller than 2.5 µm (PM-2.5) of about 1000 $\mu g/m^3$ were measured in Fairbanks, exceeding E.P.A.'s threshold (300

µg/m^3) by a factor of more than three (Rozell, 2004). Also in Fairbanks measured CO of 9.2 ppm (Rozell, 2004) nearly violated the Clean Air Act (9.5 ppm), whereas typical mid-summer background CO mixing ratios are only about 80 ppb. Emissions from the burning were also transported over long distances. High enhancements of aerosol scattering were observed at Cheeka Peak (48.3° N, 124.6° W, 480 m asl) (personal communication, D. Jaffe) and several research aircraft were guided repeatedly into the fire plumes over eastern North America, the Atlantic and over Europe during the ICARTT (International Consortium for Atmospheric Research on Transport and Transformation) campaign and measured large enhancements of fire tracers in the lower and middle troposphere (de Gouw, 2005).

During most of June 2004, anticyclonic conditions prevailed over Alaska and western Canada. However, on 22 June a low-pressure center moved in from the west and on 23 July at 0 UTC it was centered approximately at the border between Alaska and Canada (Fig. 15a). The associated cold front triggered strong convection, as shown in an infrared satellite image on 23 June at 5 UTC (Fig. 15b). Convective clouds were aligned along the cold-frontal band, but the cloud patterns were not well organized, as is typical for cyclones in summer. Instead, several centers of convective activity can be seen, with the coldest cloud top brightness temperatures (< -52° C) located over the Yukon Territory and British Columbia. Fig. 16 shows the distribution of active fires and smoke on 22nd June, from NASA's Moderate Resolution Imaging Spectroradiometer (MODIS) aboard the Terra and Aqua satellites (Kaufman et al. 2003; 1998, Justice et al. 1996). It indicates intense burning in Pingo and Winter Trail along the Yukon River (upper left of Fig. 16). The Billy Creek and Porcupine fires south-east of the Tanana River sent piles of smoke into the atmosphere. By comparing Figures 15 and 16, it can be seen that the northern cluster of deep convection on 23 June was located almost exactly over the region with the

strongest burning activity. While it is impossible to say to what extent the fires enhanced the convection, the strong correlation between fire locations and the coldest cloud tops is striking. According to radiosonde temperature measurements from Fairbanks (Fig. 17), taken approximately within the white circle indicated in Fig. 15b, the coldest cloud tops were located above 10 km, and the thermal tropopause height was at approximately 11 km, whereas, the dynamical tropopause (orange line in Fig. 17) taken from the ECMWF analysis was located at about 10.5 km (the dynamical tropopause is the altitude where the potential vorticity exceeds the value of 2 potential vorticity units). The radiosonde temperature profile indicates no significant structure in the troposphere but a very sharp tropopause at about 11 km. Both features are characteristic of an environment shaped by deep convection. The cloud top height is consistent with the simulated transport of the CO emissions from the fires. A vertical section of the FLEXPART CO tracer at 64° N with convection turned on (Fig. 18a) and off (Fig. 18b) on 23rd at 03 UTC confirms indeed the injection of fire emissions deep into the Alaskan lower stratosphere due to convection. In the simulation with convection turned on, a tracer blob can be found between about 8 and 13 km altitude that was transported upward by the convection parameterization in FLEXPART. The top of the tracer blob is in good agreement with the coldest cloud top temperatures.

On 23rd and 24th June, TOMS aerosol index (Fig. 19a and 19b, respectively) shows filaments of enhanced values that stretch from Fairbanks and the Yukon Territory through Edmonton to Wisconsin. Distinct maxima of about 4.2 are observed over Fairbanks and the Yukon Territory on both days. These locations correspond remarkably well with the locations of the very cold cloud tops in Fig. 15b. The features of enhanced TOMS aerosol index on 23rd and 24th June are in good agreement with the FLEXPART CO tracer located between 9 and 15 km (Fig. 19c and 19d) in the simulation with the convection parameterization turned

on. On 23rd June at 03 UTC (Fig. 19c), the simulated CO tracer shows a similar filament with maxima over the Yukon Territory and British Columbia while on 24th June at 03 UTC (Fig. 19d) the maxima are at eastern Fairbanks, Yukon Territory and Edmonton. Fig. 19e and 19f show the corresponding results, but with the convection parameterization turned off. The very low CO tracer in this simulation shows that the upward transport in the simulation with convection turned on was indeed due to the sub-grid-scale convection parameterization. In fact, the average of the tracer between 9 and 15 km with convection relative to without convection shows a nearly nine-fold enhancement on both days.

Other instruments that testify to the perturbation of the UT/LS by the Alaskan fires are the Polar Ozone and Aerosol Measurement (POAM III) aboard the SPOT-4 satellite (Lucke et al., 1999) and the Stratospheric Aerosol and Gas Experiment (SAGE II) aboard the Earth Radiation Budget satellite (Mauldin et al., 1985). Fig. 20a shows enhanced aerosol extinction at 1 μm wavelength in the UT/LS from SAGE II (green) and POAM III (orange) over Edmonton, Canada on early hours of 24th June. The SAGE profile shows a strong enhancement between 10 and 12 km, the ECMWF dynamical tropopause (Fig. 20b) over the location is at about 10-11 km. The POAM profile over Edmonton shows an even stronger enhancement above 12 km but no values below. This termination of POAM data at such a high altitude is what is referred to as "High Zmin" (Fromm et al., 1999). This indicates that optically sufficiently thick clouds obscure the sun from the POAM sun tracker and thereby terminate the measurements above the cloud. An investigation of GEOS infrared imagery, however, revealed that there were no high clouds in the region. Visible imagery showed some greyish features, whose color suggests these were not normal water or ice clouds. In fact, backward trajectories from the enhanced POAM profile travel back to the fire source in Alaska. Another POAM profile at Quebec (black) outside the region of the Alaskan fire emission plume shows an

unperturbed profile for reference. The two POAM profiles above 12 km show an approximately four-fold enhancement of the aerosol extinction of the perturbed relative to the unperturbed profile. In addition, the FLEXPART CO tracer across 54° N on 24th June at 03 UTC (Fig. 20b) also shows a CO plume extending well above (2 km) the local tropopause at Edmonton, confirming the fact that the enhanced POAM and SAGE extinction in the UT/LS was due to the pyro-convective blow up.

During the last four days of June 2004, the High Spectral Resolution Lidar (HSRL) (Eloranta, 2005) at the University of Wisconsin, used for long-term cloud studies (43.1° N, 89.4° W), registered unusually high values of the aerosol backscatter cross section in the upper troposphere (Fig. 21). The strong signal was presumably smoke that was transported from Alaska and the Yukon Territory. Fig. 21a-c show observed aerosol backscatter on 26th, 28th and 30th June, respectively, (note that the first two panels show the last 12 hours of the day while the last panel shows the first 12 hours of the day). It is obvious that there is a consistent aerosol layer build up high above the atmospheric boundary layer at altitudes up to 13 km. The observed patterns of the aerosol backscatter throughout this period agree well with the simulated FLEXPART CO tracer patterns from the fires both with convection on (Fig. 21d-f) and off (Fig. 21g-i). Although FLEXPART tends to underestimate the maximum plume height by about 2-3 km, the overall features are well produced. It is evident from the simulations that convection did not alter the CO tracer distribution over Madison significantly during the last 12 hours of 26th and 28th June. However, during the last 2 hours of 26th of June traces of the CO lifted into the UT/LS by pyro-convection is evident above 9 km. The strongest aerosol backscatter was observed on June 30th, with the pyro-convective plume seen at 6 to 12 km. In fact, according to a FLEXPART movie showing maps of the total tracer column (not shown), this thick plume over Madison was advected north-eastwards from

the Yukon Territory on 25th June. 24 h later, it has taken a south-eastern direction from south of Victoria Island (69°-73° N, 100°-115° W) where it was stagnant for some hours before it headed to Wisconsin, where it engulfed most of the upper troposphere over Madison and reached levels above 12 km.

Alaska and Yukon Territory saw severe forest fire blow up in summer 2004 which was triggered by extremely strong lightning strikes. Deep convection in the midst of the boreal fires injected particles up to about 3 km above the tropopause. Satellite data that were available on 24 June, one day after the pyro-convection event, showed that there was enhanced aerosol extinction up to about 12-13 km, whereas the local tropopause was at only about 10-11 km. Infact, According to POAM data at location of Edmonton, the UT/LS aerosol load was enhanced by a factor of 4 relative to an unperturbed profile, whereas model results suggest an enhancement of approximately 9 fold due to deep convection over the entire region (40°-90° N, 80°-160° W) under review. Lidar measurements at Madison, Wisconsin, showed strongly enhanced aerosol backscatter at up to about 12 km altitude on 30 June, about 1 week after the pyro-convection event.

4. Conclusions

Both long-range and vertical transport of boreal fire emissions have been reported previously (Jaffe et al., 2003b; Westphal and Toon, 1991). However, our results show that the most significant impact of the boreal fires occurs during episodic fire years, such as 1998, 2003 and 2004. In 1998, due to long-range transport of fire emissions, Siberian fire CO tracer over Canada exceeded Canadian's own CO tracer. Long-range transport of air pollutants that occurred

in May 2003 also caused Russian fire plumes to circumnavigate the globe. This underlines the large-scale influence of boreal fires on radiative forcing of the atmosphere. Finally, the results from the 2004 fires in Alaska help to explain the recent concern on the observations of fire remnants in the lower stratosphere.

As the above results suggest a linkage between boreal fire activities and elevated CO and CO2 surface concentrations, the episodic nature of boreal fires could account for the interannual variations of these gases.

5. The relevance of the work to the scientific community

The input of biomass burning emissions into the atmosphere was often discussed as a phenomenon of the tropical rain forest and savannas (Andreae, 1991; Andreae and Merlet, 2001). However, the boreal forest contains about one third of the terrestrial carbon storage. The burning of boreal forest has an important impact on climate due to the release of substantial amount of carbon and other particulate into the atmosphere. Due to long-range transport, emissions from the boreal burning are not only limited to the boreal region but can be transported across continents (Hsu et al., 1999; Formenti et al., 2002; Fiebig et al., 2002; Wandinger et al., 2002). In fact, Jaffe et al. (2004) have shown that long-range transport of these emissions contributes to the exceedance of air quality standard. For the first time, our results from **Article 1** and **Article 2** show that during strong boreal fire activity, emission at a receptor far away from the source can exceed that of the receptor's own emission. Moreover, the emission can even circumnavigate the globe within a timescale of two weeks, this adds to the concern on the impact of boreal fire emissions on both climate and air quality standard.

Convection in thunderstorms is sufficiently energetic in some circumstances to inject materials from the surface into the lower stratosphere (Poulida and

Dickerson, 1996). However, it is generally accepted that only volcanic eruptions have the needed energy to cause a stratospheric injection of surface materials (Graf et al., 1999). Recently, due to the convection associated with a fire, Fromm et al. (2000) linked the enhancement of stratospheric aerosol to boreal fire. Other studies such as Jost et al, 2004 and Immler et al, 2005 have observed fire emissions in the lower stratosphere. Findings from **Article 3** suggest that deep convection in the midst of boreal fires coupled with long-range transport can lead to 4-fold enhancement of aerosol in the lower stratosphere which is also consistent with that of Fromm et al. (2003). However, quantification and mechanisms responsible for this transport of fire remnants into the stratosphere need more investigation.

Given the likelihood of increasing boreal fires due to future climate warming (Kasischke et al., 1995), these results suggest a linkage between climate, boreal forest fires, long-range transport of air pollutants and human health.

6. Task of the candidate in the various Articles

Article 1 & 2: I retrieved the satellite data (TOMS, POAM and SAGE) including the MODIS fire product that was used in the model runs. In addition, I retrieved the ECMWF meteorological data required for the FLEXPART model and made the model simulations. Finally, I analyzed and interpreted the results.

Article 3: I retrieved the ECMWF wind fields, ATSR (Along Track Scanning Radiometer) fire product and the CMDL (Climate Monitoring and Diagnostics Laboratory) CO and CO2 data. I also assisted in the analysis and interpretation of the data.

7. References

1. Andreae, M. O.: Biomass burning: Its history, use and distribution and its impacton environmental quality and global climate, in Global Biomass Burning*:* Atmospheric, Climate, and Biospheric Implications, edited by J. S. Levine, pp. 3 – 21, MIT Press, Cambridge, Mass, 1991.
2. Andreae, M. O., Rosenfeld, D., Artaxo, P., Costa, A. A., Frank, G. P., Longo, K. M., Silva-Dias, M. A. F.: Smoking rain clouds over the Amazon, Science, 303, 1337 – 1342, 2004.
3. Atkinson, B. W.: Weather, meteorology, physics and mathematics: Dynamical meteorology, edited by Atkinson, Methuen & Co. Ltd, London, 1981.
4. Beirle, S., Platt, U., Wenig, M., and Wangner, T.: Weekly cycle of NO_2 by GOME measurements: a signature of anthropogenic sources, Atmos. Chem. Phys., 3, 2225 – 2232, 2003.
5. Bethan, S., Vaughan, G., Gerbig, C., Volz-Thomas, A., Richer, H., Tiddeman, D. A.: Chemical air mass differences near fronts, J. Geophys. Res., 103, 13413 - 13434, 1998.
6. Butchart, N., and Scaife, A. A.: Removal of chlorofluorocarbons by increased mass exchange between the stratosphere and troposphere in a changing climate, Nature, 410, 799 - 801, 2001.
7. Carlson, T. N.: Mid-latitude weather systems, America Meteo. Soc., Boston, 1998.
8. Christian, H. J., Blakeslee, R. J., Boccipio, D. J., Boeck, W. L., Buechler, D. E., Driscoll, K. T., Goodman, S. J., Hall, J. M., Koshak, W. J., Mach, D. M., Stewart, M. F.: Global frequency and distribution of lightning as observed from space by the optical transient detector, J. Geophys. Res., 108, 4005, doi:10.1029/2002JD002347, 2003.
9. Christopher, S., Chou, J., Chang, J., Lin, X., Berendes, T. A., and Welch, R. M.: Shortwave direct radiative forcing of biomass burning aerosols

estimated using VIRS and CERES data, Geophys. Res. Lett., 27, 2197 – 2200, 2000.

10. Christopherson, W. R.: Geosystems, Prentice Hall, New Jersey, 2000.
11. Cahoon, D. R., Stocks, B. J, Levine, J. S., Cofer, W. R., III, and Pierson, J. M.: Satellite analysis of the severe 1987 forest fires in northern China and southeastern Siberia, J. Geophys. Res., 99, 18,627 – 18,638, 1994.
12. Cofer, W. R., Winstead, E. L., Stocks, B. J., Goldammer, J. G., and Cahoon, D. R.: Crown fire emissions of CO_2, CO, H_2, CH_4, and TNMHC from dense jack pine boreal forest fire, Geophys. Res. Lett., 25, 3919 - 3922, 1998.
13. Conard, S. G., and Ivanova, G. A. : Wildfire in Russian boreal forests – potential impacts of fire regime characteristics on emissions and global carbon estimates, Environmental Pollution, 98, 305 – 313, 1998.
14. Cooper, O. R., Moody, J. L., Parrish, D. D., Trainer, M., Ryerson, T. B., Holloway, J. S., Hübler, G., Fehsenfeld, F. C., Evans, M. J.: Trace gas signatures of the airstreams within North Atlantic cyclones: Case studies from the North Atlantic Regional Experiment (NARE’97), J. Geophys. Res. 106, 5437 - 5456, 2001.
15. Cooper, O. R., and Parrish, D. D.: Air pollution export from and import to North America. In: Inter-continental transport of air pollution, pp. 43-67, edited by Stohl, A., Springer-Verlag Berlin Heidelberg, 2004.
16. Crutzen, P. J.: A discussion of the chemistry of some minor constituents in the stratosphere and troposphere, Pure Appl. Geophys., 106 – 108, 1385 – 1399, 1973.
17. Damoah, R., Spichtinger, N., Forster, C., James, P., Mattis, I., Wandinger, U., Beirle, S., Wagner, T., and Stohl, A.: Around the world in 17 days – hemispheric-scale transport of forest fire smoke from Russia in May 2003, Atmos. Chem. Phys., 4, 1311-1321, 2004.

18. Daniel, J. S., and Solomon, S.: On the climate forcing of carbon monoxide, J. Geophys. Res., 103, 13,249 – 13,260, 1998.
19. Dickerson, R. R., Huffman, G. J., Luke, W. T., Nunnermacker, L. J., Pickering, K. E., Leslie, A. C. D., Lindsey, C. G., Slinn, W. G. N., Kelly, T. J., Daum, P. H., Delaney, A. C., Greenberg, J. P., Zimmerman, P. R., Boatman, J. F., Ray, J. D., Stedman, D. H.: Thunderstorms: An important mechanism in the transport of air pollutants, Science, 235, 460-465, 1987.
20. Eckhardt, S., A. Stohl, H. Wernli, P. James, C. Forster, and N. Spichtinger; A 15-year climatology of warm conveyor belts, J. Climate, 17, 218-237, 2004.
21. ECMWF: User Guide to ECMWF Products 2.1, Meteorol. Bull. M3.2, ECMWF, Reading, UK, 1995.
22. Efremov, D. F. and Sheshukov, M. A.: Ecological and economical evaluation of the consequences of catastrophic fires in Russia Far East: The Khabarovsk Territory Example of 1998, IFFN, 22, 53-62, 2000.
23. Eloranta, E. W.: High spectral resolution lidar: Range-Resolved Optical Remote Sensing of the Atmosphere, edited by Weitkamp, C., pp. 143-163, in press, 2005.
24. Emanuel, K. A., and Zivkovic-Rothman, M.: Development and evaluation of a convection scheme for use in climate models, J. Atmos. Sci., 56, 1766 – 1782, 1999.
25. Fiebig, M., Petzold, A., Wandinger, U., Wendisch, M., Kiemle, C., Stifter, A., Ebert, M., Rother, T., and Leiterer, U.: Optical closure for an aerosol column: Method, accuracy, and inferable properties applied to a biomass-burning aerosol and its radiative forcing, J. Geophys. Res., 107, 8130, doi:10.1029/2000JD000192, 2002.
26. Formenti, P., et al., STAAARTE-MED 1998 summer airborne measurements over the Aegean Sea, 1, Aerosol particles and trace gases, J. Geophys. Res., 107, 4450, doi:10.1029/2001JD001337, 2002.

27. Forster, C., Wandinger, U., Wotawa, G., James, P., Mattis, I., Althausen, D., Simmonds, P., O'Doherty, S., Jennings, S., Kleefeld, C., Schnieder, J., Trickl, T., Kreipl, S., Jäger, H., and Stohl, A.: Transport of boreal forest fire emissions from Canada to Europe, J. Geophys. Res., 106, 22,887 – 22,906, 2001.
28. Fromm, M., Bevilacqua, R., Hornstein, J., Shettle, E., Hoppel, K., and Lumpe, J. D.: An analysis of Polar Ozone and Aerosol Measurement (POAM) II Arctic polar stratospheric cloud Observations, 1993-1996, J. Geophys. Res., 104, 24341–24357, 1999.
29. Fromm, M. D., and Servranckx, R.: Transport of forest fire smoke above the tropopause by supercell convection, Geophys. Res. Lett., 30, 1542, doi: 1029/2002GL016820, 2003.
30. Fromm, M., Alfred, J., Hoppel, K., Hornstein, J., Bevilacqua, R., Shettle, E., Servranckx, R., Li, Z., and Stocks, B.: Observations of boreal forest fire smoke in the stratosphere by POAM III, SAGE II, and lidar in 1998, Geophys. Res. Lett., 27, 1407 – 1410, 2000.
31. Fromm, M., Bevilacqua, R., Servranckx, R., Rosen, J., Thayer, P. J., Herman, J., and Larko, D.: Pyro-cumulonimbus injection of smoke to the stratosphere: observations and impact of a super blowup in northwestern Canada on 3-4 August 1998, J. Geophys. Res., 110, D08205, doi:10.1029/2004JD005350, 2005.
32. Global Fire Monitoring Center (GFMC): Daily/weekly updates of forest fires in the Russian Federation, 2003, *see* ***http://www.fire.uni-freiburg.de/current/globalfire.htm***.
33. de Gouw, J. A., Warneke, C, Stohl, A., Wollny, A.G., Brock, C.A., Cooper, O.R., Holloway, J.S., Trainer, M., Fehsenfeld, F.C., Atlas, E.L., Donnelly, S.G., Stroud, V., and Lueb, A.: The VOC Composition of Aged Forest Fire Plumes from Alaska and Western Canada. Submitted to J. Geophys. Res., 2005.

34. Graf, H., Herzog, M., Oberhuber, J. M., and Textor, C.: The effect of environmental conditions on volcanic plume rise, J. Geophys. Res. 104, 24309-24320, 1999.
35. Holton, J. R., Hayness, P. H., McIntyre, M. E., Douglass, A. R., Rood, R. B., and Pfister, L.: Stratosphere-troposphere exchange, Rev. Geophys., 33, 403 – 439, 1995.
36. Hooker, S. B., Mcclain, C. R., Holmes, A.: Ocean color imaging – Costal Zone Color Scanner (CZCS) to Sea WiFS, Marine Technology Society Journal, 27, 3 – 15, SPR, 1993.
37. Hsu, N. C., Herman, J., Gleason, J., Torres, O., and Seftor, C.: Satellite detection of smoke aerosols over a snow/ice surface by TOMS, Geophys. Res. Lett. 26, 1165 – 1168, 1999.
38. Immler, F., Engelbart, D., and Schrems, O.: Fluorescence from atmospheric aerosol detected by a lidar indicates biogenic particles in the stratosphere, Atmos. Chem. Phys., 5, 345-355, 2005.
39. IPCC: Climate Change, edited by Nebojsa Nakicenovic and Rob Swart, Cambridge Univ. Press, New York, 2001.
40. Jaffe, D., Bertschi, I., Jaegle, L., Novelli, P., Reid, S. J., Tanimoto, H., Vingarzan, R., and Westphal, L. D.: Long-range transport of Siberian biomass burning emissions and impact on surface ozone in western North America, Geophys Res. Lett., 31, L16106, doi:10.1029/2004GL020093, 2004.
41. Jost, H.J., Drdla, K., Stohl, A., Pfister, L., Loewenstein, M., Lopez, J.P., Hudson, P.K., Murphy, D.M., Cziczo, D.J., Fromm, M., Bui, T.P., Dean-Day, J., Gerbig, C., Mahoney, M.J., Richard, E.C., Spichtinger, N., Pittman, J.V., Weinstock, E.M., Wilson, J.C., and Xueref, I.,: In-situ observations of mid-latitude forest fire plumes deep in the stratosphere, Geophys. Res. Lett. 31, 11101, doi:10.1029/2003GL019253, 2004.

42. Justice, C. O., Kendall, J. D., Dowty, P. R., and Scholes, R.: Satellite remote sensing of fires during the SAFARI campaign using NOAA advanced very high radiometer data, J. Geophys. Res., 101, 23,851 – 23,863, 1996.
43. Kajii, Y., Kato, S., Streets, G. D., Tsai, Y. N., Shvidenko, A., Nilsson, S., McCallum, I., Minko, P. N., Abushenko, N., Altyntsev, D., and Khodzer, V. T.: Boreal forest fires in Siberia in 1998: Estimation of area burned and emissions of pollutants by advanced very high resolution radiometer satellite data, J. Geophys. Res., 107, 4745, doi:10.1029/2001JD001078, 2002.
44. Kasischke, E. S., Christensen, N. L., and Stocks, B. J.: Fire, global warming and the carbon balance of boreal forests, Ecology, 5(2), 437-451, 1995.
45. Kasischke, E. S., Stocks, B. J., Oneill, K., French, N. H., and Bourgeau-Chavez: Direct effects of fire on the boreal forest carbon budget, in Biomass burning and its Inter – Relationships with the Climate System, edited by J. L. Innes, M. Beniston and M. M. Verstraete, pp. 51 – 68, Kluwer Academic Publishers, Dordrecht, Netherlands, 2000.
46. Kato, S., Pochanart, P., Hirokawa, J., Kajii, Y., Akimoto, H., Ozaki, Y., Obi, K., Katsuno, T., Streets, D.G., and Minko, N.P.: The influence of Siberian forest fires on carbon monoxide concentrations at Happo, Japan, Atmos. Env., 36, 385-390, 2002.
47. Kaufman, Y. J., Justice, C. O., Flynn, L. P., Kendall, J. D., Prins, E. M., Giglio, L., Ward, D. E., Menzel, W. P., and Setzer, A. W.: Potential global fire monitoring from EOS-MODIS, J. Geophys. Res., 103, 32,215 – 32,238, 1998.
48. Kaufman, Y. J., Ichoku, C., Giglio, L., Korontzi, S., Chu, D. A., Hao, W. M., Li, R.-R., and Justice, C. O.: Fire and smoke observed from Earth

Observing System MODIS instrument – products, validation, and operational use, Int. J. Remote Sensing, 24, 1765 – 1781, 2003.

49. Lavoue, D. C., Liousse, C., Cachier, H., Stocks, B. J., and Goldammer, J. G.: Modelling of carbonaceous particles emitted by boreal and temperate wildfires at northern latitudes, J. Geophys. Res., 105, 26871 – 26890, 2000.
50. Lelieveld, J., and Dentener, F. J.: What controls tropospheric ozone?, J. Geophys. Res., 105, 3531 – 3551, 2000.
51. Livesey, N. J., Fromm, M. D., Waters, J. W., Manney, G. L., Santee, M. L., and Read, W. G.: Enhancement in lower stratospheric CH_3CH observed by the Upper Atmosphere Research Satellite Microwave Limb Sounder following boreal forest fires, J. Geophys. Res., 109, D06308, doi:10.1029/2003JD004055, 2004.
52. Logan, J. A., Prather, M. J., Wofsy, S. C., and McElroy, M. B.: Tropospheric chemistry: A global perspective, J. Geophys. Res., 86, 7210 – 7254, 1981.
53. Lucke, R., Korwan, D., Bevilacqua, R., Hornstein, J., Shettle, E., Chen, D., Daehler, M., Lumpe, J., Fromm, M., Debrestian D., Neff, B., Squire,M., König-Langglo, and Davis J.: The Polar Ozone and Aerosol Measurement (POAM) III instrument and early validation results , J. Geophys. Res., 104, 18785-18799, 1999.
54. Mattis, I., Ansmann, A., Wandinger, U., and Müller, D.: Unexpectedly high aerosol load in the free troposphere over Central Europe in spring/summer 2003, Geophys. Res. Lett., 30, 2178, dio:10.1029/2003GL018442, 2003.
55. Mauldin, L., Zuan, N., McCormic, M., Guy, J., and Vaughn, W.,: Stratospheric Aerosol and Gas Expriment II instrument: A functional description, Opt Eng., 24, 307-312, 1985.

56. Merrill, J. T., and Moody, J. L.: Synotic meteorology and transport during the North Atlantic Regional Experiment (NARE) intensive: Overview, J. Geophys. Res., 101, 28903 - 28922, 1996.
57. Nedelec P., Thouret, V., Brioude, J., Sauvage, B., Cammas, J.-P., and Stohl, A.: Extreme CO concentrations in the upper troposphere over northeast Asia in June 2003 from in situ MOZAIC aircraft data, Geophys. Res. Lett. 32, L14807, doi:10.1029/2005GL023141, 2005.
58. Ogawa, T., Miyata, A.: Seasonal variation of the tropospheric ozone: A summer minimum in Japan, J. Meteorol. Soc. Jpn, 63, 937-946, 1985.
59. Orville, R. E., Huffines, G. R., Burrows, W. R., Holle, R. L., Cummins, K. L.: The North American Lightning Detection Network (NALDN) – First results: 1998-2000, Mon. Wea. Rev., 130, 2098 - 2109, 2002.
60. Plumb, R. A., and Eluszkiewicz, J.: The Brewer-Dobson circulation: dynamics of the tropical upwelling. J. Atmos. Sci., 56, 868-890, 1999.
61. Pochanart, P., Hirokawa, J., Kajii, Y., Akimoto, H., Nakao, M.: Influence of regional-scale anthropogenic activity in northeast Asia on seasonal variations of surface ozone and carbon monoxide observed at Oki, Japan, J. Geophys. Res., 104, 3621 - 3632, 1999.
62. Pochanart, P., Akimoto, H., Kinjo, Y., Tanimoto, H.: Surface ozone at four remote Island sites and preliminary assessment of the exceedances of its critical level in Japan, Atmos. Environ., 36, 4235-4250, 2002.
63. Rozell, N.: Smoked pike on menu for Yukon Flats scientists, Alaska Science Forum, 1710, 2004.
64. Seinfeld, H. J., and Pandis, N. S.: Atmospheric chemistry and physics: From air pollution to climate change, pp. 11 – 17, John Wiley & Sons Inc., New York, 1998.
65. Shvidenko, A., and Goldammer, J. G.: Fire situation in Russia, International Forst Fire News, 24, 41 – 59, 2001.

66. Spichtinger, N., Wenig, M., James, P., Wagner, T., Platt, U., and Stohl, A.: Satellite detection of a continental-scale plume of nitrogen oxides from boreal forest fires, Geophys. Res. Lett., 28, 4579 – 4583, 2001.
67. Spichtinger, N., Damoah, R., Eckhard, S., Forster, C., James, P.,Beirle, T., Wagner, T., Novelli, P.C., and Stohl, A.: Boreal forest fires in 1997 and 1998: A seasonal comparison using transport model simulations and measurement data, Atmos. Chem. Phys., 4, 1857 – 1868, 2004.
68. Stocks, J. B.: Forest fires in the boreal zone: Climate change and carbon implications, IFFN, 31, 122-131, 2004.
69. Stohl, A., and Trickl, T.: A textbook example of long-range transport: Simultaneous observation of ozone maxima of stratospheric and North American origin in the free troposphere over Europe, J. Geophys. Res., 104, 30,445 – 30,462, 1999.
70. Stohl, A.: A one-year Lagrangian climatology of airstreams in the northern hemisphere troposphere and lowermost stratosphere, J. Geophys. Res., 106, 7263 – 7279, 2001.
71. Stohl, A., Eckhardt, S., Forster, C., James, P., and Spichtinger, N.: On the pathways and timescales of intercontinental air pollution transport, J. Geophys. Res.,107, 4684, dio:10.1029/2001JD001396, 2002.
72. Stohl, A., Wernli, H., James, P., Bourqui, M., Forster, C., Liniger, A. M., Seibert, P., and Sprenger, M.: A new perspective of stratosphere-troposphere exchange, American Meteo. Soc., DOI: 10.1175/BAMS-84-11-1565, 2003.
73. Stohl, A., Seibert, P., and Forster, C.: The FLEXPART particle dispersion model version 6.1 user guide, 2005.
74. Tanimoto, H., Kajii, Y., Hirokawa, J., Akimoto, H., and Minko, N.P.: The atmospheric impact of boreal forest fires in far eastern Siberia on the seasonal variation of carbon monoxide: observations at Rishiri, a northern remote island in Japan, Geophys. Res. Lett., 27, 4073-4076, 2000.

75. Tsuruta, H., Shinya, K., Mizoguchi, T., Ogawa, T.: Seasonal behaviour of the tropospheric ozone in rural Japan. In: Ozone in the atmosphere, pp. 433, edited by Bojkov, R. D., and Fabian, P., Deepak, Hampton, 1989.
76. United Nation Economic Commission for Europe: Forest fire statistics 1996-1998, Timber Bulletin, 52, 1999.
77. Valendick, E. N.: Ecological aspects of forest fires in Siberia, Sib. Ecol. J., 1, 1 – 8, 1996.
78. Wandinger, U., et al., Optical and microphysical characterization of biomass- burning and industrial-pollution aerosols from multiwavelength lidar and aircraft measurements, J. Geophys. Res., 107, 8125, doi:10.1029/2000JD000202, 2002.
79. Waugh, D. W.: Seasonal variation of isentropic transport out of the tropical stratosphere, J. Geophys. Res., 101, 4007 – 4023, 1996.
80. Wotawa, G., and Trainer, M.: The influence of Canadian forest fires on pollutant concentrations in the United States, Science, 288, 324 – 328, 2000.
81. Yurganov, N. L., Blumenstock, T., Grechko, E. I., et al.: A quantitative assessment of the 1998 carbon monoxide emission anomaly in the Northern Hemisphere based on total column and surface concentration measurements, J. Geophys. Res., 109, D15305, doi:10.1029/2004JD004559.
82. Zajac, B. A., and Rutledge S. A.: Cloud-to-ground lightning activity in the contiguous United States from 1995-1999, Mon. Wea. Rev., 129, 999 - 1019, 2001.

8. Figures

(a)

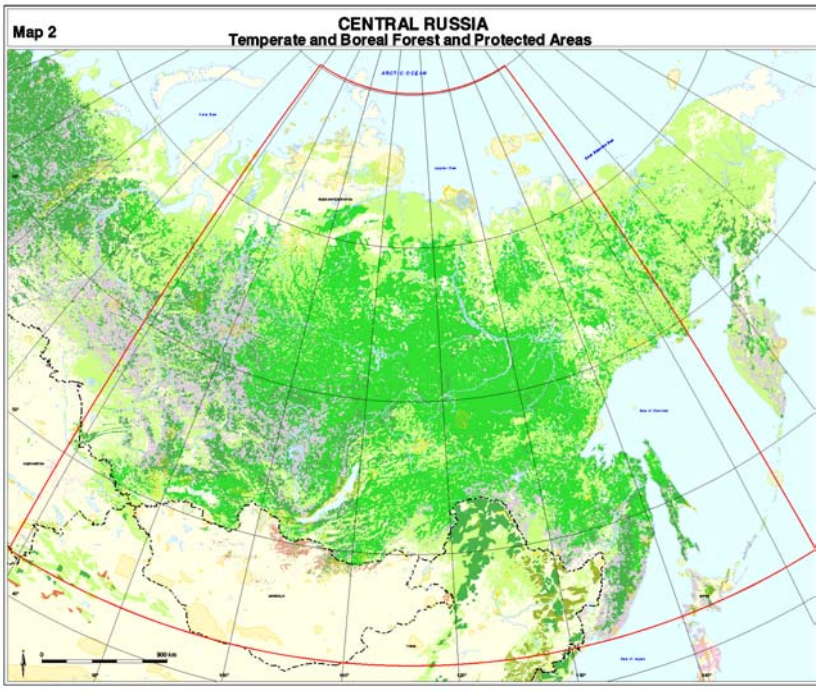
Map 2
CENTRAL RUSSIA
Temperate and Boreal Forest and Protected Areas

(b)

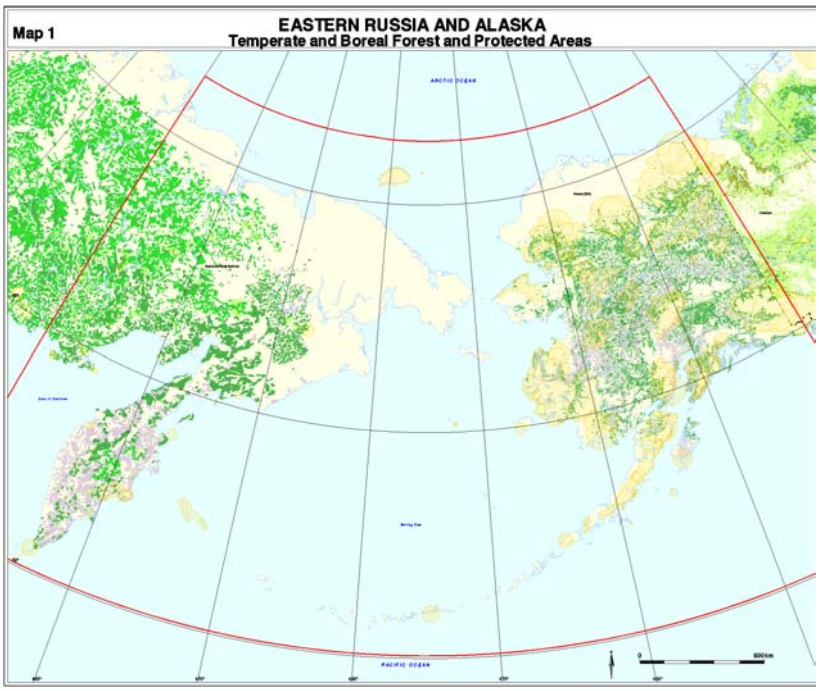
Map 1
EASTERN RUSSIA AND ALASKA
Temperate and Boreal Forest and Protected Areas

(c)

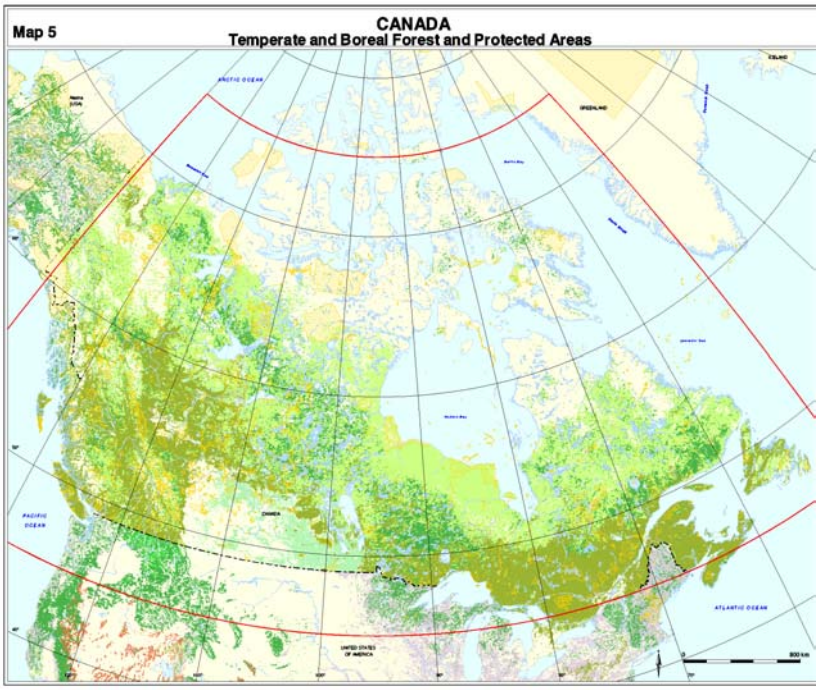

(d)

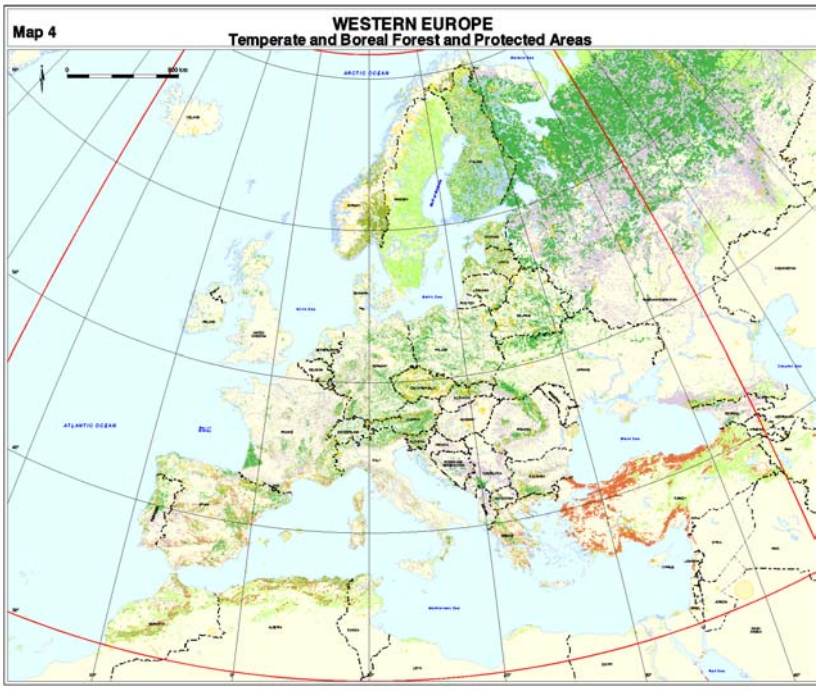

Figure 1 A map of the distribution of protected boreal and temperate forests in (a) Russia (b) Alaska (c) Canada and (c) Scandinavia according to the World Conservation Monitoring Centre (WCMC).

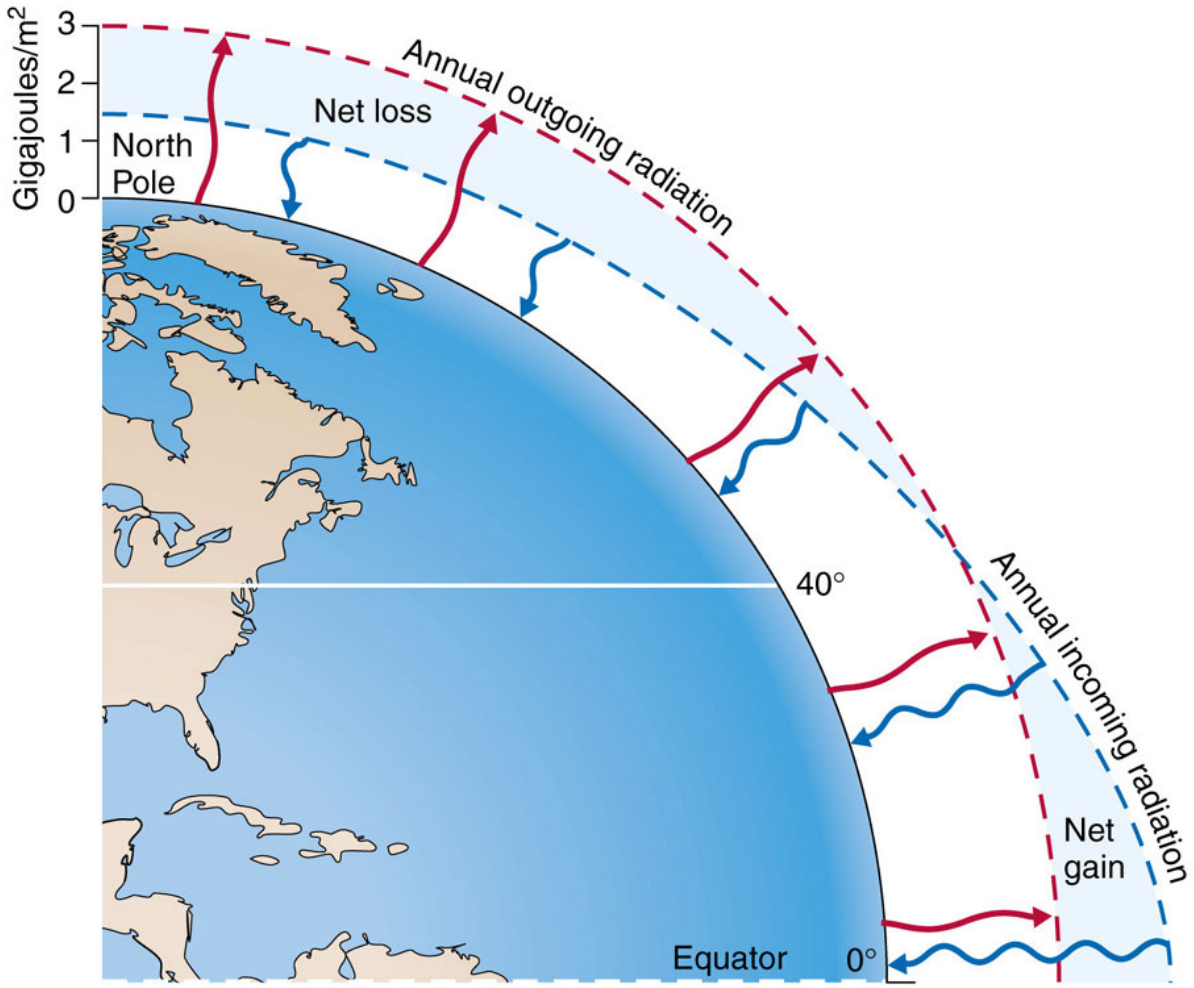

Figure 2 Shows the representation of annual incoming (blue arrows) and outgoing (red arrows) radiation over the globe.

(a)

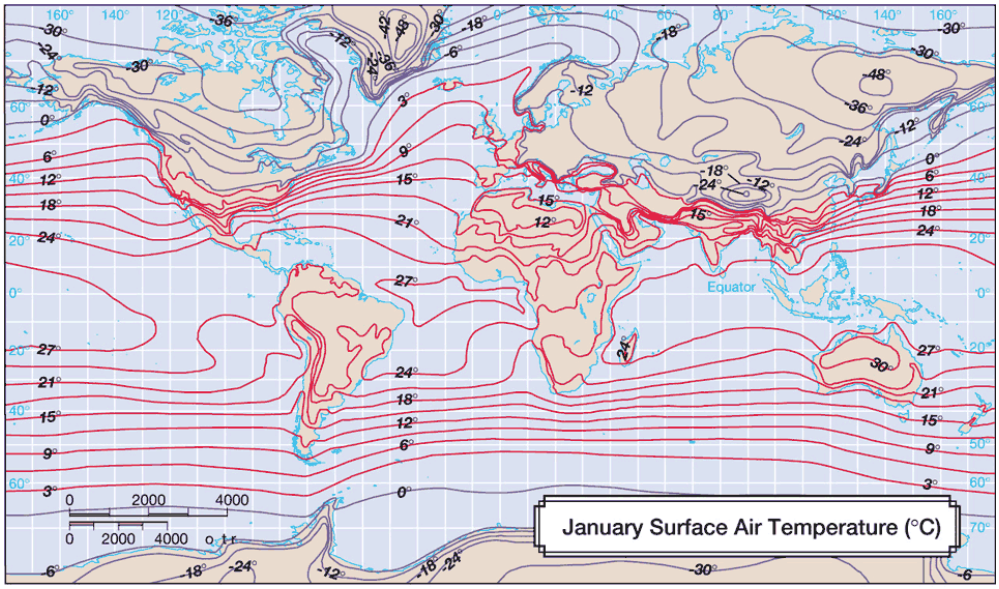

(b)

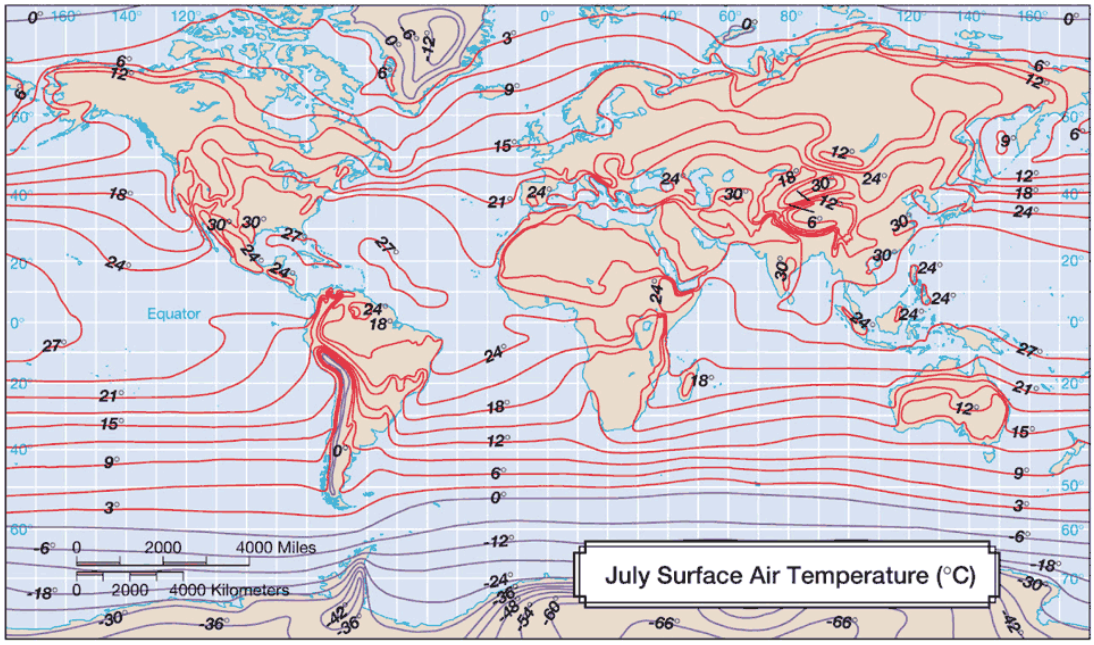

Figure 3 Average surface air temperatures for (a) January and (b) July in ° C. Red contour lines indicate temperatures above 0° C and voilet show 0° C or below.

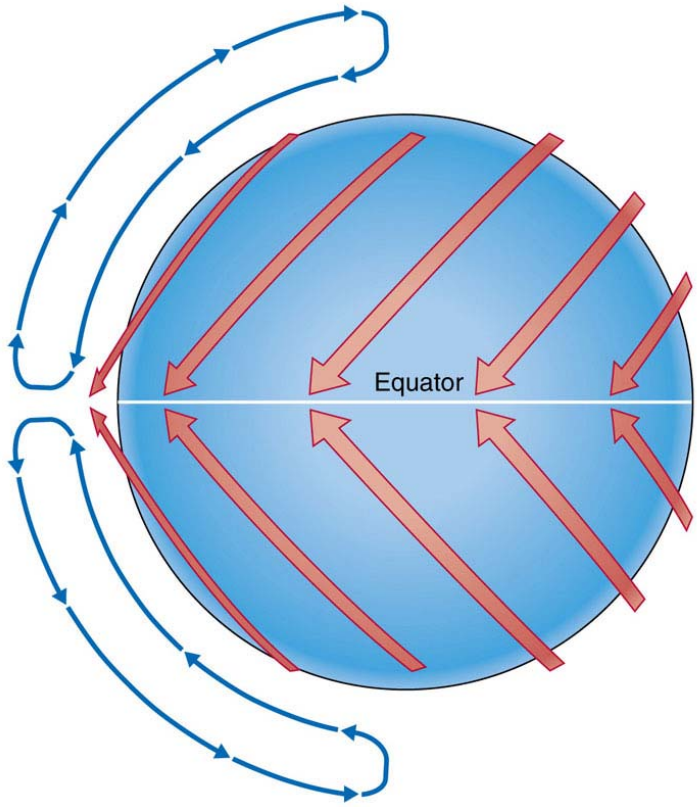

Figure 4 Hadley cell global air circulation of the atmosphere. Surface air (red arrows) is from the poles to the equator whiles upper atmospheric air (blue) is from the equator to the poles.

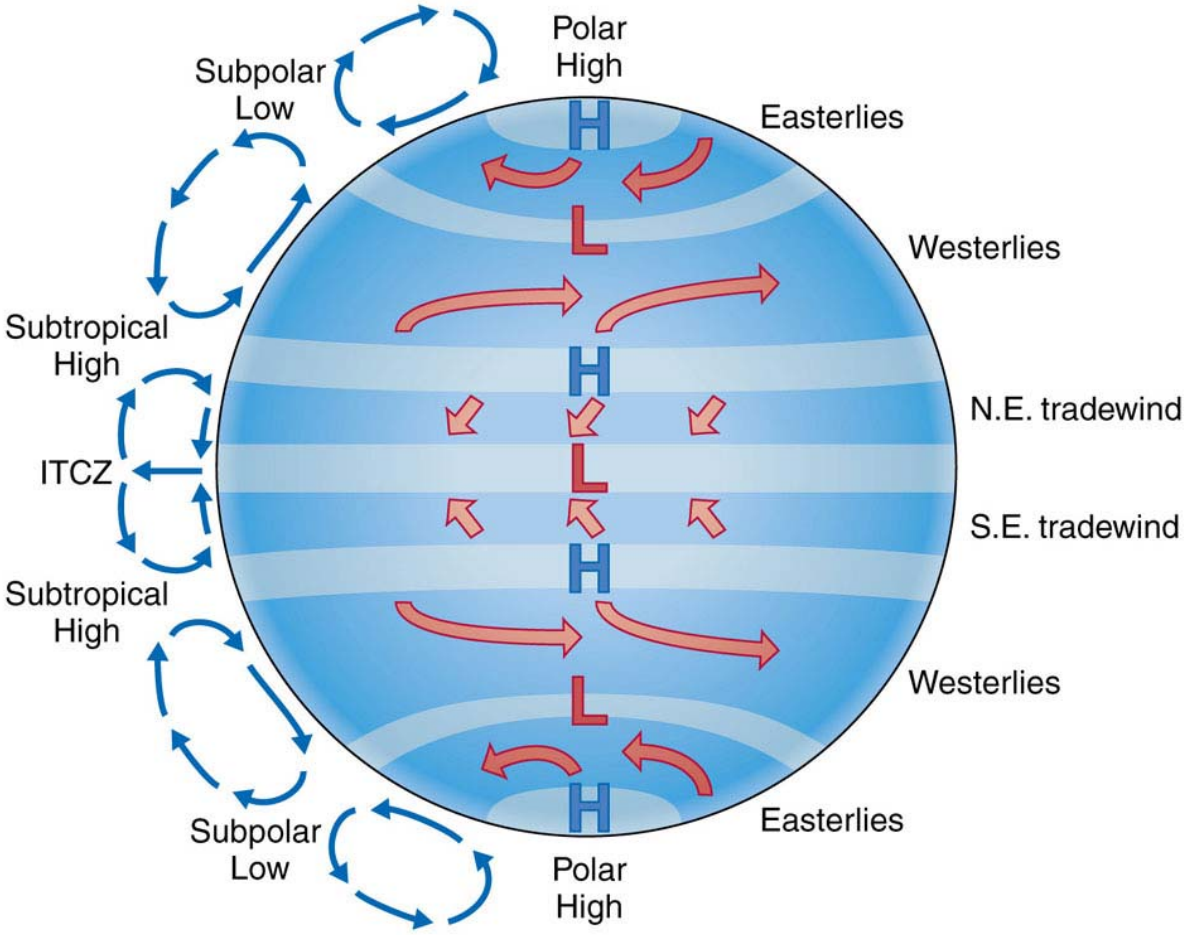

Figure 5 Simplified three cell (Hadley, Ferrel and Polar) surface and upper air circulation patterns.

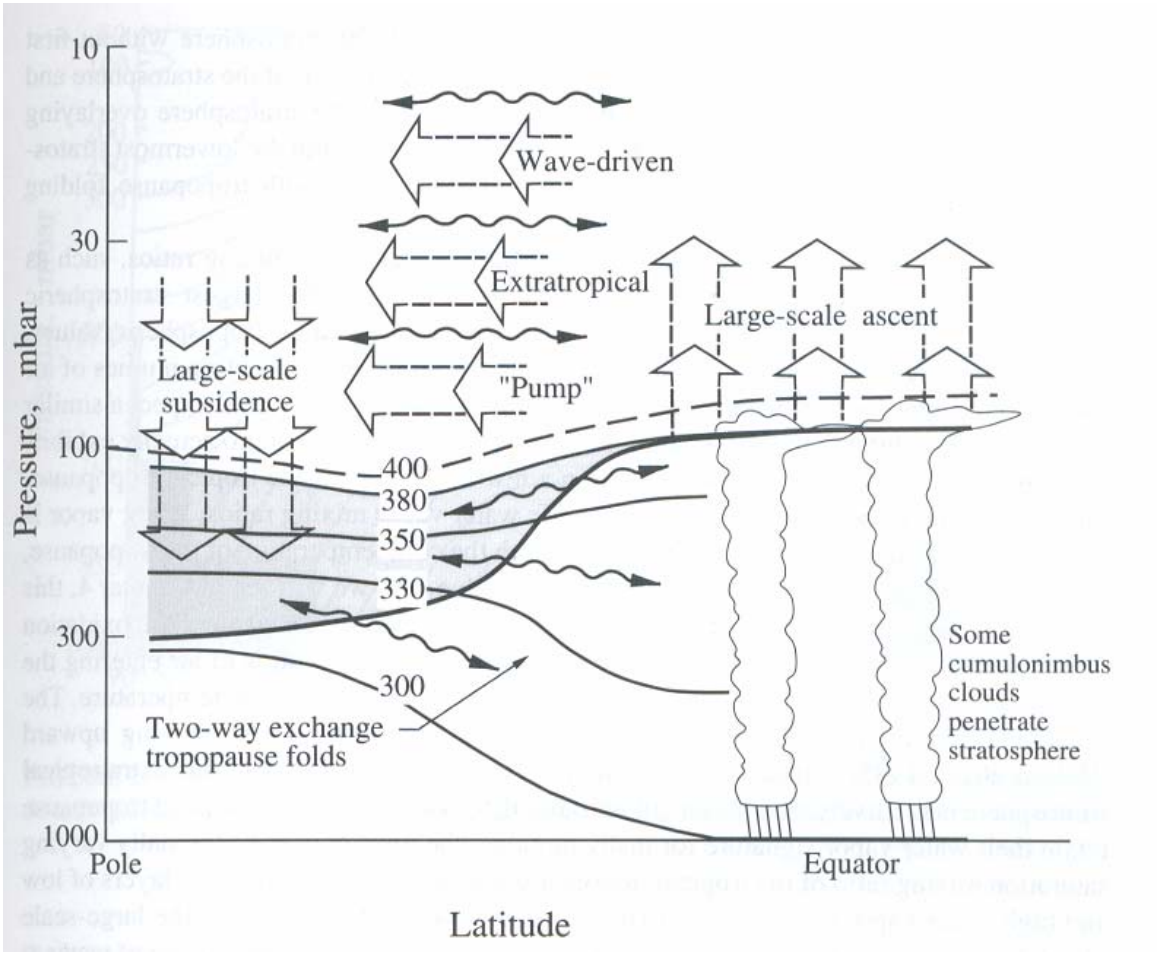

Figure 6 The Global representation of stratosphere-troposphere transport from Holton et al., (1995).

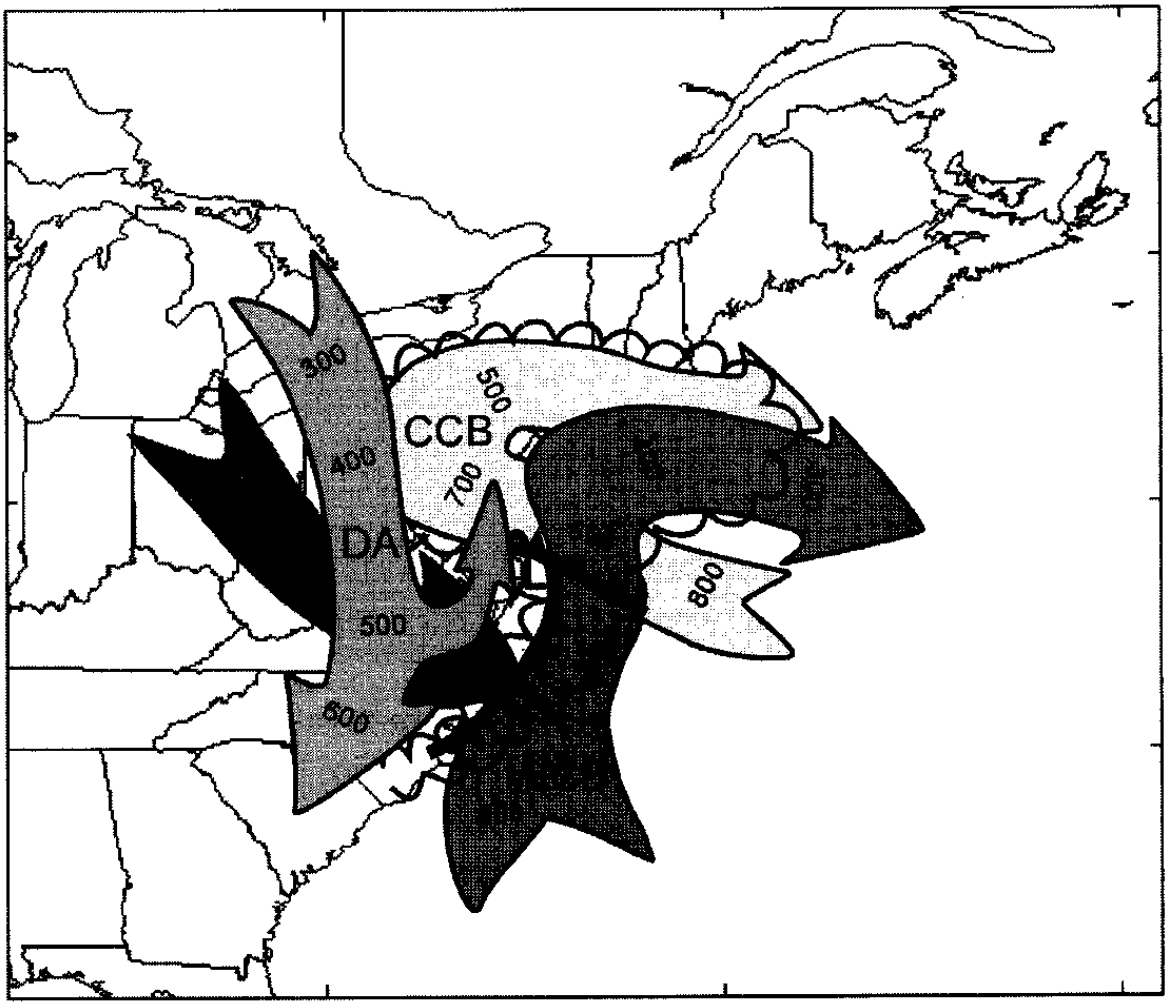

Figure 7 Mid-latitude cyclone showing the WCB, CCB, DA and PCFA. The centre of cyclone is indicated by L and the scalloped lines indicate the edges of the comma-cloud formed by the airstreams. The numbers on the WCB and CCB show the pressure (hPa) at the top of these airstreams, while that on the DA indicates the pressure at the bottom of the air stream.

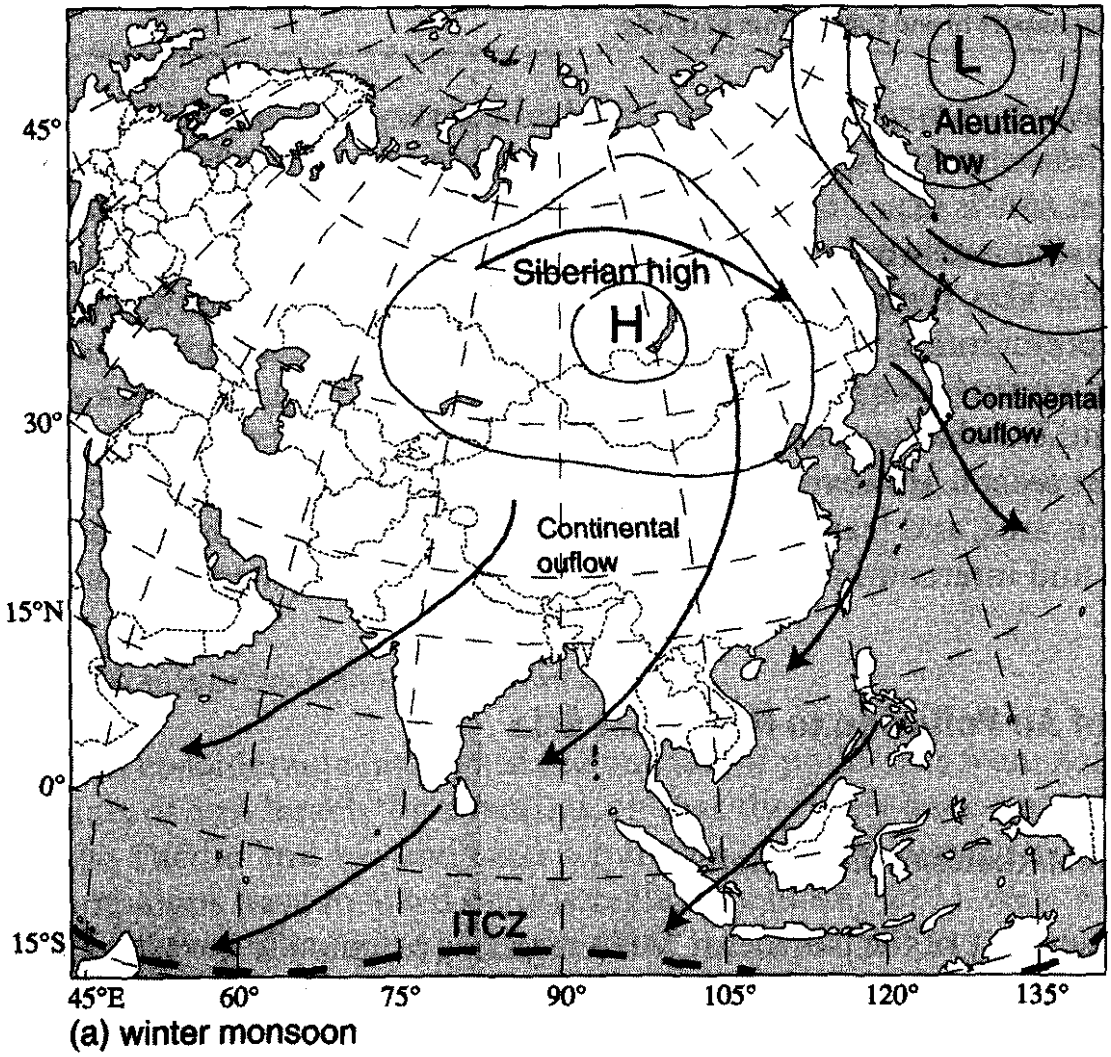

(a) winter monsoon

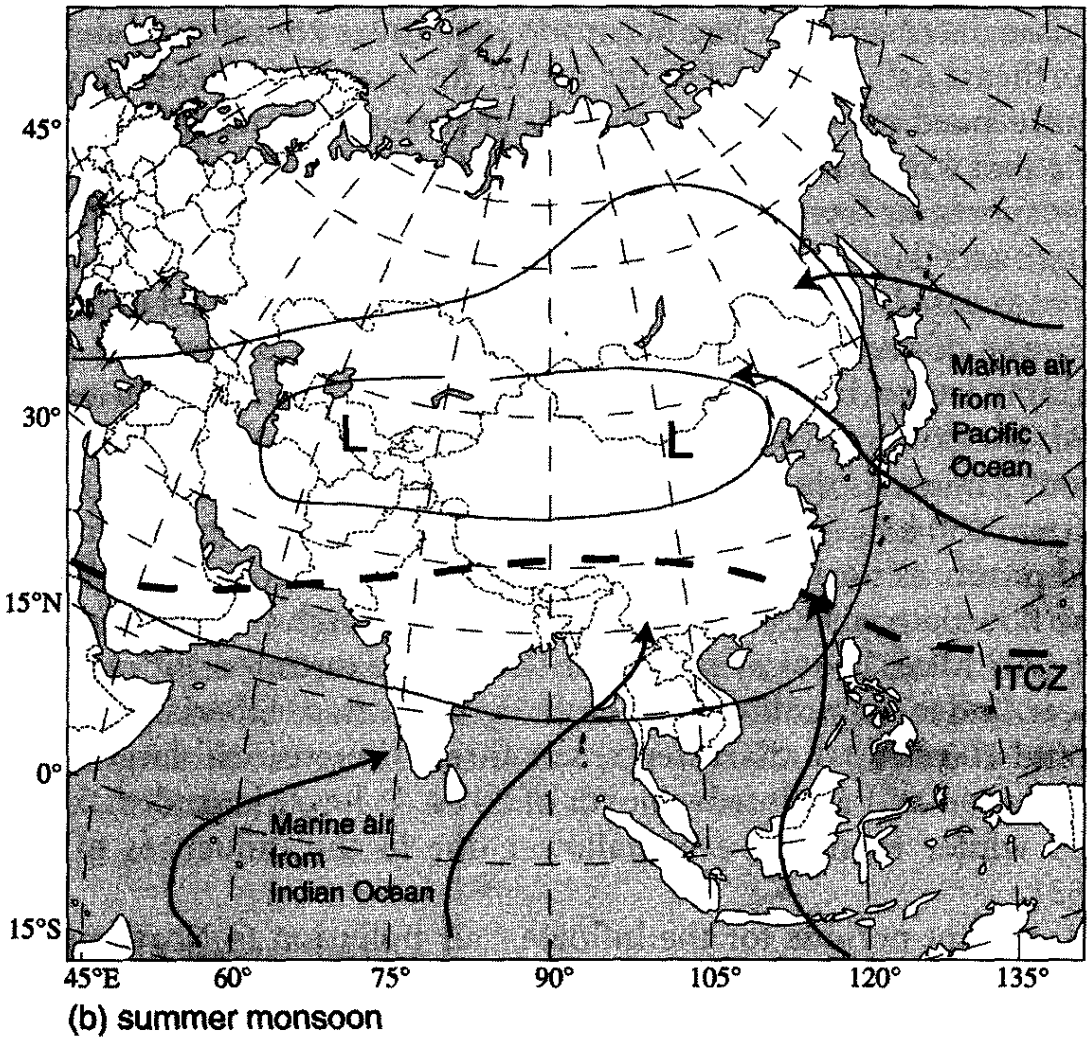

Figure 8 (a) and (b) are the surface wind flow and pressure distribution during winter and summer monsoons, respectively. The heavy dashed line denotes the Inter-tropical convergence zone (ITCZ).

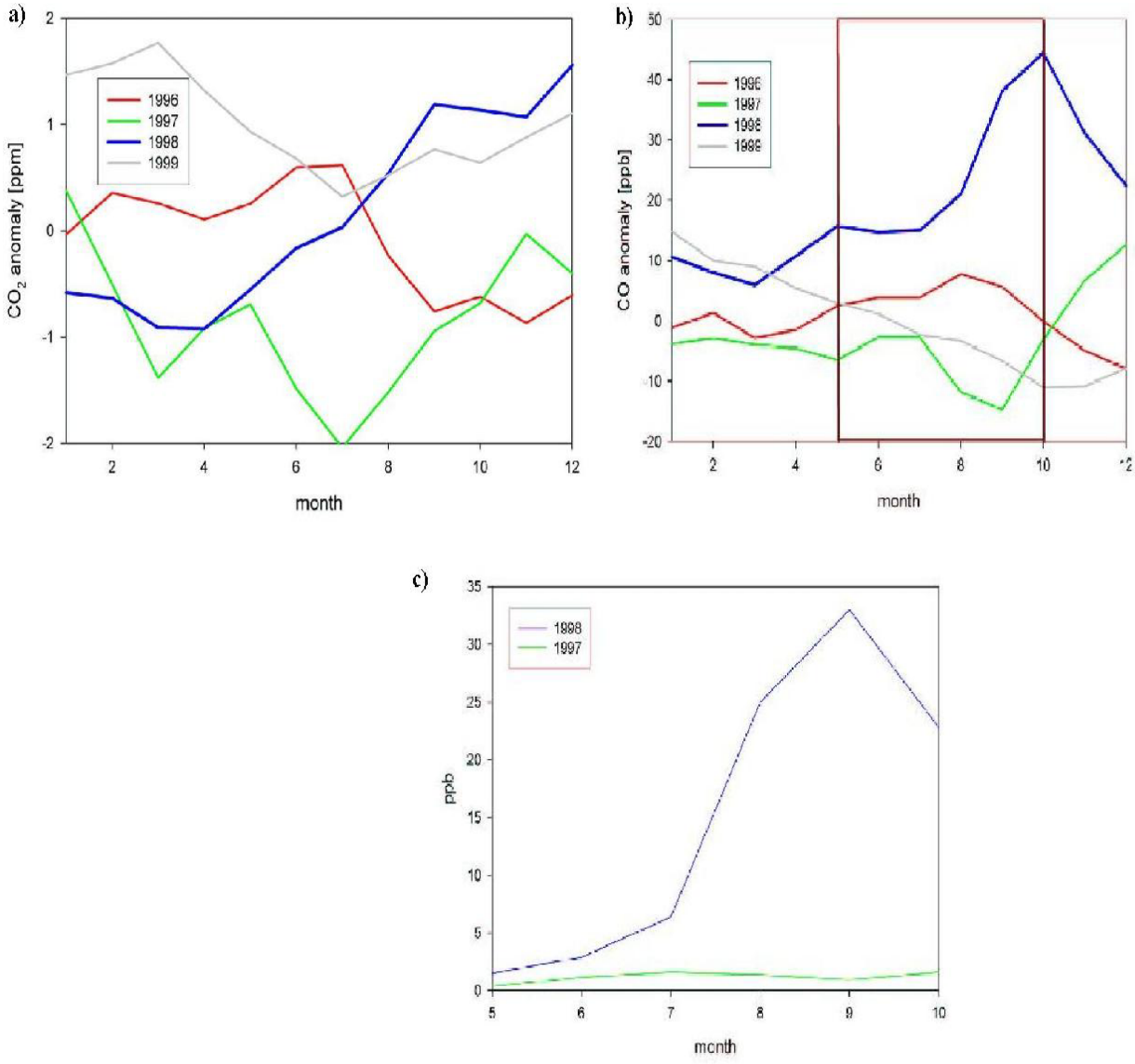

Figure 9 Seasonal variation of the detrended anomalies of (a) CO2 and (b) CO averaged over all CMDL stations north of 35° (c) Monthly mean FLEXPART CO tracer mixing ratios averaged for the positions of the CMDL stations.

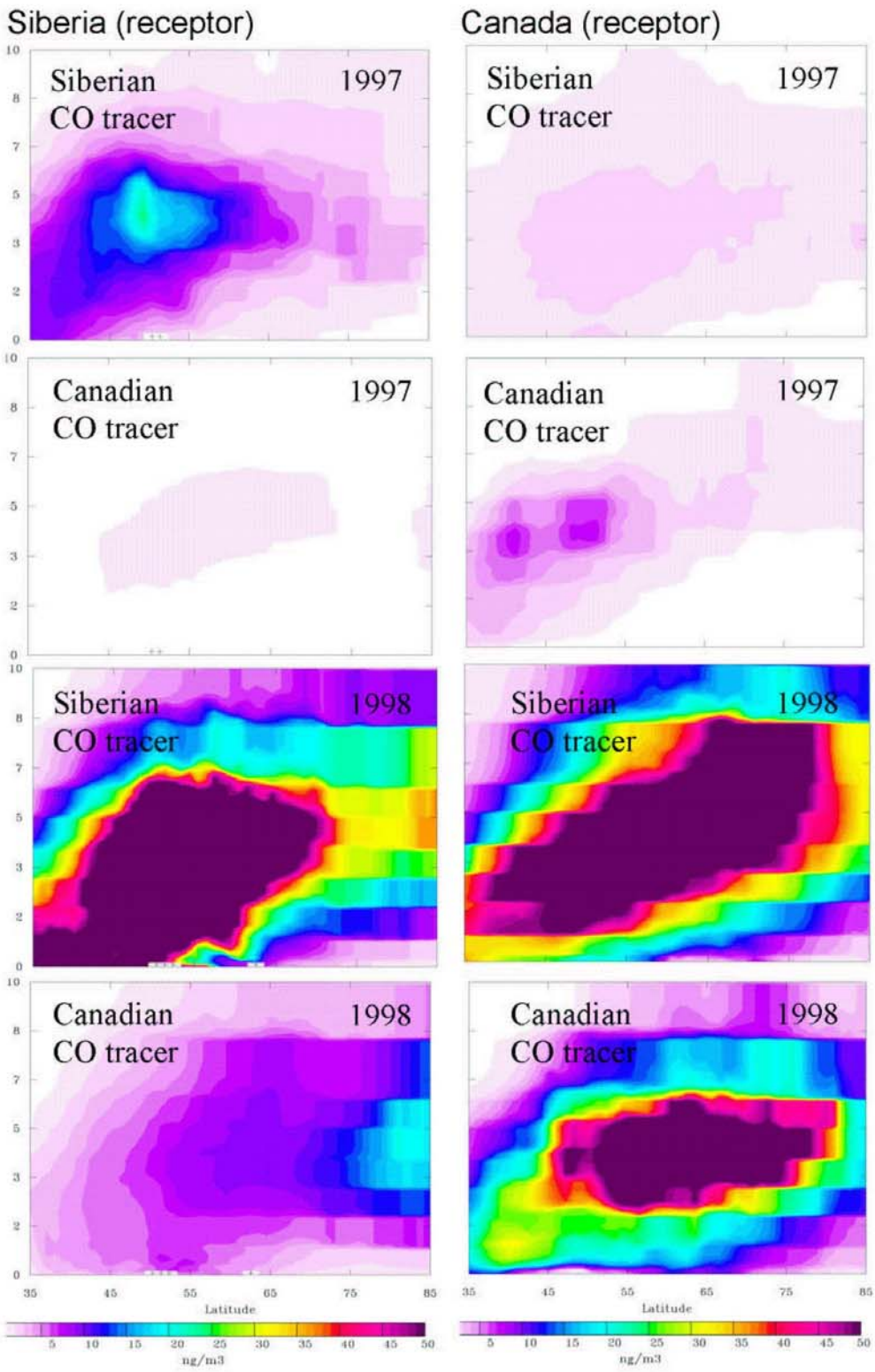

Figure 10 Vertical cross sections of zonal means of the averaged CO tracer concentrations for the receptor regions of Siberia (left column) and Canada (right column). First two rows show Siberian and Canadian CO tracer in 1997 and the last two that for 1998.

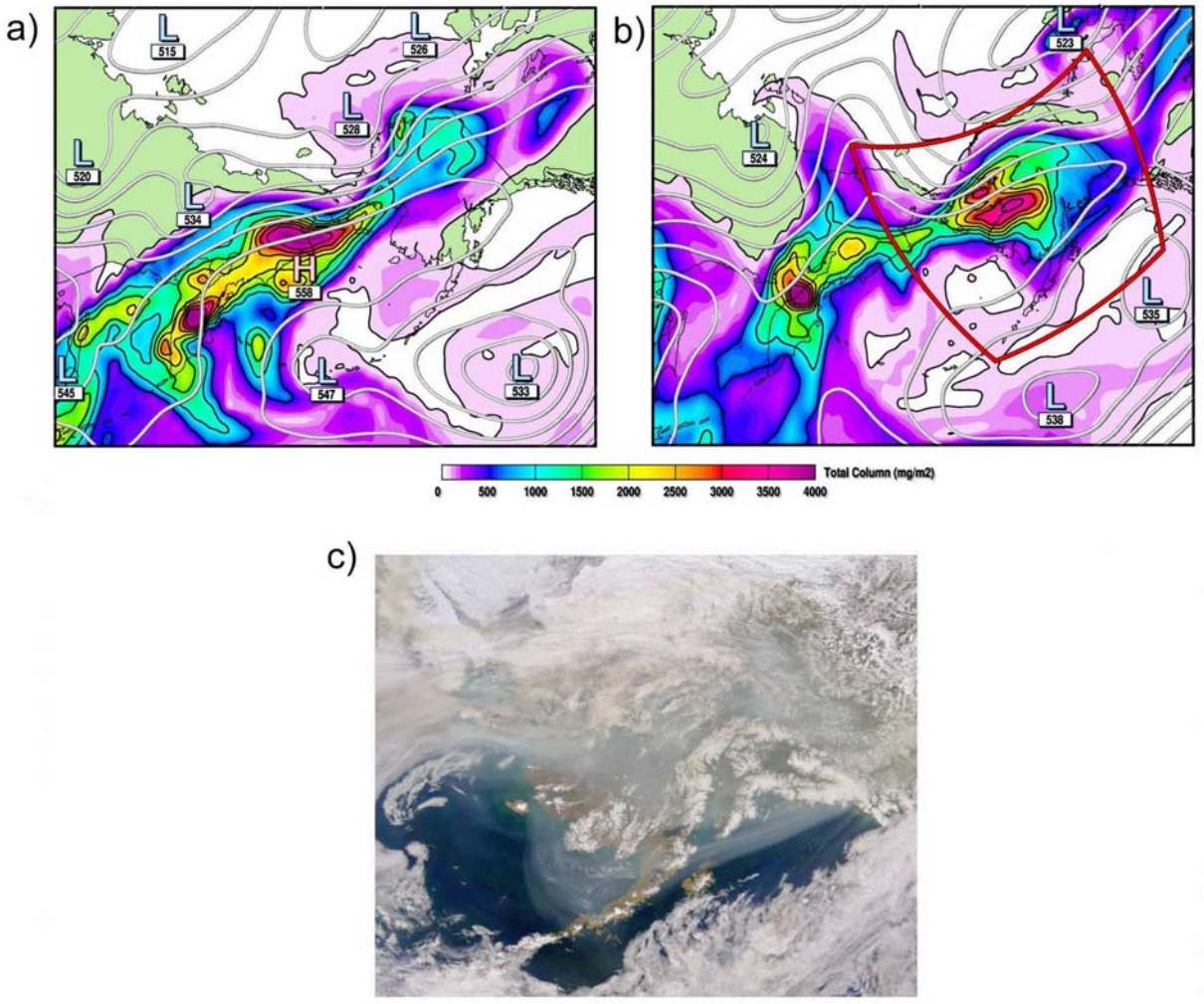

Figure 11 FLEXPART ECMWF CO tracer columns over the Bering Sea and adjacent regions with superimposed contours of the 500 hPa geopotential surface, on (a) 20 May 12 UTC, (b) 22 May 00 UTC; The hatched area represents the topography. Green areas represent land surface, oceans are white. The red rectangle in b) shows approximately the area shown in panel c); (c) SeaWiFS image showing smoke over Alaska at 23 UTC on 21 May; Whitish colors are snow, ice and clouds, whereas the blue-grey indicate smoke.

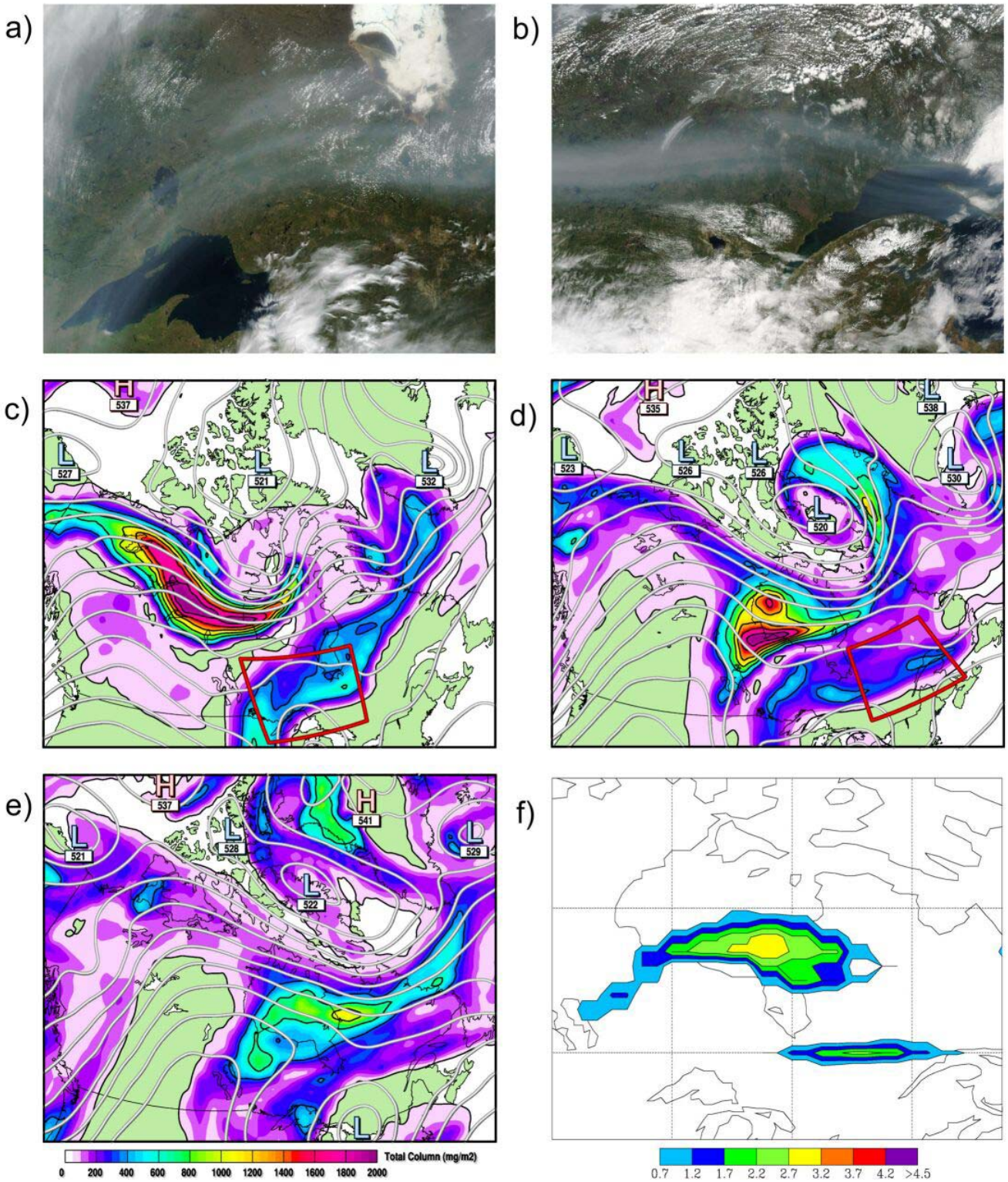

Figure 12 MODIS Terra satellite images over (a) central Canada at 16:30 UTC, 23 May and (b) eastern Canada at 15:35 UTC, 24 May; (c-e) FLEXPART ECMWF CO tracer columns over Canada with superimposed contours of the 500 hPa geopotential surface, based on GFS analyses, contour interval 5 dam, at (c) 23 May 18 UTC, (d) 24 May 18 UTC and (e) 25 May 18 UTC; (f) TOMS aerosol index over eastern Canada on 24 May, 2003.

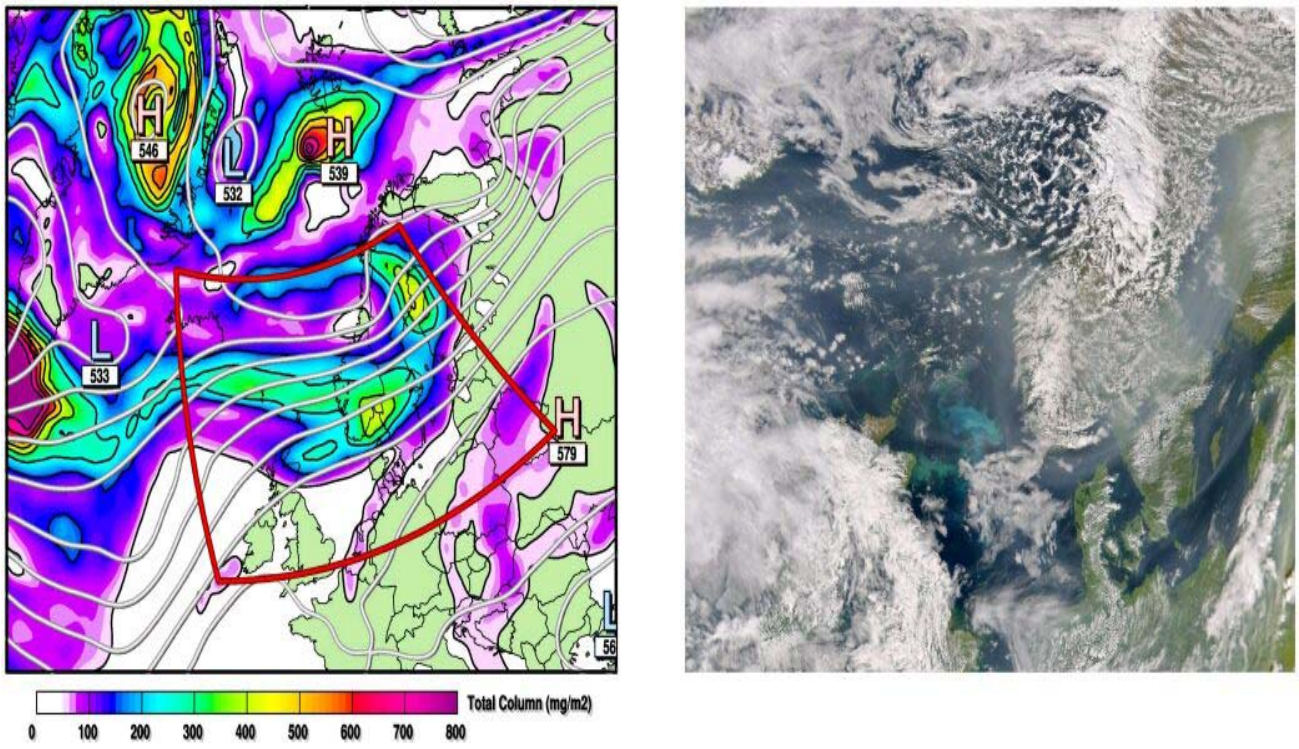

Figure 13 (a) FLEXPART ECMWF CO tracer columns over the north-east Atlantic, Europe and Greenland with superimposed contours of the 500 hPa geopotential surface, at 27 May 15 UTC; (b) Image of SeaWiFS sensor showing smoke over Scandinavia on 27 May, 2003 at 12:54 UTC.

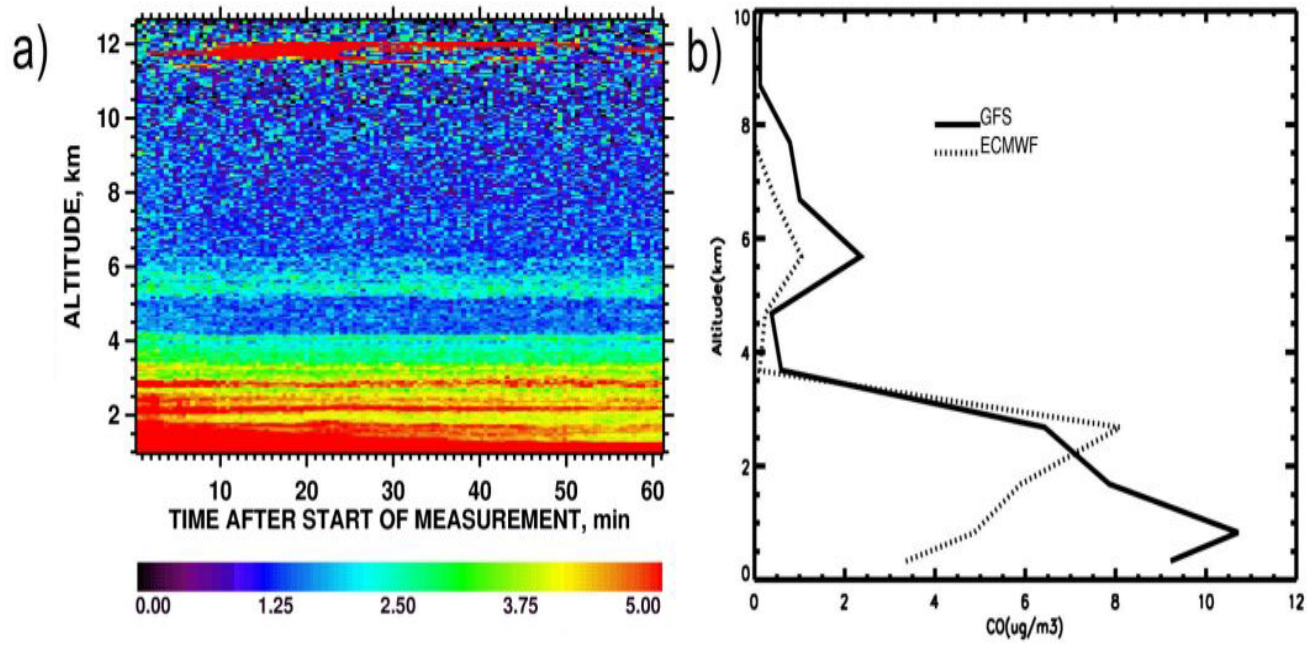

Figure 14 (a) Lidar time-height plot of particle backscatter ratio at 1064 nm over Leipzig, Germany on 29 May, 2003 from 20 UTC to 21 UTC. The vertical and temporal resolutions

are 60 m and 30 s, respectively. (b) ECMWF (dotted line) and GFS (solid line) FLEXPART simulation profiles over Leipzig averaged between 18 and 21 UTC of 29 May, 2003.

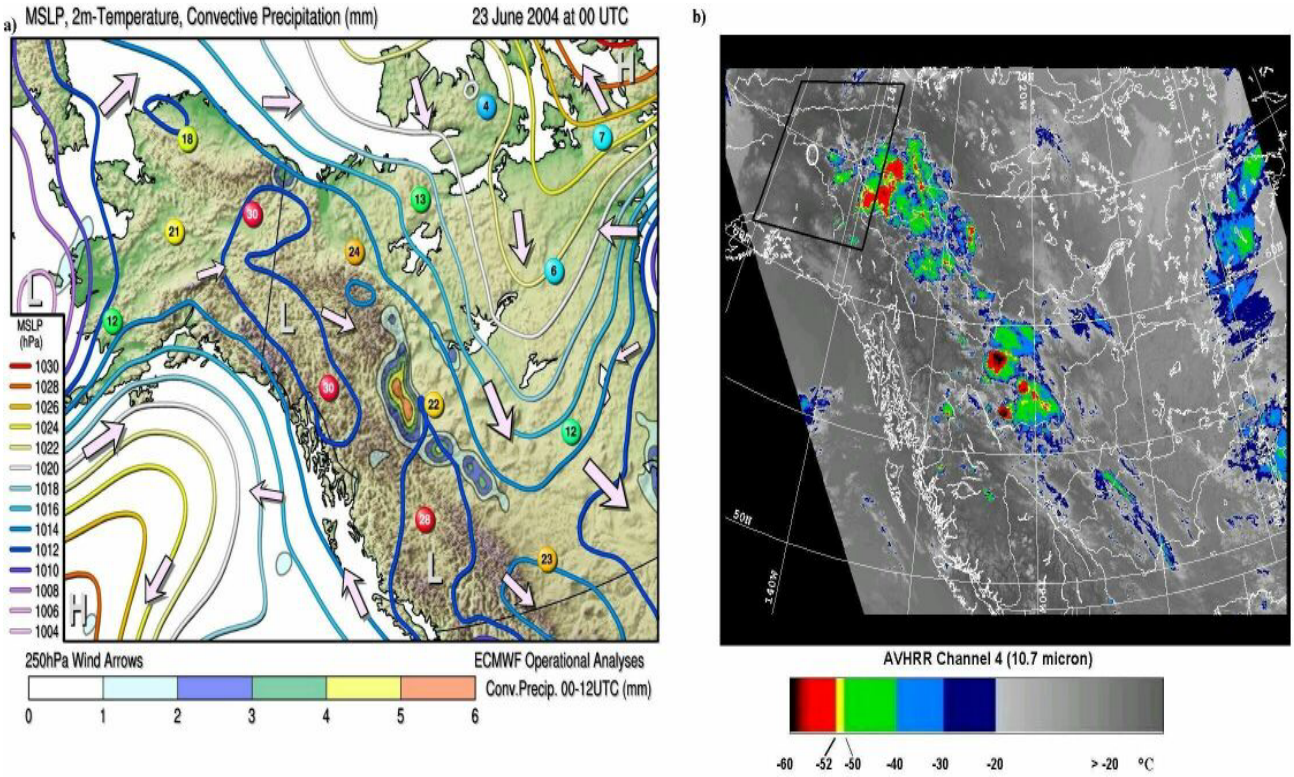

Figure 15 (a) ECMWF analyses of mean sea level pressure (colored contour lines), 2-meter temperatures at selected locations (colored buttons) and 250 hPa winds (arrows) for 23rd June at 0 UTC, plotted over a topography map of Alaska and western Canada. Shaded areas show the convective precipitation from a 12-hour forecast from the 0 UTC analysis. (b) Brightness temperatures from the NOAA-12 satellite at channel 4 (10.7 µm) on 23rd June at 05 UTC. The black rectangle and white circle indicate approximately the area shown in Fig. 15 and location of the radiosonde (Fig. 16), respectively.

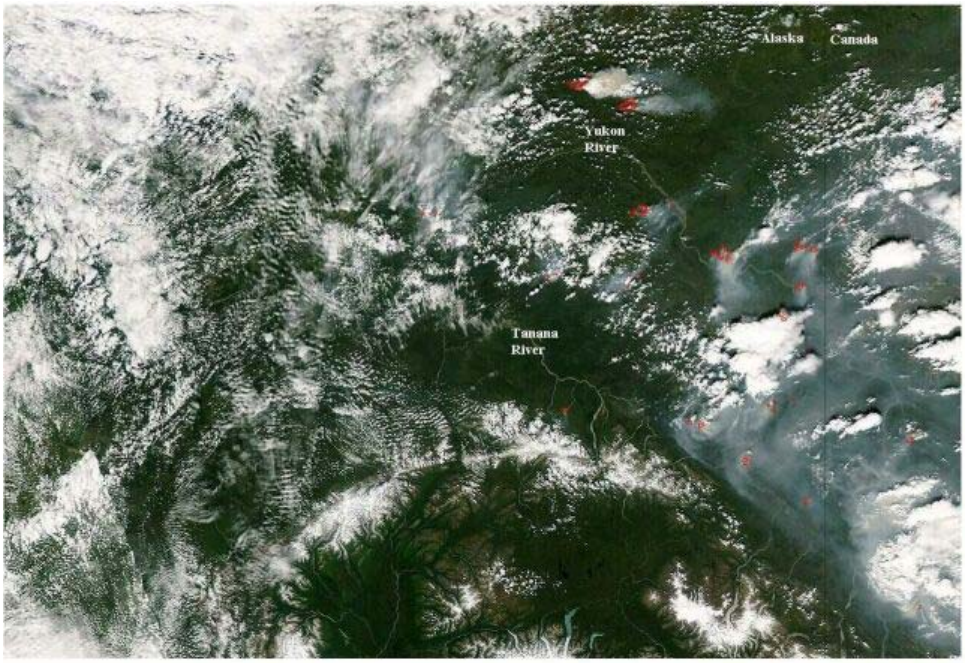

Figure 16 MODIS Aqua satellite image over Alaska and the Yukon Territory on 22nd June at about 22 UTC. Red spots show active fires, whereas blue-grey colors indicate smoke, and the whitish colors show snow, ice and clouds

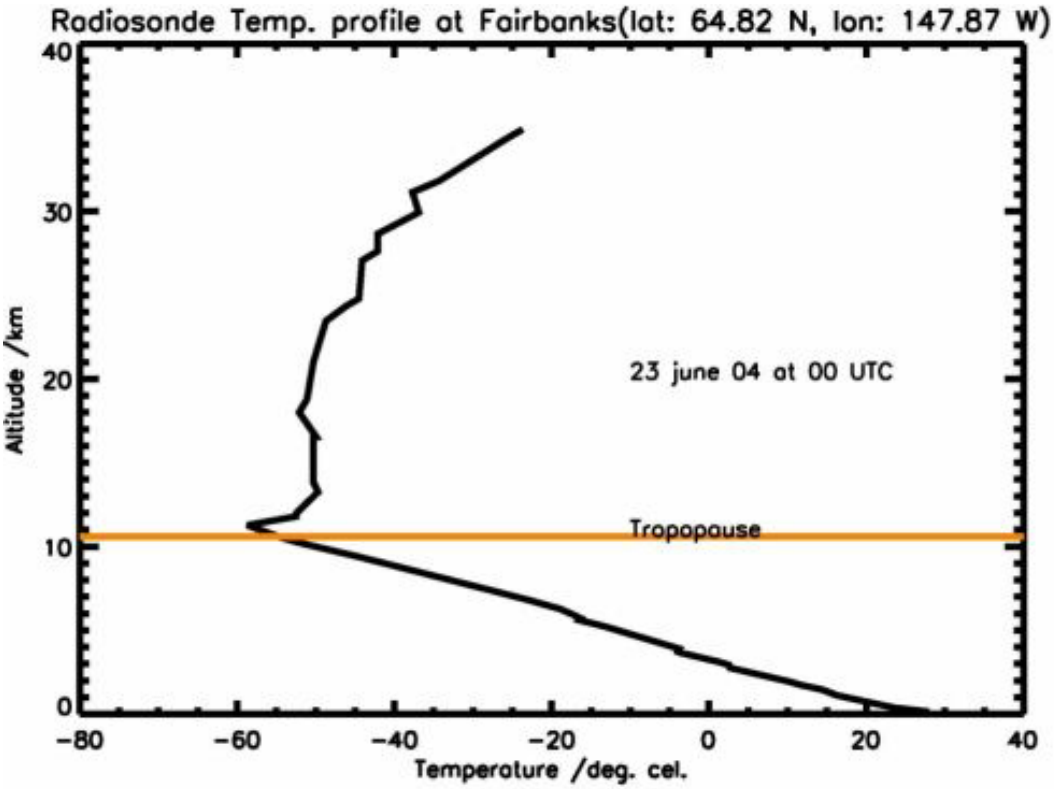

Figure 17 Radiosonde temperature profile at Fairbanks, Alaska on 23rd June at 00 UTC. The horizontal orange line indicates the dynamical tropopause height calculated from ECMWF data.

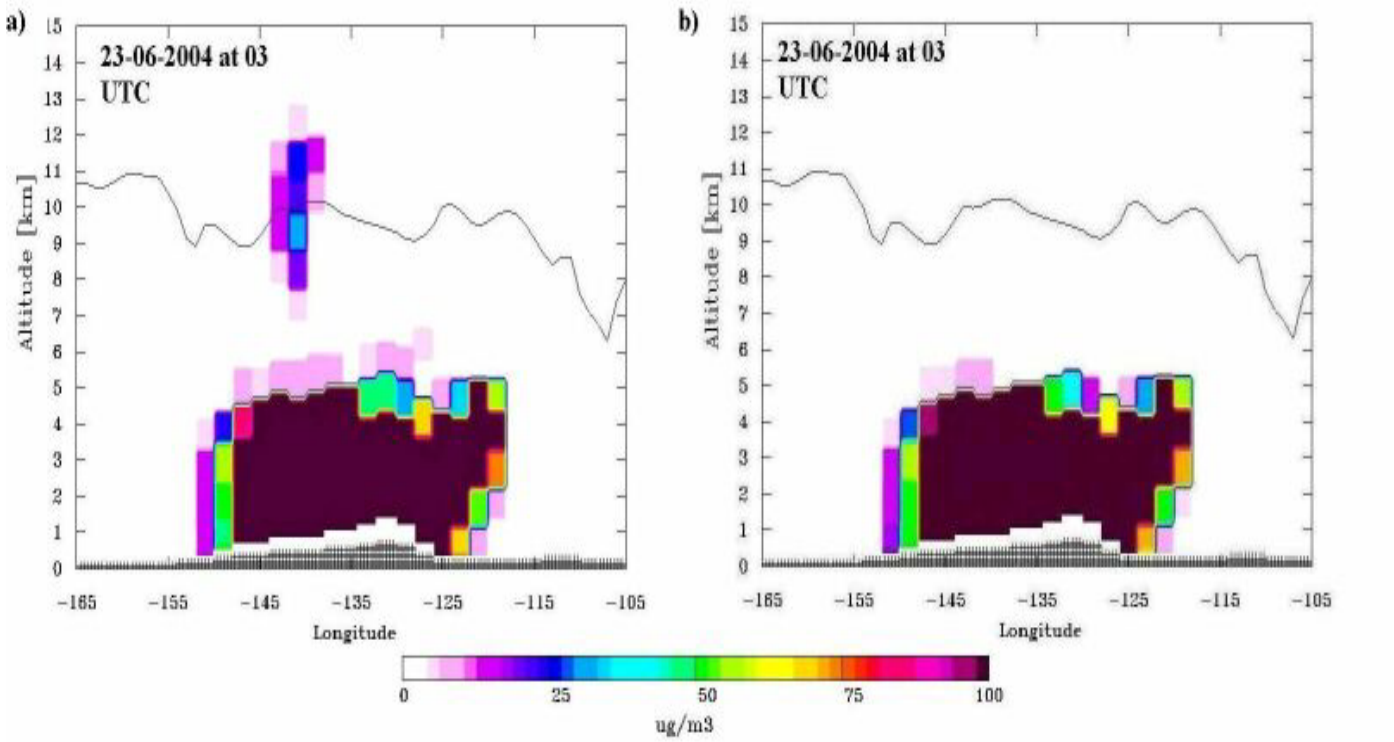

Figure 18 Vertical sections through the FLEXPART CO tracer at 64^{o} latitude on 23rd June at 03 UTC with convection turned on (a) and off (b), respectively.

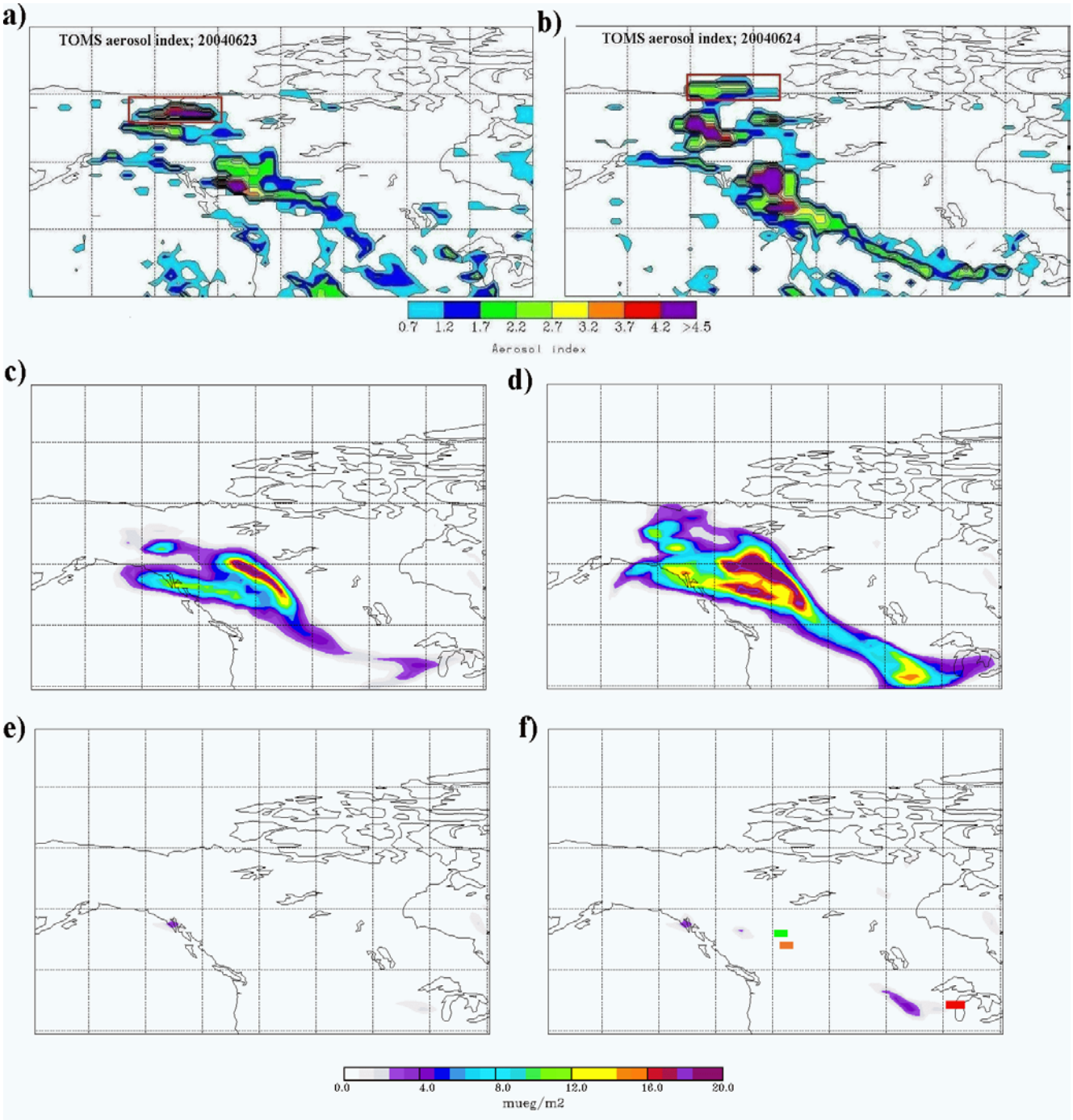

Figure 19 TOMS aerosol index over North America on (a) 23rd and (b) 24th June, 2004. FLEXPART 9-15 km CO tracer columns over North America with convection turned on, at (c) 23rd June 03 UTC, (d) 24th June 03 UTC. (e) and (f) Same as c) and d), respectively, but with convection turned off. The orange and green rectangles shown in panel f indicate the locations of the POAM and SAGE measurements, respectively, shown in Figure 19. The red rectangle shows the location of the lidar measurements shown in Figure 20.

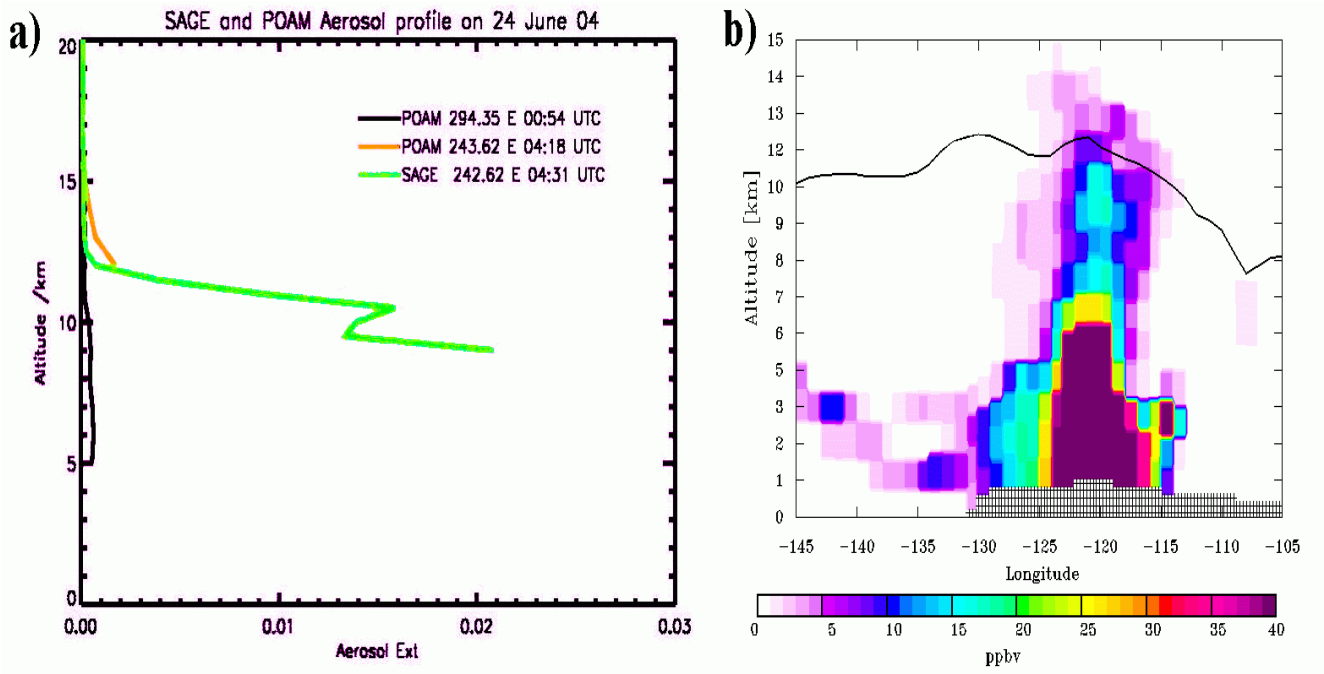

Figure 20 (a) POAM III (orange) and SAGE II (green) aerosol extinction profiles at 1 µm approximately over Edmonton on 24th June at 04 UTC. The location of the profiles is shown in Figure 8d. The unperturbed black profile is the POAM aerosol extinction over Quebec at 00 UTC. (b) Vertical section through the FLEXPART CO tracer at 54° latitude on 24th June at 03 UTC with convection turned on.

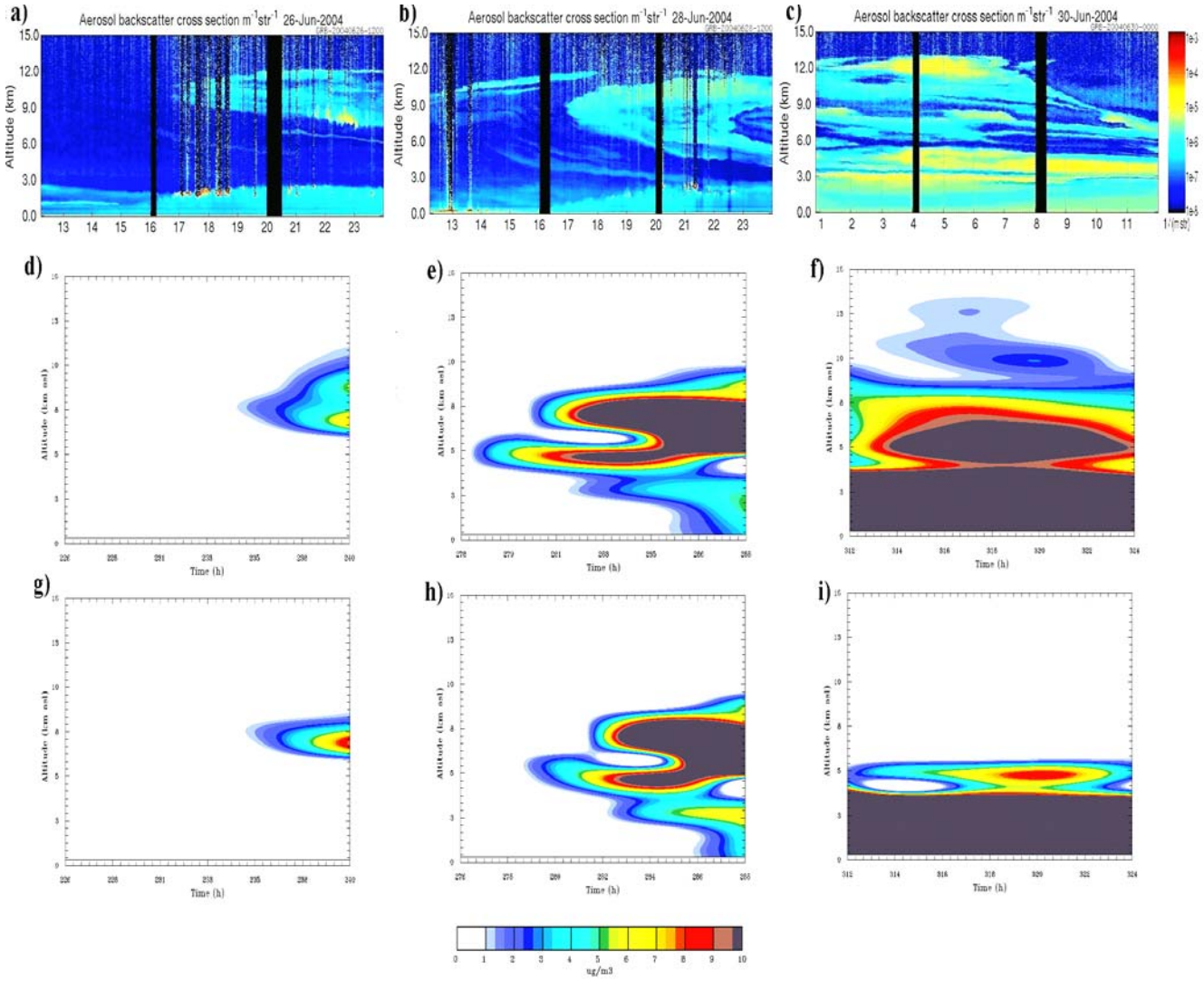

Figure 21 Lidar time-height plot of aerosol backscatter cross section over Madison (red rectangle in Fig. 8d) on (a) 26th June from 12 UTC to 24 UTC, (b) 28th June from 12 UTC to 24 UTC and (c) 30th June 2004 from 01 UTC to 12 UTC. The vertical resolution is 7.5 m. FLEXPART time-height plots of the CO tracer from the simulation with convection turned on at the lidar location on (d) 26th, (e) 28th (f) 30th June for the same time periods as the corresponding lidar data plots (a-c). (g), (h) and (i) Same as d), e) and f), respectively, but with convection switched off.

9. Appendix

ARTICLE 1

Atmos. Chem. Phys. Discuss., 5, 6185–6214, 2005
www.atmos-chem-phys.org/acpd/5/6185/
SRef-ID: 1680-7375/acpd/2005-5-6185
European Geosciences Union

Atmospheric Chemistry and Physics Discussions

Transport Modelling of a pyro-convection event in Alaska

R. Damoah[1], N. Spichtinger[1], R. Servranckx[2], M. Fromm[3], E. W. Eloranta[4], I. A. Razenkov[4], P. James[5], M. Shulski[6], C. Forster[7], and A. Stohl[7]

[1]Department of Ecology, Technical University of Munich, Freising, Germany
[2]Canadian Meteorological Centre, Montreal, Canada
[3]Naval Research Laboratory, Washington, D.C., USA
[4]University of Wisconsin-Madison, Madison, WI, USA
[5]Hadley Centre for Climate Prediction and Research, Exeter, UK
[6]Alaska Climate Research Center, Fairbanks, AK, USA
[7]Norwegian Institute for Air Research, Kjeller, Norway

Received: 8 July 2005 – Accepted: 21 July 2005 – Published: 18 August 2005

Correspondence to: R. Damoah (damoah@forst.tu-muenchen.de)

Abstract

Summer 2004 saw severe forest fires in Alaska and the Yukon Territory that were mostly triggered by lightning strikes. The area burned (>2.7×10^6 ha) in the year 2004 was the highest on record to date in Alaska. Pollutant emissions from the fires lead to violation of federal standards for air quality in Fairbanks.

This paper studies deep convection events that occurred in the burning regions at the end of June 2004. The convection was likely enhanced by the strong forest fire activity (so-called pyro-convection) and penetrated into the lower stratosphere, up to about 3 km above the tropopause. Emissions from the fires did not only perturb the UT/LS locally, but also regionally. POAM data at the approximate location of Edmonton (53.5° N, 113.5° W) show that the UT/LS aerosol extinction was enhanced by a factor of 4 relative to unperturbed conditions. Simulations with the particle dispersion model FLEXPART with the deep convective transport scheme turned on showed transport of forest fire emissions into the stratosphere, in qualitatively good agreement with the enhancements seen in the POAM data. A corresponding simulation with the deep convection scheme turned off did not result in such deep vertical transport. Lidar measurements at Wisconsin on 30 June also show the presence of substantial aerosol loading in the UT/LS, up to about 13 km. In fact, the FLEXPART results suggest that this aerosol plume originated from the Yukon Territory on 25 June.

1 Introduction

Emissions of aerosols and trace gases like carbon monoxide, nitrogen oxides and non-methane hydrocarbons from forest fires play an important role for atmospheric chemistry (Crutzen, 1973) and radiation transmission in the atmosphere (Robock, 1991). Due to long-range transport of forest fire emissions, they affect not only local surroundings but also influence the atmosphere on regional (Tanimoto et al., 2000; Kato et al., 2002) and even continental (Wotawa and Trainer, 2000) and hemispheric scales

(Forster et al., 2001; Wotawa et al., 2001; Damoah et al., 2004; Spichtinger et al., 2004; Yurganov et al., 2004; Novelli et al., 2005).

It is well known that volcanic eruptions can produce the explosive force to inject material from the surface deep into the stratosphere (Graf et al., 1999). Only recently, however, it was realized that deep convection triggered or enhanced by forest fires (so-called pyro-convection) can also penetrate deeply into the stratosphere, leading to the deposition of gaseous and particulate products of the burning in the upper troposphere and lower stratosphere (UT/LS) (Fromm et al., 2003, 2004). The mechanisms causing this deep convection are not yet entirely clear, but it appears that normal deep convection that occurs regularly in the boreal region in summer-time under favourable meteorological conditions can be greatly enhanced by the heat released by the fire as well as by microphysical and radiative processes due to the large amounts of aerosols emitted. These aerosols reduce cloud droplet numbers, suppress precipitation formation, and enhance the significance of the ice phase (thence, also enhance the amount of latent heating available at high altitudes) (Andreae et al., 2004). Similar processes have also been observed to be effective in tropical biomass burning plumes (Andreae et al., 2004). Furthermore, the radiation absorption by black carbon particles emitted by the fires and the associated heating of the atmosphere above the cloud tops could lead to further lifting after the initial convective injection into the UT/LS region. While the relative importance of these different mechanisms is not clear, several recent papers have presented cases where pyro-convection transported forest fire emissions relatively deep into the stratosphere, using satellite (Fromm et al., 2003; Livesey et al., 2004), lidar (Immler et al., 2005; Fromm et al., 2004) and aircraft (Jost et al., 2004) observations. Some of the observations (e.g., Jost et al., 2004) even show that the emission products can be transported to levels in the stratosphere with potential temperatures above 380 K, a region that is commonly referred to as the stratospheric overworld.

In June 2004, dry conditions, above normal temperatures and strong lightning activity caused severe forest fires in Alaska and the Canadian Yukon Territory. Air quality

was significantly degraded in large regions by these fires. For instance, particulate matter smaller than 2.5 μm (PM-2.5) of about 1000 μg/m^3 were measured in Fairbanks, exceeding E.P.A.'s threshold (300 μg/m^3) by a factor of more than three (Rozell, 2004). Also in Fairbanks measured CO of 9.2 ppm nearly violated the Clean Air Act (9.5 ppm), whereas typical mid-summer CO background mixing ratios are only about 80 ppb. Emissions from the burning were also transported over long distances. High enhancements of aerosol scattering were observed at Cheeka Peak (48.3° N, 124.6° W, 480 m a.s.l.) (Jaffe, D., personal communication) and several research aircraft were guided repeatedly into the fire plumes over eastern North America, the Atlantic and over Europe during the ICARTT (International Consortium for Atmospheric Research on Transport and Transformation) campaign and measured large enhancements of fire tracers in the lower and middle troposphere. In fact, Cammas et al. (2005)[1] linked an enhanced CO measurements taking during a commercial airliner cruising at about 11 km over the North Atlantic to biomass burning. Using convective mass fluxes from a mesoscale model, they show that deep convection was responsible for the high CO concentrations in the stratosphere.

In this paper we focus on a particular episode of burning in June 2004 when pyro-convection transported fire emissions into the UT/LS. Section 2 describes model calculations used to study the transport of the plume, and Sect. 3 gives the meteorological conditions in the observed area during the event. Model results, satellite and lidar measurements during the event are reported in Sect. 4 and, finally, summary and conclusions are presented in Sect. 5.

[1] Cammas, J.-P., Brioude, J., Chaboureau, J.-P., Duron, J., Mari, C., Mascart, P., Nedelec, P., Smit, H., Volz-Thomas, A., Stohl, A., and Fromm, M.: Stratospheric injection of biomass fire smoke followed by long-range transport: a MOZAIC case study, in preparation, 2005.

2 Model description

For studying the transport phenomena associated with the pollution plumes, we used the Lagrangian particle dispersion model FLEXPART (Stohl et al., 1998; Stohl and Thomson, 1999) to simulate the transport of a CO tracer. CO tracer was used because CO has a relatively long life time that ranges from 1 month (in the tropics) to 4 months (in the mid-latitudes) (Seinfeld and Pandis, 1998) and because we want to focus here on the transport only, and do not consider chemical processes.

FLEXPART simulates long-range transport, diffusion, dry and wet deposition and radioactive decay of air pollutants released from point, line or volume sources. It treats advection and turbulent diffusion by calculating the trajectories of a multitude of particles. Stochastic fluctuations, obtained by solving Langevin equations (Stohl and Thomson, 1999), are superimposed on the grid-scale winds from global meteorological datasets to represent transport by turbulent eddies, which are not resolved. Global data sets also do not resolve individual convective cells, although they reproduce some of the large-scale effects of convection. Therefore, FLEXPART has recently been equipped with a convection scheme (Emanuel and Zivkovic-Rothman, 1999) to account for sub grid-scale convective transport. FLEXPART can be driven by meteorological analysis data either from the European Centre for Medium-Range Weather Forecasts (ECMWF, 1995) or from the Global Forecast System (GFS) of the National Center for Environmental Prediction (NCEP). Due to the significantly higher vertical resolution of the ECMWF data and the higher intrinsic horizontal resolution of the operational ECMWF forecast model, compared to the GFS model, we use ECMWF data in this study.

The ECMWF model version used here has 60 hybrid model levels in the vertical and data were retrieved on a global $1^{\circ}\times1^{\circ}$ latitude-longitude grid. Six hourly analyses were supplemented by 3-h forecast step data to provide a 3-hourly temporal resolution. An output grid with a $1^{\circ}\times2^{\circ}$ latitude/longitude resolution, a vertical spacing of 1000 m and an output interval of 3 h was employed.

In the tracer simulations, 5×10^{6} particles were released to calculate the transport of CO emissions from fires in Alaska. For our simulation we considered the 2-week period from 17 to 30 June 2004, during which the strongest deep convection and transport event occurred. In order to describe the regional and daily variations of the fires, the MODIS hot spot data were counted daily on a $1^{\circ}\times1^{\circ}$ grid. For every 3-day period the maximum daily number of hot spots in a grid cell was taken in order to minimize the effect of missing hot spot data in the presence of clouds. The daily area burned in North America on a per-province (in Canada) and per-fire-state (in the United States) basis, taken from a web page at the Center for International Disaster Information (http://www.cidi.org/wildfire), was distributed to those cells in the respective province containing the hot spots. Then, a constant CO emission factor of 4500 kg per hectare of forest burned, which is similar to recent estimates based on emissions from the Canadian Northwest Territories (Cofer et al., 1998), was applied to release CO on a $1^{\circ}\times1^{\circ}$ grid. The altitude at which fire emissions are effectively released into the atmosphere varies from day to day and is actually not known. Lacking this information, we released the CO tracer into the lowest 3 km of the model atmosphere which is consistent with other fire simulations (Damoah, 2004; Spichtinger, 2004). Transport to high altitudes must be produced by the model itself, either as a result of resolved vertical transport or by the convection scheme. It must be noted that all the processes related to the fire itself are not treated in the ECMWF model. It is, thus, likely that convective transport over the fires is underestimated by FLEXPART. However, to some extent the effects of the fires (e.g., a destabilization of the atmosphere) are introduced into the analyses through the assimilation of observations (e.g., temperature data from satellites and radiosondes in the vicinity of the fires).

3 Meteorological conditions in the burning area

It is known that, climatologically, maximum daily temperatures are related to the number of lightning strikes, and the number of lightning strikes is in turn related to the num-

ber of started fires. During the year 2004, most of Alaska experienced the warmest summer on record. In June, temperatures were warmer than normal across the State (Alaska Climate Research Center; see http://climate.gi.alaska.edu). Anomalies of the monthly mean temperature ranged from 2.5°C to 4°C. In Anchorage, southern Alaska, the monthly average temperature in June was about 14°C, 2.5°C above normal. The highest temperature of the month (28°C) occurred on 26 June (Fig. 1a). More than 65% of the daily maximum temperatures were above normal. The conditions in Juneau were extreme; a string of 7 days (18–24 June) had record highs (red asterisks, Fig. 1b). The highest measured temperature was above 29°C. Nome also registered three record high temperatures (Fig. 1c). The monthly mean temperature in Fairbanks was almost 19.5°C, 4°C above normal.

The high temperatures also caused a large number of lightning strikes. Between 14 and 15 June, about 17 000 cloud-ground flashes were reported to have hit Alaska within 24 h, the highest number in 25 years (AICC, 2004). Of the 707 fires reported in 2004, almost 300 were triggered by lightning strikes (see, http://fire.ak.blm.gov). Being the third driest summer on record (Rozell, 2004), the fires, also fanned by surface winds of about 32 km/h (Rozell, 2004) on average in June, consumed large areas in Alaska and its surroundings. Figure 2 shows the annual area burned in Alaska from 1997 to 2004. In 2004, 707 fires burned a new record of about 2.7×10^6 ha. The old record of 2×10^6 ha was registered in 1957.

During the second half of June 2004, anti-cyclonic conditions prevailed over Alaska and north-western Canada (Fig. 3a). However, on 21 June a mid-tropospheric low-pressure system developed west of the Canadian west coast weakening the anticyclone over Alaska and north-western Canada over the next two days (Figs. 3b, c, d). Then the anticyclone strengthened again (Figs. 3e, f) and remained until the end of June. The low pressure system caused only a slight decrease in surface pressure and did not bring a major change in surface temperatures (see colored buttons in Fig. 4a and temperature time series in Fig. 1), but colder temperatures associated with the mid-tropospheric cut-off low triggered strong convection, as shown in an infrared satel-

lite image on 23 June at 05:00 UTC (Fig. 4b). Several centers of convective activity can be seen, with the coldest cloud top brightness temperatures (<−52°C) located over the Yukon Territory and British Columbia. On the following days even lower brightness temperatures (<−60°C) were observed (Fig. 4c). As we shall show below, the convective activity was strongest during the afternoon and evening hours and weakened over night. This daily cycle was repeated several days after 20 June. The northern cluster of convection seen in Figs. 4b and c was responsible for the upward transport of forest fire emissions into the UT/LS.

4 Transport of fire emissions into the upper troposphere and lower stratosphere

Figures 5a and b show the distribution of active fires and smoke on 23 and 22 June, respectively, from NASA's Moderate Resolution Imaging Spectroradiometer (MODIS) aboard the Terra and Aqua satellites (Kaufman et al., 2003, 1998; Justice et al., 1996). It indicates intense burning in Pingo and Winter Trail along the Yukon River (upper left of Fig. 5b). The Billy Creek and Porcupine fires south-east of the Tanana River sent piles of smoke (blue-grey) into the atmosphere. Another cluster of hot spots can be seen in Yukon Territory through to Juneau and in the north-west of British Columbia (Fig. 5a). These fires had been burning for weeks and also continued to burn into July.

By comparing Figs. 4b, 4c and 5, it can be seen that the northern clusters of deep convection were located almost exactly over the region with the strongest burning activity. While it is impossible to say to what extent the fires enhanced the convection, the strong correlation between fire locations and the coldest cloud tops is striking, such that a causal relationship is suggested. In support of this view, Fig. 6 shows a picture taken out of the window of a commercial aircraft on 27 June within the region. The picture shows a pyro-cumulonimbus cloud with cloud tops above 10 km. Three things about this image are striking: Firstly, the cloud's brownish color, which is reminiscent of pictures of volcanic eruptions and is caused by the huge mass of aerosols transported

upward by the cloud from the forest fires seen to be burning underneath. Secondly, the exact co-location of the convective cloud and the forest fire and its considerable depth. The cloud top is obviously much higher than the tops of the convective clouds seen in the background. Thirdly, despite the maturity and depth of the convection, the cloud doesn't seem to precipitate. This supports our suggestion that, in addition to the heat and water vapor (i.e., latent heat) released by the fire, microphysical mechanisms similar to those reported by Andreae et al. (2004) suppressed precipitation and, thus, allowed the latent heat of freezing to be released at high altitude.

Based on radiosonde temperature measurements from Fairbanks (Fig. 7), taken approximately within the white circle indicated in Fig. 4b, the coldest cloud tops were located at around 11 to 12 km. According to the soundings, the thermal tropopause height was at approximately 11 km on 23 June at 00:00 UTC and at 12 km on 24 June at 12:00 UTC. The dynamical tropopause (orange lines in Fig. 7) taken from the ECMWF analysis was located somewhat lower at about 10.5 km on 23 June (the dynamical tropopause is the altitude where the potential vorticity exceeds the value of 2 potential vorticity units). The radiosonde temperature profiles show a strong gradient and no significant structure in the free troposphere but a very sharp tropopause. These features are characteristic of an environment shaped by deep convection. Note that the sounding from 24 June was taken during night hours and shows a very shallow surface inversion. The cloud top height is consistent with the simulated transport of the CO emissions from the fires. The fires were located east of Fairbanks, and a vertical section of the FLEXPART CO tracer at 64° N with convection turned on (Fig. 8a) and off (Fig. 8b) on 24th at 12:00 UTC confirms the injection of fire emissions into the Alaskan lower stratosphere due to convection at around 138° W. In the simulation with convection turned on, forest fire tracer can be found up to about 12 km altitude. The top of the tracer cloud at about 12 km is in good agreement with the coldest cloud top temperatures (Fig. 7). No injection into the stratosphere takes place in the simulation without convection showing that the use of the convection scheme in FLEXPART brings a better agreement between measurements and model results.

Figure 9 shows FLEXPART vertical cross sections along 64° N cutting through the region with the strongest burning activity at around 140° W. It demonstrates how the convection weakens during the night and morning hours, and how the forest fire emission injected into the free troposphere and lower stratosphere during the day are transported eastwards (Figs. 9a, b). In the afternoon hours of the following day the convection gets active again (Fig. 9c) and transports forest fire emissions to regions above the tropopause within a couple of hours (Figs. 9d, e). This cycle is repeated every day in the period from 20 June until the end of June, and forest fire emissions were repeatedly injected into the stratosphere during this period. Figures 9f–j show the same as in Figs. 9a–e, but for a FLEXPART simulation with the convective parameterization turned off. No transport into the stratosphere takes place reflecting again the importance of the representation of convection in transport models.

4.1 UT/LS observations of forest fire smoke

The aerosol index derived from data provided by the Total Ozone Mapping Spectrometer (TOMS) instrument on board the Earth Probe satellite (see http://toms.gsfc.nasa.gov for details) gives information on the spatial distribution of UV-absorbing tropospheric aerosols (Hsu et al., 1996). On 23 and 24 June, the TOMS aerosol index (Figs. 10a and b, respectively) shows filaments of enhanced values that stretch from Fairbanks and the Yukon Territory through Edmonton to Wisconsin. Distinct maxima of more than 4.5 are observed over Fairbanks and the Yukon Territory on both days. These locations correspond remarkably well with the locations of the very cold cloud tops in Figs. 4b and c. The sensitivity of the TOMS aerosol index to the presence of absorbing aerosols increases strongly with altitude. Thus, the maximum values of the TOMS aerosol index are likely due to aerosols located at high altitudes, which have passed through the deep convective clouds.

The features of enhanced TOMS aerosol index on 23 and 24 June are in remarkable agreement with the FLEXPART CO tracer located between 9 and 15 km (Figs. 10c and d) in the simulation with the convection parameterization turned on. On 23 June at

03:00 UTC (Fig. 10c), the simulated CO tracer shows a similar filament over the Yukon Territory and British Columbia while on 24 June at 03:00 UTC (Fig. 10d) the maxima are at eastern Fairbanks, Yukon Territory and Edmonton. Figures 10e and f show the corresponding results, but with the convection parameterization turned off. The very low CO tracer in this simulation shows again that the upward transport in the simulation with convection turned on was indeed due to the sub-grid-scale convection parameterization. In fact, the average of the tracer between 9 and 15 km with convection relative to without convection shows a nearly nine-fold enhancement on both days. The feature in the TOMS image which is close to the Beaufort Sea on 23 and over the sea on 24 (red rectangle) is not visible in the FLEXPART 9–15 km column (Figs. 10c and d). However, inspection of the 0–15 km column (not shown) indeed shows CO tracer over the Beaufort Sea. Thus we contend that the feature is located at lower (<9 km) altitude.

Other instruments that testify to the perturbation of the UT/LS by the Alaskan fires are the Polar Ozone and Aerosol Measurement (POAM III) aboard the SPOT-4 satellite (Lucke et al., 1999) and the Stratospheric Aerosol and Gas Experiment (SAGE II) aboard the Earth Radiation Budget satellite (Mauldin et al., 1985). Figure 11a shows enhanced aerosol extinction at 1 μm wavelength in the UT/LS from SAGE II (green) and POAM III (orange) over Edmonton (green and orange rectangles in Fig. 10f) on early hours of 24 June. The SAGE profile shows a strong enhancement between 10 and 12 km, the ECMWF dynamical tropopause (Fig. 11b) over the location is at about 10–11 km. The POAM profile over Edmonton shows an even stronger enhancement above 12 km but no values below. This termination of POAM data at such a high altitude is what is referred to as "High Zmin" (Fromm et al., 1999). This normally indicates that optically sufficiently thick clouds obscure the sun from the POAM sun tracker and, thus, measurements are available only above the cloud. An investigation of GEOS infrared imagery, however, revealed that there were no high clouds in the region. Visible imagery showed some greyish features, whose color suggests these were not normal water or ice clouds. In fact, backward trajectories (not shown) from the enhanced POAM profile travel back to the fire source in Alaska. Thus, it seems that the aerosol

layer was optically sufficiently thick to terminate the POAM sun tracker measurements. Another POAM profile over Quebec at 54° N, 66° W (black line in Fig. 11a) outside the region of the Alaskan fire emission plume shows an unperturbed profile for reference. The two POAM profiles above 12 km show an approximately four-fold enhancement of the aerosol extinction of the perturbed relative to the unperturbed profile. Although the FLEXPART CO tracer across 54° N on 24 June at 06:00 UTC (Fig. 11b) shows the main part of the forest fire plume west of Edmonton, there is clear evidence of forest fire CO plume well above (1–2 km) the local tropopause at Edmonton. This underlines that the enhanced POAM and SAGE extinction in the UT/LS were likely due to a pyro-convective blow up.

4.2 Lidar observations at Madison

During the last four days of June 2004, the High Spectral Resolution Lidar (HSRL) (Eloranta, 2005) at the University of Wisconsin (red rectangle in Fig. 10d), used for long-term cloud studies (43.1° N, 89.4° W), registered unusually high values of the aerosol backscatter cross section in the upper troposphere (Fig. 12). The strong signal was presumably smoke that was transported from Alaska and the Yukon Territory. Figures 12a–c show observed aerosol backscatter on 26, 28 and 30 June, respectively, (note that the first two panels show the last 12 h of the day while the last panel shows the first 12 h of the day). It is obvious that there is a consistent aerosol layer build up high above the atmospheric boundary layer at altitudes up to 13 km.

The observed patterns of the aerosol backscatter throughout this period agree well with the simulated FLEXPART CO tracer patterns from the fires both with convection on (Figs. 12d–f) and off (Figs. 12g–i). Although FLEXPART tends to underestimate the plume height by about 2–3 km, the overall features are well produced. It is evident from the simulations that convection did not alter the CO tracer distribution over Madison significantly during 26 and 28 June. However, during the last 2 h of 26 of June traces of the CO lifted into the UT/LS by pyro-convection is evident above 9 km. The strongest aerosol backscatter was observed on 30 June, with the pyro-convective CO plume

seen at 6 to 13 km. In fact, according to a FLEXPART movie showing maps of the total tracer column (not shown), this thick plume over Madison was advected northeastwards from the Yukon Territory on 25 June. 24 h later, it has taken a south-eastern direction from south of Victoria Island (69°–73° N, 100°–115° W) where it was stagnant for some hours before it headed to Wisconsin, where it engulfed most of the upper troposphere over Madison and reached levels above 12 km.

5 Summary and conclusions

In this paper, we have used satellite and lidar data and the Lagrangian transport model FLEXPART to study a pyro-convection event that occurred in Alaska and the Yukon Territory in June, 2004. After a mostly dry period of anticyclonic conditions over Alaska with unusually high temperatures, a cyclone developed west of the Canadian coast on 21 June. It weakened the anticyclone over Western Canada and Alaska and triggered strong convection. Several deep convective centers with very low cloud top brightness temperatures were observed. The cluster of the coldest cloud top temperatures (below −60°C) was located almost exactly over the region with the strongest fire activity in the boreal forest, suggesting that the fires may have enhanced the convection. A picture taken from a commercial airliner a few days later over another fire also shows the pyro-convection over the fire to be much higher than the convective clouds in the environment. The picture clearly shows how smoky the pyro-convection was, suggestive of microphysical processes being active to influence the release of latent heat in the atmosphere, in addition to the heat generated by the fire itself.

POAM and SAGE extinction profiles that were available on 24 June, one day after one of the pyro-convection events, showed that there was enhanced aerosol extinction up to about 13 km, whereas the local tropopause was at about 11 km. Lidar measurements at Madison, Wisconsin, showed strongly enhanced aerosol backscatter at up to about 12 km altitude on 30 June, about 1 week after the strongest pyro-convection.

The Lagrangian particle dispersion model FLEXPART was used to establish rela-

tionships between the different observations of the fire plume. These simulations could indeed trace back the POAM and SAGE observations as well as the lidar observations to the pyro-convection events in the second half of June 2004. However, the simulations were only successful when the deep convection parameterization of FLEXPART was switched on. Without the convection parameterization the deep transport of the fire emissions into the stratosphere could not be simulated at all. Even with the convection parameterization turned on, the maximum altitude of the simulated pollution plume over the lidar location was somewhat lower than observed. This is likely because the convection parameterization does not account for processes related directly to the fire. However, the ECMWF data used to drive FLEXPART likely benefited from the assimilation of close-by (only about 557 km from the coldest cloud top temperatures) radiosonde data that clearly showed the signatures of the deep convection taking place. In other cases, where there are no such close-by radiosonde data available, tracer simulations of pyro-convection may be much less successful. This demonstrates the need to include information about fire activity in numerical weather forecast models and observation assimilation schemes.

Finally, measurements of CO on board a commercial airliner showed strongly enhanced CO concentrations of almost 300 ppb at cruising altitude (about 11 km) in the stratosphere over the North Atlantic. This CO plume could be traced back to the same pyro-convection events as described here (Cammas et al., 2005[1]). Using convective mass fluxes taken from a simulation with a mesoscale model, Cammas et al. also show that deep convection was responsible for the strong stratospheric CO enhancements.

Acknowledgements. We acknowledge ECMWF and the German Weather Service for permitting access to the ECMWF archives. We appreciate the provision of data via the internet by the science teams at the Alaska climate research centre including those of MODIS, TOMS, POAM, SAGE and lidar group in Madison. We are thankful to N. Todo of Japan Airlines International Co. Ltd. for his image of a pyro-cb. This study was funded by the European Commission in the European Research Framework 5 program as part of the PARTS (no. EVK2CT200100112) project and the German Federal Ministry for Education and Research in the Framework of the Atmospheric Research 2000 program as part of NOXTRAM (07 ATF05).

References

Alaska Interagency Coordination Center (AICC) Report: Review of the 2004 fire season (see, http://fire.ak.blm.gov), 2004.

Andreae, M. O., Rosenfeld, D., Artaxo, P., Costa, A. A., Frank, G. P., Longo, K. M., and Silva-Dias, M. A. F.: Smoking rain clouds over the Amazon, Science, 303, 1337–1342, 2004.

Cofer, W. R., Winstead, E. L., Stocks, B. J., Goldammer, J. G., and Cahoon, D. R.: Crown fire emissions of CO_2, CO, H_2, CH_4, and TNMHC from dense jack pine boreal forest fire, Geophys. Res. Lett., 25, 3919–3922, 1998.

Crutzen, P. J.: A discussion of the chemistry of some minor constituents in the stratosphere and troposphere, Pure Appl. Geophys., 106–108, 1385–1399, 1973.

Damoah, R., Spichtinger, N., Forster, C., James, P., Mattis, I., Wandinger, U., Beirle, S., Wagner, T., and Stohl, A.: Around the world in 17 days – hemispheric-scale transport of forest fire smoke from Russia in May 2003, Atmos. Chem. Phys., 4, 1311–1321, 2004, SRef-ID: 1680-7324/acp/2004-4-1311.

ECMWF: User Guide to ECMWF Products 2.1, Meteorol. Bull. M3.2, ECMWF, Reading, UK, 1995.

Eloranta, E. W.: High spectral resolution lidar: Range-Resolved Optical Remote Sensing of the Atmosphere, edited by: Weitkamp, K., Springer-Verlag, New York, pp. 143–163, 2005.

Emanuel, K. A. and Zivkovic-Rothman, M.: Development and evaluation of a convection scheme for use in climate models, J. Atmos. Sci., 56, 1766–1782, 1999.

Forster, C., Wandinger, U., Wotawa, G., James, P., Mattis, I., Althausen, D., Simmonds, P., O'Doherty, S., Jennings, S., Kleefeld, C., Schnieder, J., Trickl, T., Kreipl, S., Jäger, H., and Stohl, A.: Transport of boreal forest fire emissions from Canada to Europe, J. Geophys. Res., 106, 22 887–22 906, 2001.

Fromm, M., Bevilacqua, R., Hornstein, J., Shettle, E., Hoppel, K., and Lumpe, J. D.: An analysis of Polar Ozone and Aerosol Measurement (POAM) II Arctic polar stratospheric cloud Observations, 1993–1996, J. Geophys. Res., 104, 24 341–24 357, 1999.

Fromm, M. D. and Servranckx, R.: Transport of forest fire smoke above the tropopause by supercell convection, Geophys. Res. Lett., 30, 1542, doi:10.1029/2002GL016820, 2003.

Fromm, M., Bevilacqua, R., Servranckx, R., Rosen, J., Thayer, P. J., Herman, J., and Larko, D.: Pyro-cumulonimbus injection of smoke to the stratosphere: observations and impact of a super blowup in northwestern Canada on 3–4 August 1998, J. Geophys. Res., 110,

doi:10.1029/2004JD005350, 2005.

Graf, H., Herzog, M., Oberhuber, J. M., and Textor, C.: The effect of environmental conditions on volcanic plume rise, J. Geophys. Res., 104, 24 309–24 320, 1999.

Hsu, N. C., Herman, J., Gleason, J., Torres, O., and Seftor, C.: Satellite detection of smoke aerosols over a snow/ice surface by TOMS, Geophys. Res. Lett., 26, 1165–1168, 1999.

Immler, F., Engelbart, D., and Schrems, O.: Fluorescence from atmospheric aerosol detected by a lidar indicates biogenic particles in the stratosphere, Atmos. Chem. Phys., 5, 345–355, 2005, SRef-ID: 1680-7324/acp/2005-5-345.

Jost, H. J., Drdla, K., Stohl, A., Pfister, L., Loewenstein, M., Lopez, J. P., Hudson, P. K., Murphy, D. M., Cziczo, D. J., Fromm, M., Bui, T. P., Dean-Day, J., Gerbig, C., Mahoney, M. J., Richard, E. C., Spichtinger, N., Pittman, J. V., Weinstock, E. M., Wilson, J. C., and Xueref, I.: In-situ observations of mid-latitude forest fire plumes deep in the stratosphere, Geophys. Res. Lett. 31, 11101, doi:10.1029/2003GL019253, 2004.

Justice, C. O., Kendall, J. D., Dowty, P. R., and Scholes, R.: Satellite remote sensing of fires during the SAFARI campaign using NOAA advanced very high radiometer data, J. Geophys. Res., 101, 23 851–23 863, 1996.

Kato, S., Pochanart, P., Hirokawa, J., Kajii, Y., Akimoto, H., Ozaki, Y., Obi, K., Katsuno, T., Streets, D. G., and Minko, N. P.: The influence of Siberian forest fires on carbon monoxide concentrations at Happo, Japan, Atmos. Environ., 36, 385–390, 2002.

Kaufman, Y. J., Justice, C. O., Flynn, L. P., Kendall, J. D., Prins, E. M., Giglio, L., Ward, D. E., Menzel, W. P., and Setzer, A. W.: Potential global fire monitoring from EOS-MODIS, J. Geophys. Res., 103, 32 215–32 238, 1998.

Kaufman, Y. J., Ichoku, C., Giglio, L., Korontzi, S., Chu, D. A., Hao, W. M., Li, R.-R., and Justice, C. O.: Fire and smoke observed from Earth Observing System MODIS instrument – products, validation, and operational use, Int. J. Remote Sensing, 24, 1765–1781, 2003.

Livesey, N. J., Fromm, M. D., Waters, J. W., Manney, G. L., Santee, M. L., and Read, W. G.: Enhancement in lower stratospheric CH_3CH observed by the Upper Atmosphere Research Satellite Microwave Limb Sounder following boreal forest fires, J. Geophys. Res., 109, D06308, doi:10.1029/2003JD004055, 2004.

Lucke, R., Korwan, D., Bevilacqua, R., Hornstein, J., Shettle, E., Chen, D., Daehler, M., Lumpe, J., Fromm, M., Debrestian D., Neff, B., Squire,M., König-Langglo, and Davis J.: The Polar Ozone and Aerosol Measurement (POAM) III instrument and early validation results , J.

Geophys. Res., 104, 18 785–18 799, 1999.
Mauldin, L., Zuan, N., McCormic, M., Guy, J., and Vaughn, W.,: Stratospheric Aerosol and Gas Expriment II instrument: A functional description, Opt. Eng., 24, 307–312, 1985.
Novelli, P. C., Masarie, K. A., Land, P. M., Hall, B. D., Myers, R. C., and Elkins, J. W.: Reanalysis of tropospheric CO trends: Effects on the 1997–1998 wildfires, J. Geophys. Res., 108, 4464, 2003.
Robock, A.: Surface cooling due to forest fire smoke, J. Geophys. Res., 96, 20 869–20 878, 1991.
Rozell, N.: Smoked pike on menu for Yukon Flats scientists, Alaska Science Forum, 1710, 2004.
Seinfeld, J. H. and Pandis, S. N.: Atmospheric Chemistry and Physics, 1326 pp., John Wiley, Inc., New York, 1998.
Spichtinger, N., Damoah, R., Eckhard, S., Forster, C., James, P.,Beirle, T., Wagner, T., Novelli, P. C., and Stohl, A.: Boreal forest fires in 1997 and 1998: A seasonal comparison using transport model simulations and measurement data, Atmos. Chem. Phys., 4, 1857–1868, 2004,
SRef-ID: 1680-7324/acp/2004-4-1857.
Stohl, A., Hittenberger, M., and Wotawa, G.: Validation of the Lagrangian particle dispersion model FLEXPART against large scale tracer experiment data, Atmos. Environ., 32, 4245–4264, 1998.
Stohl, A. and Thomson, D. J.: A density correction for Lagrangian particle dispersion models, Boundary-Layer Meteorol., 90, 155–167, 1999.
Tanimoto, H., Kajii, Y., Hirokawa, J., Akimoto, H., and Minko, N. P.: The atmospheric impact of boreal forest fires in far eastern Siberia on the seasonal variation of carbon monoxide : observations at Rishiri, a northern remote island in Japan, Geophys. Res. Lett., 27, 4073–4076, 2000.
Wotawa, G. and Trainer, M.: The influence of Canadian forest fires on pollutant concentrations in the United States, Science, 288, 324–328, 2000.
Wotawa, G., Novelli, P. C., Trainer, M., and Granier, C.: Inter-annual variability of summertime CO concentrations in the Northern Hemisphere explained by boreal forest fires in North America and Russia, Geophys. Res. Lett., 28, 4575–4578, 2001.
Yurganov, N. L., Blumenstock, T., Grechko, I. E., Hase, F., Hyer, J. E., Kasischke, E. S., Koike, M., Kondo, Y., Kramer, I., Leung, F.-Y., Mahieu, E., Mellqvist, J., Notholt, J., Novelli, C.

P., Rinsland, P. C., Scheel, E. H., Schulz, A., Strandberg, A., Sussmann, R., Tanimoto, H., Velazco, V., Zander, R., and Zhao, Y.: A quantitative assessment of the 1998 carbon monoxide emissions anomaly in the Northern Hemisphere based on total column and surface concentration measurements, J. Geophys. Res., 109, doi:10.1029/2004JD004559, 2004.

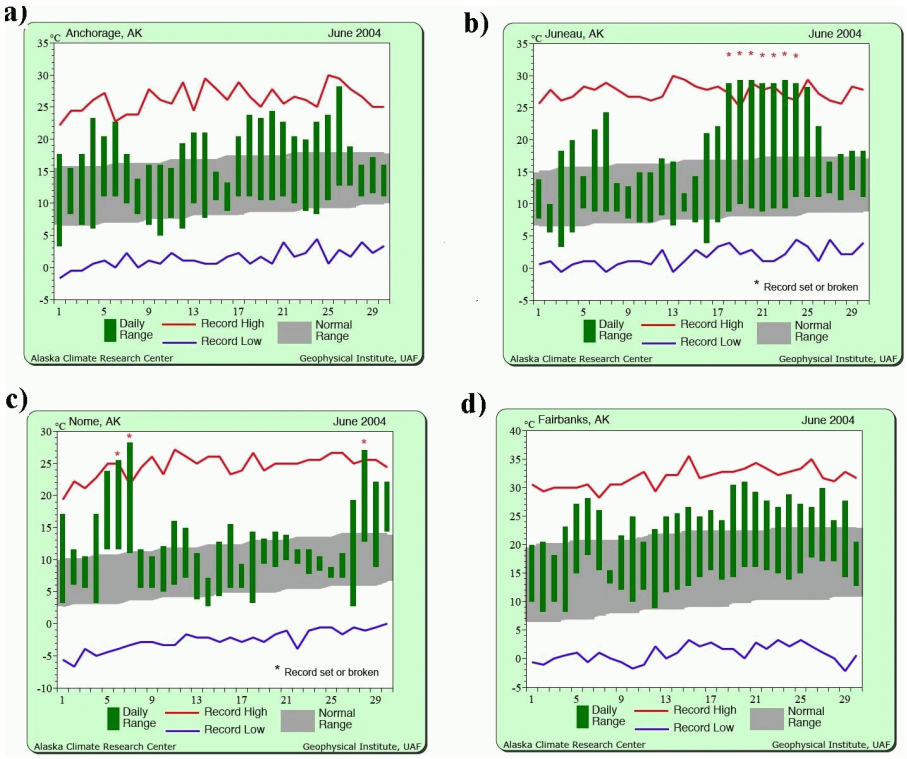

Fig. 1. June daily temperatures (green) for **(a)** Anchorage, **(b)** Juneau, **(c)** Nome and **(d)** Fairbanks, respectively. The horizontal red and blue lines indicate record high and low temperatures, respectively (see from http://climate.gi.alaska.edu).

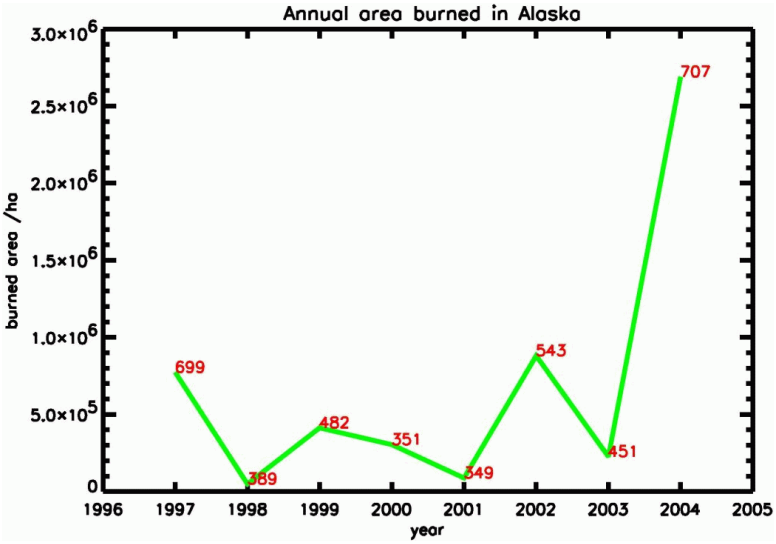

Fig. 2. The annual area burned in Alaska during the fire seasons between the years 1997 and 2004 (see http://climate.gi.alaska.edu).

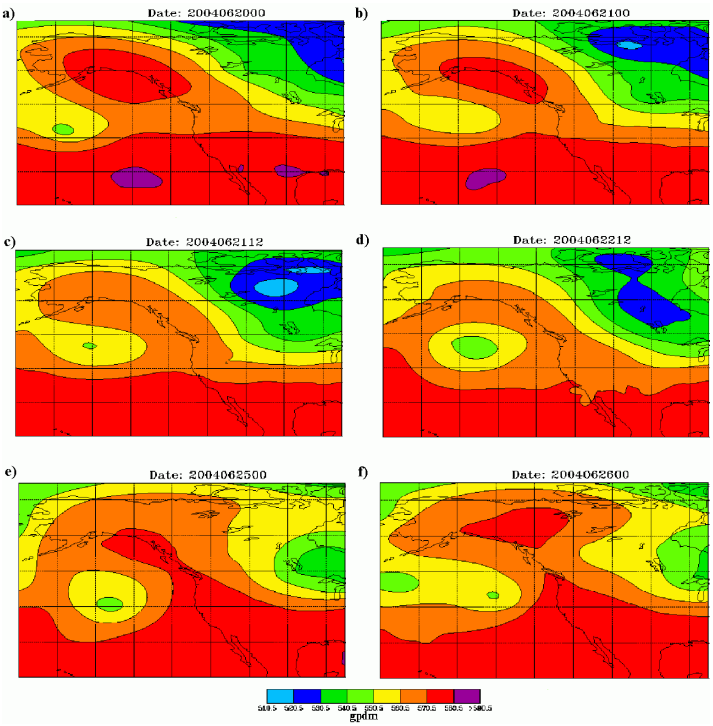

Fig. 3. ECMWF (European Centre for Medium-Range Weather Forecasts) Geopotential Height in gpdm (geopotential decametres) at 500 hPa on **(a)** 20 June 2004 at 00:00 UTC, **(b)** 21 June 2004 at 00:00 UTC, **(c)** 21 June 2004 at 12:00 UTC, **(d)** 22 June 2004 at 12:00 UTC, **(e)** 25 June 2004 at 00:00 UTC and **(f)** 26 June 2004 at 00:00 UTC.

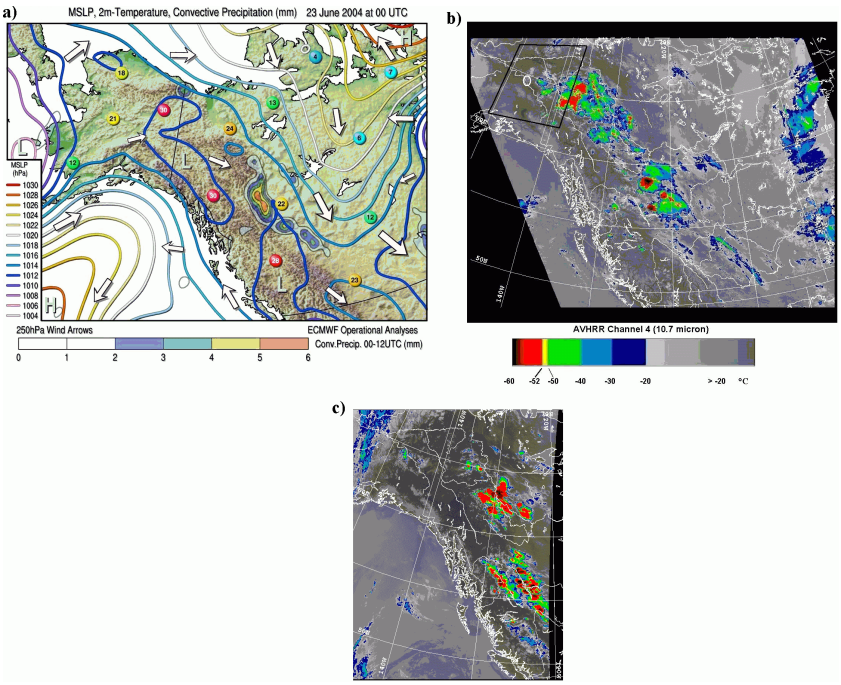

Fig. 4. **(a)** ECMWF analyses of mean sea level pressure (colored contour lines), 2-meter temperatures at selected locations (colored buttons) and 250 hPa winds (arrows) for 23 June at 00:00 UTC, plotted over a topography map of Alaska and western Canada. Shaded areas show the convective precipitation from a 12-h forecast from the 00:00 UTC analysis. **(b)** Brightness temperatures from the NOAA-12 satellite at channel 4 (10.7 μm) on 23 June at 05:00 UTC and **(c)** on 24 June at 01:00 UTC. The black rectangle and white circle in (b) indicate approximately the area shown in Fig. 5b and location of the radiosonde (Fig. 7), respectively.

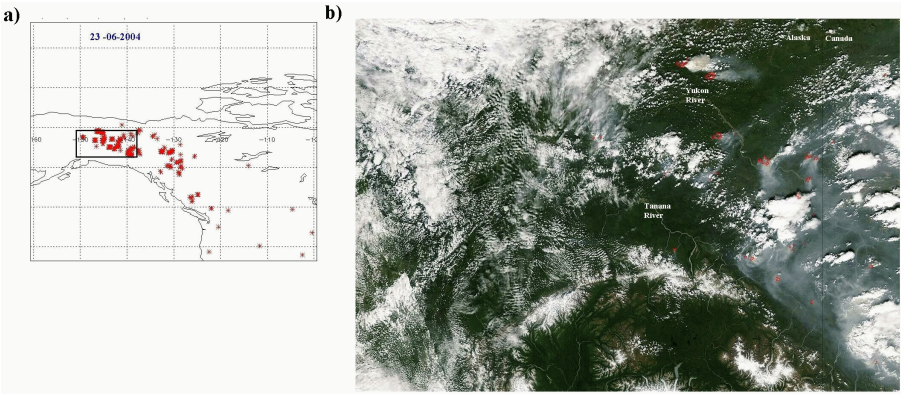

Fig. 5. **(a)** MODIS fire hot spots for 23 June, 2004. The black rectangle is approximately the area shown in panel b). **(b)** MODIS Aqua satellite image over Alaska and the Yukon Territory on 22 June at about 22:00 UTC. Red spots show active fires, whereas blue-grey colors indicate smoke, and the whitish colors show snow, ice and clouds.

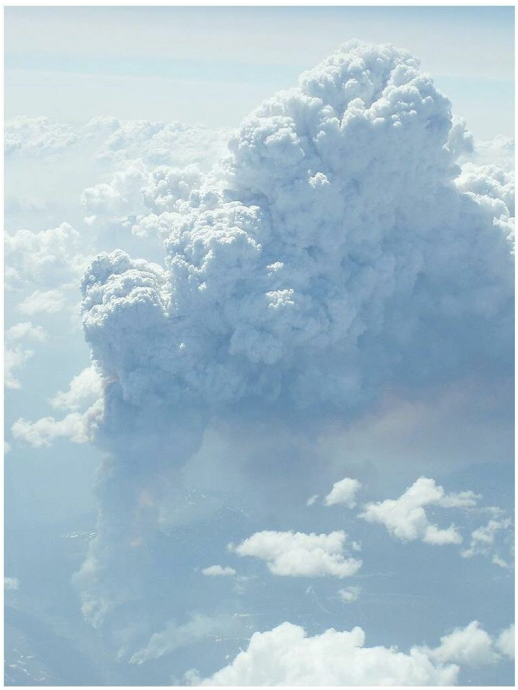

Fig. 6. Picture of a pyro-cumulonimbus located at 58° N, 126° W on 27 June at 21:00 UTC. The picture was taken out of the cockpit of a commercial airliner cruising at about 10 km (Picture courtesy of Noriyuki Todo of Japan Airlines).

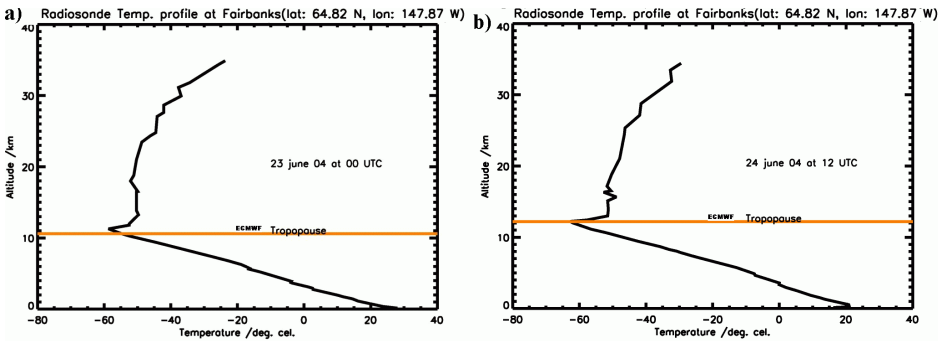

Fig. 7. Radiosonde temperature profile at Fairbanks, Alaska **(a)** on 23 June at 00:00 UTC and **(b)** on 24 June at 12:00 UTC. The horizontal orange line indicates the dynamical tropopause height calculated from ECMWF data.

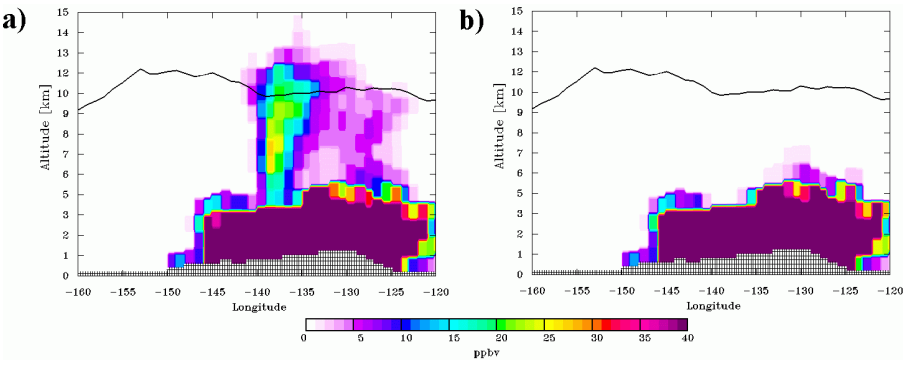

Fig. 8. Vertical sections through the FLEXPART CO tracer at 64° latitude on 24 June at 12:00 UTC with convection turned on **(a)** and off **(b)**, respectively. The black solid line is the dynamical tropopause height (height of the 2PVU surface) determined from ECMWF operational data.

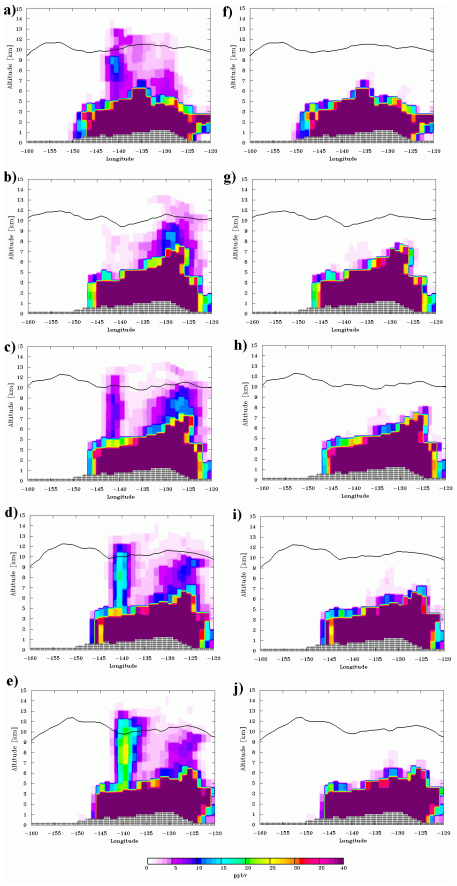

Fig. 9. Vertical sections through the FLEXPART CO tracer at 64° latitude on **(a, f)** 23 June at 09:00 UTC and **(b, g)** 21:00 UTC, **(c, h)** on 24 June at 00:00 UTC, **(d, i)** 03:00 UTC and **(e, j)** 06:00 UTC. Panels a-e show simulations with convection turned on, panels **(f–j)** show simulations with convection turned off. The black solid line is the dynamical tropopause height (height of the 2PVU surface) determined from ECMWF operational data.

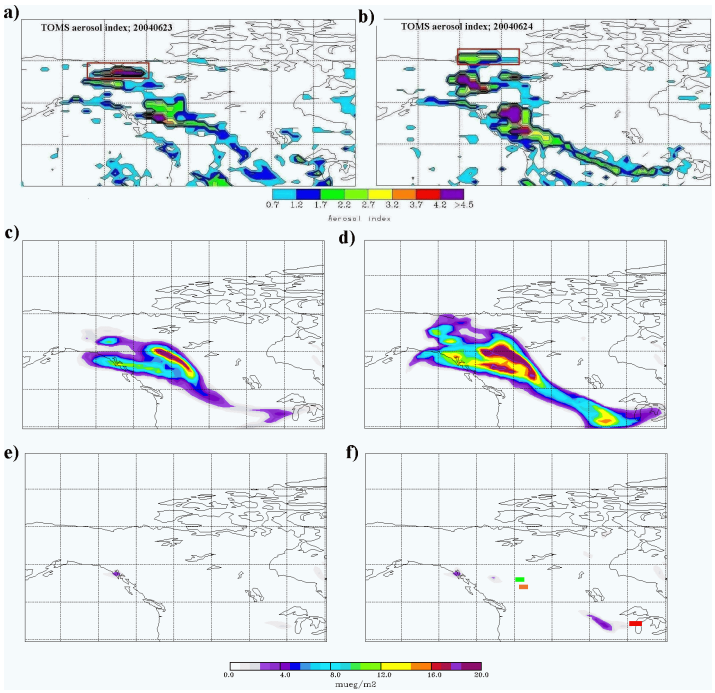

Fig. 10. TOMS aerosol index over North America on **(a)** 23 and **(b)** 24 June, 2004. FLEXPART 9–15 km CO tracer columns over North America with convection turned on, at **(c)** 23 June 03:00 UTC, **(d)** 24 June 03:00 UTC. **(e)** and **(f)** Same as (c) and (d), respectively, but with convection turned off. The orange and green rectangles shown in panel (f) indicate the locations of the POAM and SAGE measurements, respectively, shown in Fig. 11a. The red rectangle shows the location of the lidar measurements shown in Fig. 12.

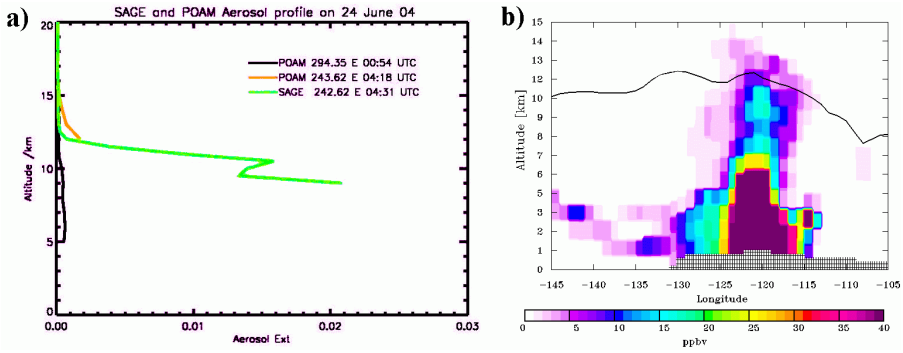

Fig. 11. (a) POAM III (orange) and SAGE II (green) aerosol extinction profiles at 1 μm approximately over Edmonton on 24 June at 04:00 UTC. The location of the profiles is shown in Fig. 10f. The unperturbed black profile is the POAM aerosol extinction over Quebec at 00:00 UTC. **(b)** Vertical section through the FLEXPART CO tracer at 54° latitude on 24 June at 03:00 UTC with convection turned on. The black solid line is the dynamical tropopause height (height of the 2PVU surface) determined from ECMWF operational data.

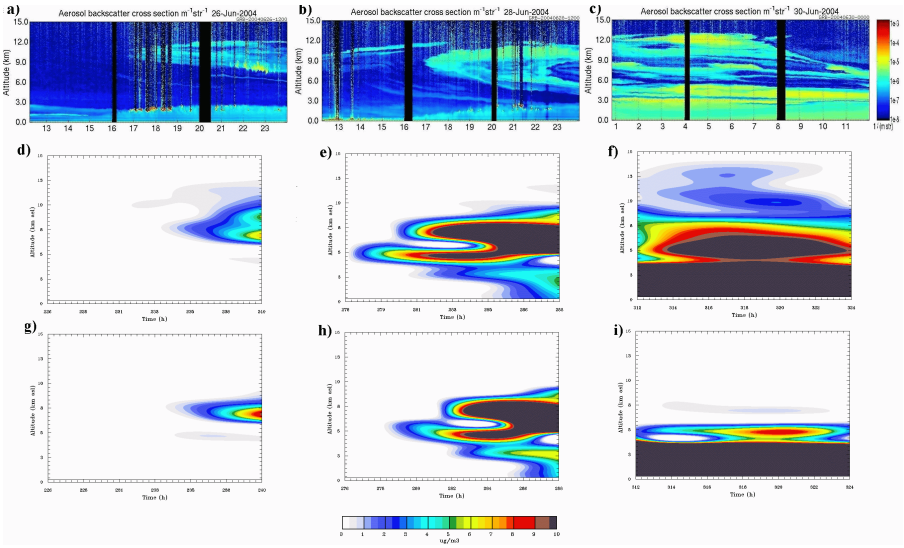

Fig. 12. Lidar time-height plot of aerosol backscatter cross section over Madison (red rectangle in Fig. 10f) on **(a)** 26 June from 12:00 UTC to 24:00 UTC, **(b)** 28 June from 12:00 UTC to 24:00 UTC and **(c)** 30 June 2004 from 01:00 UTC to 12:00 UTC. The vertical resolution is 7.5 m. FLEXPART time-height plots of the CO tracer from the simulation with convection turned on at the lidar location on **(d)** 26, **(e)** 28 **(f)** 30 June for the same time periods as the corresponding lidar data plots (a–c). **(g)**, **(h)** and **(i)** Same as d), e) and f), respectively, but with convection switched off.

ARTICLE 2

Atmos. Chem. Phys., 4, 1311–1321, 2004
www.atmos-chem-phys.org/acp/4/1311/
SRef-ID: 1680-7324/acp/2004-4-1311

Atmospheric Chemistry and Physics

Around the world in 17 days – hemispheric-scale transport of forest fire smoke from Russia in May 2003

R. Damoah[1], N. Spichtinger[1], C. Forster[1], P. James[1], I. Mattis[2], U. Wandinger[2], S. Beirle[3], T. Wagner[3], and A. Stohl[4]

[1]Department of Ecology, Technical University of Munich, Freising, Germany
[2]Institute for Tropospheric Research, Leipzig, Germany
[3]Institute for Environmental Physics, University of Heidelberg, Heidelberg, Germany
[4]Cooperative Inst. for Research in Environmental Science, Univ. of Colorado/NOAA Aeronomy Laboratory, Boulder, USA

Received: 14 January 2004 – Published in Atmos. Chem. Phys. Discuss.: 15 March 2004
Revised: 9 June 2004 – Accepted: 27 July 2004 – Published: 23 August 2004

Abstract. In May 2003, severe forest fires in southeast Russia resulted in smoke plumes extending widely across the Northern Hemisphere. This study combines satellite data from a variety of platforms (Moderate Resolution Imaging Spectroradiometer (MODIS), Sea-viewing Wide Field-of-view Sensor (SeaWiFS), Earth Probe Total Ozone Mapping Spectrometer (TOMS) and Global Ozone Monitoring Experiment (GOME)) and vertical aerosol profiles derived with Raman lidar measurements with results from a Lagrangian particle dispersion model to understand the transport processes that led to the large haze plumes observed over North America and Europe. The satellite images provided a unique opportunity for validating model simulations of tropospheric transport on a truly hemispheric scale. Transport of the smoke occurred in two directions: Smoke travelling northwestwards towards Scandinavia was lifted over the Urals and arrived over the Norwegian Sea. Smoke travelling eastwards to the Okhotsk Sea was also lifted, it then crossed the Bering Sea to Alaska from where it proceeded to Canada and was later even observed over Scandinavia and Eastern Europe on its way back to Russia. Not many events of this kind, if any, have been observed, documented and simulated with a transport model comprehensively. The total transport time was about 17 days. We compared transport model simulations using meteorological analysis data from both the European Centre for Medium-Range Weather Forecast (ECMWF) and the National Center for Environmental Prediction (NCEP) in order to find out how well this event could be simulated using these two datasets. Although differences between the two simulations are found on small scales, both agree remarkably well with each other and with the observations on large scales. On the basis of the available observations, it cannot be decided which simulation was more realistic.

Correspondence to: R. Damoah
(damoah@forst.tu-muenchen.de)

1 Introduction

About 85% of biomass burning takes place in the tropics (Andreae, 1991) and causes pollutant emissions that have a strong impact on the tropospheric chemistry (Galanter et al., 2000). Aerosols and trace gases such as carbon monoxide, nitrogen oxides and non-methane hydrocarbons from biomass burning play an important role for atmospheric chemistry and radiative properties of the atmosphere. Carbon monoxide, for instance, is involved in tropospheric ozone chemistry (Crutzen, 1973) and aerosols can be transported into the stratosphere (Fromm et al., 2000) where they may influence concentrations of stratospheric ozone through catalytic chemical reactions. Therefore changes in the concentrations of aerosols and carbon monoxide also affect ozone, which plays an important role in the global climate system (Daniel and Solomon, 1998; Logan et al., 1981). Furthermore, aerosols by themselves can strongly influence the radiation in the atmosphere (Christopher et al., 2000; Hsu et al., 1999) and represent the largest source of uncertainty in current climate model simulations (IPCC, 2001).

In addition to biomass burning in the tropics, fires in the boreal forest are a further strong emission source. Recently it was found that through long-range transport, emissions from boreal forest fires can affect the concentrations of many trace substances in distant regions. Wotawa and Trainer (2000) found that the high CO and O_3concentrations over southeastern United States in 1995 over a period of 2 weeks were caused by the transport of a pollution plume from Canadian fires and photochemical ozone formation in this plume, while long-range transport events of aerosols (Hsu et al., 1999; Formenti et al., 2002; Fiebig et al., 2002; Wandinger et al., 2002), CO and O_3 (Forster et al., 2001) and NO_x (Spichtinger et al., 2001) from Canadian forest fires have also been observed over Europe. According to model simulations, the time scale of intercontinental transport of pollutant emissions

is on the order of 3–30 days (Stohl et al., 2002). The upper range of this estimate may be a typical time scale for the mixing of pollutants in the northern hemisphere middle latitudes. In case studies, Wotawa and Trainer (2000) reported a duration of about 2 weeks for the transport of Canadian fire emissions to the southeastern United States, Forster et al. (2001) quoted a period of about 1 week for the transport of Canadian fire emissions to Europe. Emissions from the fires can be transported upward in warm conveyor belts (WCBs) (Stohl, 2001) or by – sometimes extreme – convection (Fromm and Servranckx, 2003) into the upper troposphere where fast intercontinental transport may occur (Stohl and Trickl, 1999; Yienger et al., 2000; Stohl et al., 2002).

Fires in Canada have received much attention recently, whereas fires in Russia are much less well studied. The world's total closed boreal forest covers about 1 billion ha (29% of the world's forest area), of which Russian boreal forests contribute about two thirds (Kasischke et al., 2000). Fire is a major natural disturbance in Russian forests because: (1) Boreal forests are dominated by coniferous stands of high fire hazard; (2) Considerable part of the forest territory is unmanaged and unprotected; (3) The forests contain large amounts of accumulated organic matter due to slow decomposition of plant material; and (4) most of the boreal regions have limited amounts of precipitation and long periods of drought in the fire season. Despite the large areas burning in Russian forests almost every year, until recently relatively little attention has been paid to fires there compared to Canadian fires. However, recently Siberian forest fires have been the subject of several studies (e.g. Yoshizumi et al., 2002; Conard et al., 2002; Kasischke and Bruhwiler, 2003, Shvidenko and Goldammer, 2001, Shvidenko and Nilsson, 2000).

A long-period (1970–1999) average estimate of burned areas for all Russian forests and tundra is 5.1×10^6 ha yr^{-1} (Shvidenko and Goldammer, 2001), Lavoue et al. (2000) gave an annual average of 4×10^6 ha yr^{-1} (1960–1997), but some other estimates are as high as $10–12\times10^6$ ha yr^{-1} (Conard and Ivanova, 1998; Valendik, 1996). In fact, recent estimates of the annual area burned in Russia vary considerably. Partly this is due to the large interannual variability and a strong increase in fire activity since the late 1990s. In 1987, when 14.5×10^6 ha of forest and other lands were destroyed was an extreme year. Assuming typical emission factors (Andreae and Merlet, 2001), this contributed about 20% of CO_2, 36% of CO and 69% of total CH_4 produced by savanna burning during an average year (Cahoon et al., 1994). 1998 was another severe year when about 12×10^6 ha were destroyed according to recent estimates (Kasischke and Bruhwiler, 2003). It was even worse in the year 2003. The first fires were detected as early as April within the Trans-Baikal region. In May the situation in the south of Russia escalated. By the end of May, tens of thousands of fires had destroyed more than 15×10^6 ha of land in the Russian Federation. The most affected regions were Chitinskaya Oblast (55–56° N, 114–120° E), Buryatiya Repulic (55–59° N, 107–114° E) and Amurskaya Oblast (52–56° N, 120–132° E) (GFMC, 2003). At the end of the 2003 fire season, more than 19×10^6 ha of land had been destroyed in Russia (Slightly less than the size of Iraq).

In this paper, we study a hemispheric-scale transport event in May 2003. Over a period of about 17 days, satellite images in several regions of the northern hemisphere show the transport around the world of smoke from the Siberian fires. Lidars in eastern Asia, North America and Europe (Mattis et al., 2003) took vertical profiles of the smoke. The transport model and data used in this paper are described in the following section. Results from the smoke transport simulations are presented in Sect. 3, together with discussions about the relevant meteorological aspects of the event, and conclusions are drawn in Sect. 4.

2 Tools and methodology

The GOME instrument has been operational aboard the ERS-2 satellite since April 1995. With a spectral range from 240 nm to 790 nm, GOME measures the scattered and reflected sunlight from the surface using the nadir viewing mode. Operational data products of GOME result from radiance and solar irradiance spectra which are taken through several processing steps to obtain global distributions of total column amounts of NO_2 and other species using the DOAS approach (Differential Optical Absorption Spectroscopy) (Platt, 1994). Tropospheric NO_2 columns used in this study are derived from a stratosphere/troposphere separation algorithm (Beirle et al., 2003).

NASA's Moderate Resolution Imaging Spectroradiometer (MODIS) aboard the Terra and Aqua satellites measures radiances in 36 spectral bands, from which a large number of different products are derived. Of importance for this study are the locations of active fires (hot spots), burn scars and aerosols (including smoke from forest fires) (Chu et al., 2002; Remer et al., 2002; Kaufman et al., 1998a; Justice et al., 1996). Its main fire detection channels saturate at high brightness temperatures of 500 K at 4 μm and 400 K at 11 μm.

Other platforms that observed the smoke were Total Ozone Mapping Spectrometer (TOMS) aboard the Earth Probe satellite which provides data on UV-absorbing tropospheric aerosols including smoke from biomass burning (Hsu et al., 1999). And the Sea-viewing Wide Field Sensor (Sea WiFS) (Hook et al., 1993) aboard the Sea Star spacecraft, which operates in 8 wavelength channels ranging from 403–887 nm but uses channels 765 and 865 nm for the estimation of aerosol radiance (Gordon and Wang, 1994).

The Raman lidar at Leipzig, Germany (Mattis et al., 2003) measured vertical smoke profiles in terms of volume extinction coefficients of aerosols at 355 and 532 nm, and backscatter coefficients at 355, 532 and 1064 nm wavelengths.

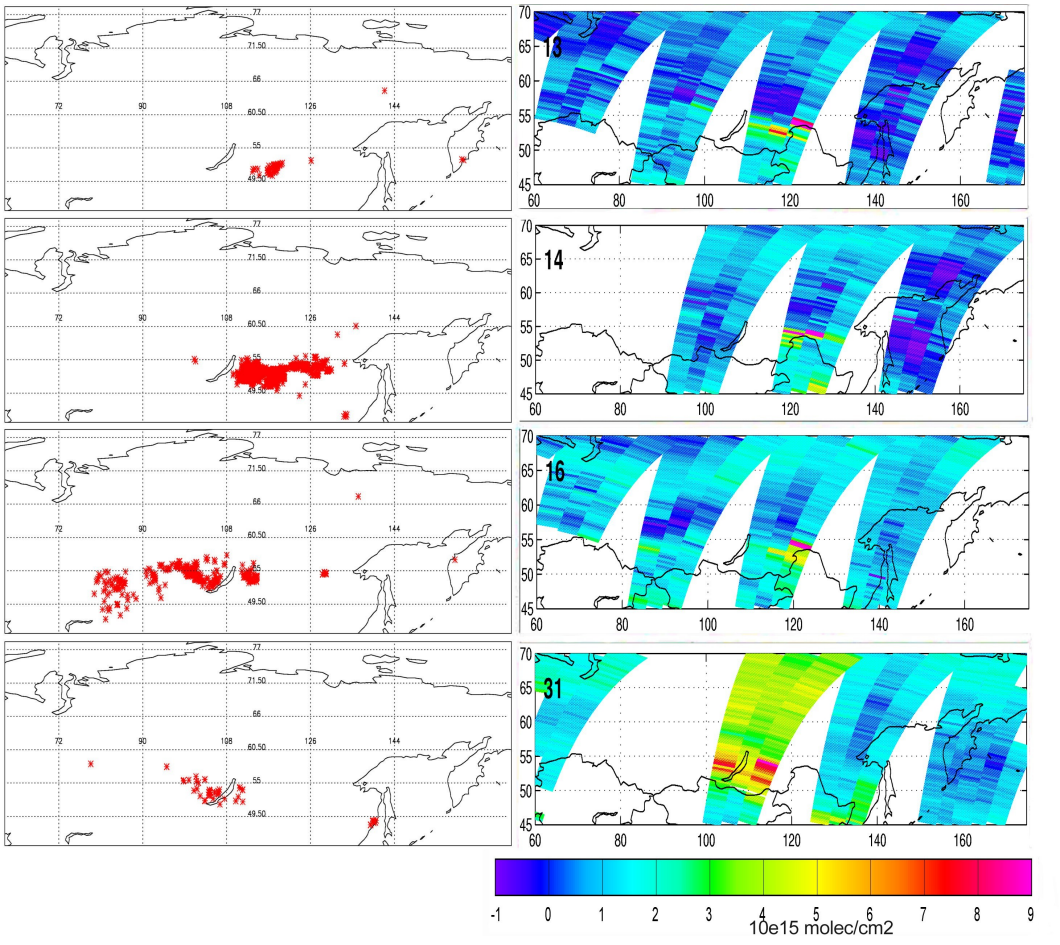

Fig. 1. MODIS fire product for 13, 14, 16 and 31 May, 2003, respectively (left column) and corresponding daily GOME tropospheric NO_2 (right column).

In order to determine the origin and the transport of these plumes, we used the Lagrangian particle dispersion model FLEXPART (Stohl et al., 1998; Stohl and Thomson, 1999) to simulate the transport of a CO tracer. A CO tracer was used because CO has a relatively long life time that ranges from 1 month (in the tropics) to 4 months (in the mid-latitudes) (Seinfeld and Pandis, 1998). As the emphasis in this paper is on the transport, we used a passive tracer (CO) not undergoing removal processes so that observed structures will always be present in the model results for qualitative comparison.

FLEXPART simulates the long-range transport, diffusion, dry and wet deposition and radioactive decay of air pollutants released from point, line or volume sources. It treats advection and turbulent diffusion by calculating the trajectories of a multitude of particles. Stochastic fluctuations, obtained by solving Langevin equations (Stohl and Thomson, 1999), are superimposed on the grid-scale winds from global meteorological datasets to represent transport by turbulent eddies, which are not resolved. Global data sets also do not resolve individual convective cells, although they reproduce the large-scale effects of convection (e.g. the strong ascent within WCBs). Therefore, FLEXPART has recently been equipped with a convection scheme (Emanuel and Zivkovic-Rothman, 1999) to account for sub-grid scale transport. FLEXPART can be driven by meteorological analysis data either from the European Centre for Medium-Range Weather Forecasts (ECMWF, 1995) or from the Global Forecast System (GFS) of the National Center for Environmental Prediction (NCEP). Simulations using data from both sources were made in order to possibly find out which dataset provided a more accurate simulation of the transport event.

The ECMWF model version used here has 60 hybrid model levels in the vertical, while the GFS output is available on 26 pressure levels. In the horizontal, both datasets are global with a $1^\circ \times 1^\circ$ regular grid. 6-hourly analyses are supplemented by 3-hour forecast step data to provide a 3-hourly temporal resolution in both cases. An output grid with a $1^\circ \times 2^\circ$ latitude/longitude resolution, a vertical spacing of 1000 m and an output interval of 3 h was employed. Due to the significantly higher vertical resolution of the ECMWF

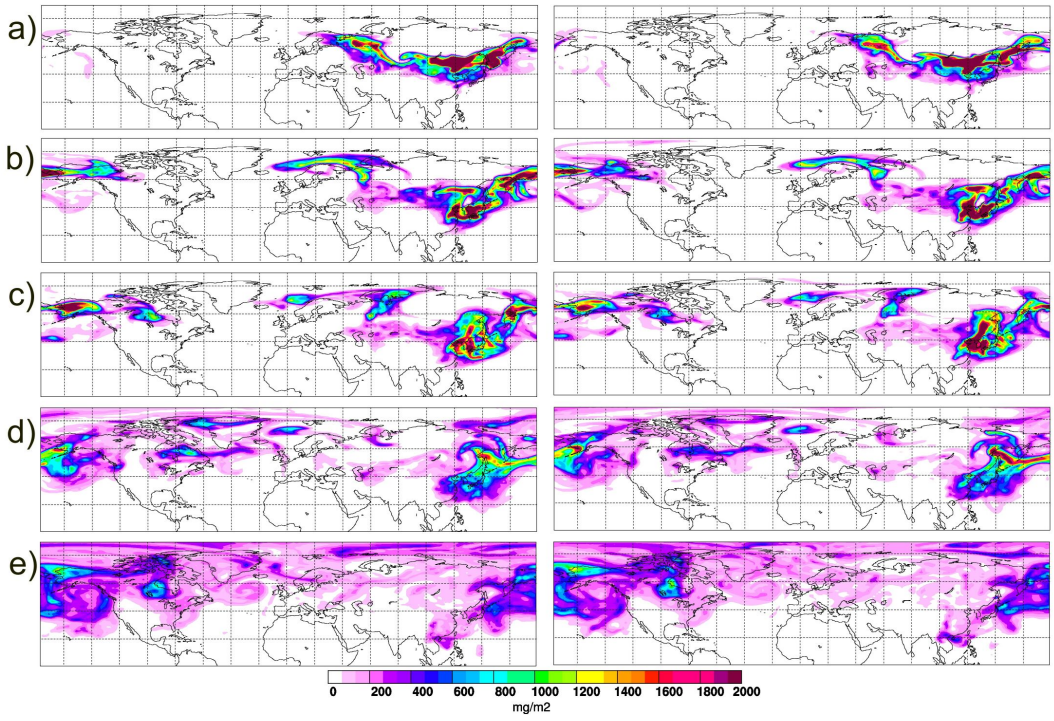

Fig. 2. Total CO tracer columns from simulations using ECMWF data (left column) and GFS data (right columns) on **(a)** 18 May 2003 at 00 UTC, **(b)** 21 May at 00 UTC, **(c)** 22 May at 06 UTC, **(d)** 26 May at 06 UTC and **(e)** 31 May at 00 UTC, respectively.

data grid and the higher intrinsic horizontal resolution of the operational ECMWF forecast model, compared to the GFS model, the simulation based on ECMWF data is our primary simulation of the smoke transport and will be used to highlight specific transport phenomena. However, the GFS simulation is very useful as a control run to indicate how differences in the meteorological analyses might affect the accuracy of the transport and its comparison with satellite data.

In the tracer simulations, 5×10^6 particles were released to calculate the transport of CO emissions from fires in Russia. For our simulation we considered the 3-week period from 10 to 31 May 2003, when the most spectacular long-range transport event occurred. Between 10 and 31 May, with approximately 0.26×10^6 ha burning per day, a total area of about 5.5×10^6 ha was burned in Chitinskaya Oblast, Buryatiya Repulic and Amurskaya Oblast, according to weekly estimates of the Global Fire Monitoring Center (GFMC, 2003). In order to describe the regional and daily variations of the fires, the MODIS hot spot data (MOD14 product) were used to spatially and temporally disaggregate the total burned area taken from GFMC (2003), assuming that the 10 310 hot spots detected during that period (Fig. 1) all burned an equal area. CO emissions were taken to be proportional to the area burned. Assuming a CO release of 4500 kg per hectare of forest burned, which is similar to recent estimates based on emissions from the Canadian Northwest Territories (Cofer et al., 1998), we estimate that 24.75 Tg of CO were released into the atmosphere due to the burning during May 10 to May 31 2003. The altitudes at which the emissions were effectively released into the atmosphere vary from day to day and are actually not known. Lacking this information, we released the CO tracer into the lowest 3 km of the model atmosphere. Sensitivity studies performed on this event by varying the upper release level from 0.5 km to 4 km altitude did not change the results much (less than 4% of the global mean concentration).

3 Results

The left column of Fig. 1 shows Moderate-Resolution Imaging Spectroradiometer (MODIS) fire products (MOD14) for 13, 14, 16 and 31 May, 2003, respectively. At the example of these four days it can be seen that there is a relatively high day-to-day variability, which to some extent may be real, but partly may also be due to the presence or non-presence of clouds and/or smoke over the fires. Because we have used the hot spot data to estimate the emissions in our model this may also introduce artificial variability into the transport model simulations. At the locations of these fires, distinct maxima of GOME's NO_2 tropospheric columns are found (right column). Despite the general agreement between fire locations and NO_2 maxima, the number of the fires does not correlate well to the strength of the NO_2 signal. For instance, on 14 May, the hot spots show a strong burning east of Lake Baikal

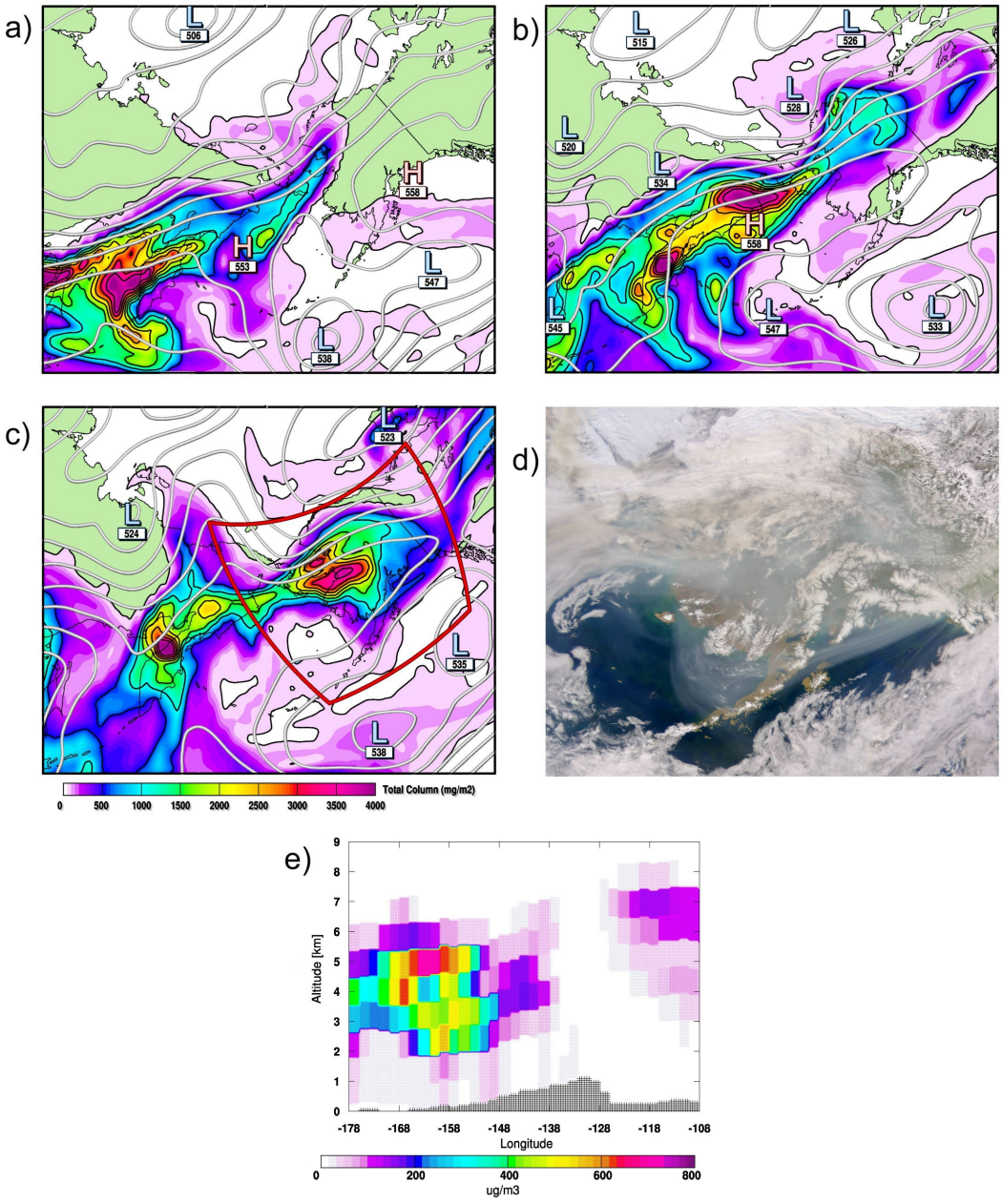

Fig. 3. (a–c) FLEXPART ECMWF CO tracer columns over the Bering Sea and adjacent regions with superimposed contours of the 500 hPa geopotential surface, based on GFS analyses, contour interval 5 dam, at (a) 19 May 00 UTC, (b) 20 May 12 UTC and (c) 22 May 00 UTC; The hatched area represents the topography. Green areas represent land surface, oceans are white. The red rectangle in c) shows approximately the area shown in panel d); **(d)** SeaWiFS image showing smoke over Alaska at 23 UTC on 21 May; Whitish colors are snow, ice and clouds, whereas the blue-grey indicate smoke. **(e)** vertical section through the FLEXPART CO tracer at 64° latitude on 22 May at 00 UTC using ECMWF data.

but relatively low NO_2columns were observed over the fires by GOME. On the other hand, fewer hot spots were detected east of Lake Baikal on 13 and 31 May, but the GOME NO_2 enhancements over the fires were much larger. This may be due to the presence of clouds which hamper both the detection of hot spots and NO_2 beneath the clouds, differences in the temporal coverage of the two intstruments, or may reflect true variability of the NO_2 emissions (for instance, different emissions strengths during flaming versus smoldering burning condition) and their transport away from their sources.

Before considering the specific meteorological events which were significant for the intercontinental transport of aerosols from the Russian fires, it is worthwhile looking at the spread of the pollution with time over the hemisphere.

Figure 2 shows total columns of the CO tracer simulated by FLEXPART using ECMWF (left column) and GFS (right column) data as input. At around 18 May (Fig. 2a), there were two main modes of transport, one northwestwards towards Northern Europe and the other eastwards to the Okhotsk Sea. The CO tracer travelling towards Europe was lifted over the Urals and was heading to Scandinavia (Fig. 2a). Four days later it split up over the Norwegian Sea with one part reversing to Asia (Fig. 2c). The more interesting to us is the other mode of the transport, which took the fire emissions around the globe. The CO tracer was lifted over the Okhotsk Sea, where it travelled rapidly through Alaska (Fig. 2b) to Canada (Fig. 2c), then crossed the Atlantic to Europe (Fig. 2d) where it began to merge with the tracer which had been advected directly out of Russia from the east. On 31 May, 2003 the CO tracer could be seen over much of the northern hemisphere (Fig. 2e). By this time the plume that had travelled across the Pacific and Atlantic oceans had also indeed crossed Eurasia, taking about 17 days to circle the entire globe. A closer look at the two data sets reveals regional differences between simulations using ECMWF and GFS data, respectively. Generally, however, the two simulations were remarkably similar to each other. Both showed the two modes of transport and the hemispheric-scale transport event.

3.1 Smoke over Alaska (8th day)

During the period 19–22 May, the north Pacific jet was split into two components: a southern component near 40° N associated with the north Pacific storm track, not relevant to this discussion, and a zonally elongated polar jet component stretching from north-east Siberia across the Bering Sea into Alaska; the latter is shown at 500 hPa in Figs. 3a–c. A large body of tracer was advected out of Siberia by this strong westerly flow which was further intensified by the growth of two synoptic waves on the jet, which cross the Bering Strait within 36 h of each other (Figs. 3b and c). The first of these waves cuts off the leading edge of the plume which is then advected quickly into northwestern Canada. The main body of the plume is pushed by the second wave over Alaska and has been very well simulated by the FLEXPART CO tracer using both ECMWF (Fig. 3c) and GFS data (not shown). On 21 May 2003, Sea WiFS captured an aerosol plume (Fig. 3d) over Alaska that was presumably transported from the intense forest fire burning in Russia. Images from the MOPITT (Measurement Of Pollution In The Troposphere) instrument (not shown) studied within this period also shows forest fire emissions (Edwards et al., 2003) over Alaska. When comparing this available satellite image. In particular, the sharp edges of the plume in the image over the Gulf of Alaska, westwards to the Aleutians and then northwards over the Bering Sea, coincide well with the edges of the CO tracer plume. A vertical section through the FLEXPART-ECMWF CO tracer at 64° N indicates that the main plume over Alaska is concentrated between 2 and 5 km altitude while the advanced plume over northwestern Canada is somewhat higher, primarily lying between 4 and 7 km. Clouds in Fig. 3d are mostly at lower altitudes, partly lying underneath the smoke.

3.2 Smoke over Canada (11th day)

On 21 May a smoke plume which arrived first over north-western Canada (see description above) was advected quickly south-eastwards before arriving and becoming slow-moving near the Great Lakes in a diffluent mid-tropospheric flow on 23 May. On 24 May 2003 (Fig. 4c) simulated FLEXPART CO tracer showed elongated plumes which stretches from the north-western edge of Lake Superior up towards James Bay and reaches across to Quebec and the St. Lawrence River. The plume coincides well with the image of MODIS instrument aboard the Terra satellite which also showed elongated smoke plumes (Figs. 4a and b) on 23 and 24 May. An anticyclonic ridge builds between the polar cylconic vortex and a small new cut-off low which develops quickly to the south of the Great Lakes. As a result, the plume is stretched out and its western flank is advected around the developing low south- and eastwards into the eastern United States. Meanwhile its eastern flank is pulled out by strong westerly winds past the southern tip of Greenland and reaches Iceland by 24 May (Figs. 4c and d).

Another smoke maximum is indicated over part of Manitoba on 23 May in the upper left corner of Fig. 4a. This is the edge of the main plume body which was seen over Alaska on 22 May (Fig. 3c) and moved into Canada about 48 h behind the leading plume above. This large main plume is advected in the strong westerly flow and arrives over the Hudson Bay on 25 May, where much of it slows down as it comes under the influence of diffluent flow ahead of a developing ridge. The leading edge of this plume, however, is pulled away from the rest in two bursts by strong flow on the edge of a trough centred over Baffin Island. One part is advected northwards to western Greenland on 24 May (Fig. 4d) and another over the Labrador Sea on 25 May (Fig. 4e).

Figure 4f shows the TOMS aerosol index on 24 May. It also shows a maximum over Hudson Bay and a filament stretching from south-east of James Bay to the St. Lawrence river, in fairly good agreement with the FLEXPART tracer simulation. However, no significant aerosols registered in TOMS near Lake Superior. This can be partly attributed to the dissipation of the smoke in this region later on 24 May (note that local midday, significant for TOMS measurements, was after 18 UTC) or the possible presence of clouds.

3.3 Smoke over Scandinavia (14th day)

The rapid advection of the plume across the Atlantic was caused by the development of a small but intense and mobile synoptic wave and associated strong winds near Iceland on 25 May (Fig. 5a). This wave moves quickly eastwards

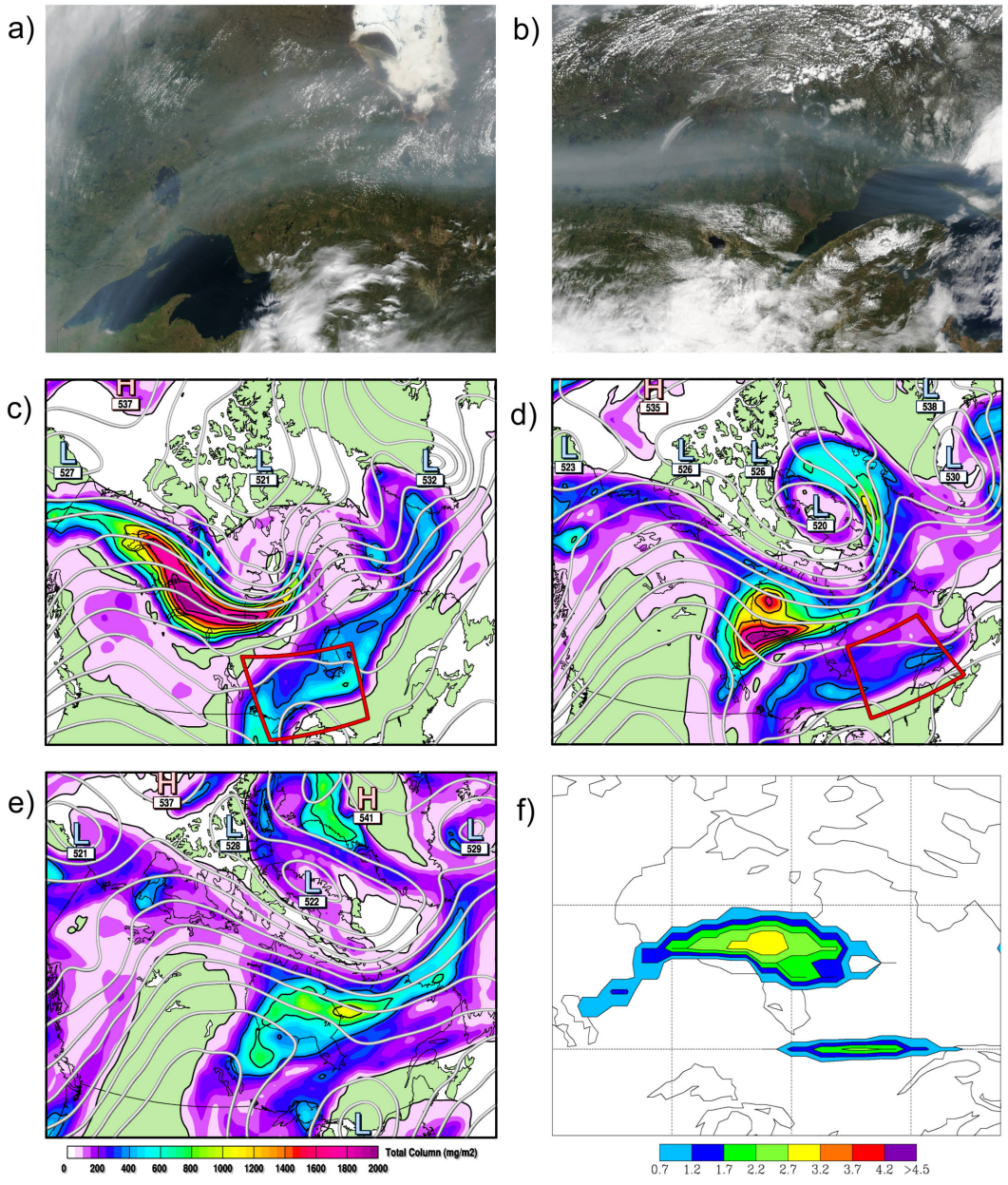

Fig. 4. MODIS Terra satellite images over **(a)** central Canada at 16:30 UTC, 23 May and **(b)** eastern Canada at 15:35 UTC, 24 May; **(c–e)** FLEXPART ECMWF CO tracer columns over Canada with superimposed contours of the 500 hPa geopotential surface, based on GFS analyses, contour interval 5 dam, at (c) 23 May 18 UTC, (d) 24 May 18 UTC and (e) 25 May 18 UTC; (f) TOMS aerosol index over eastern Canada on 24 May, 2003.

and is followed by an increasingly zonal flow which advects the remains of the plumes which had been over south-eastern Canada in streams across the Atlantic. FLEXPART simulations with both ECMWF (Fig. 5c) and GFS data (not shown), both of which showed CO tracer over parts of the North Atlantic, Scandinavia and the Baltic Sea. It also show tracer maxima at altitudes of about 5 km (Fig. 5e) The haze plume formed a curve from just to the south of Iceland down across to southern Norway and south-central Sweden and back up across western and central Finland. Further filaments are in evidence across the Skagerrak Strait near Denmark and over parts of the Baltic Sea, while further regions of haze plume are over parts of the European mainland, notably over Latvia, Lithuania and Poland.

The primary plume curve has been very well captured by the SeaWiFS sensor On 27 May 2003 (Fig. 5a). The positions of the maxima over southern Norway and western Finland have been well captured, although the leading edge of the smoke appears in the satellite image to have reached slightly further east over Finland than in the simulation. The

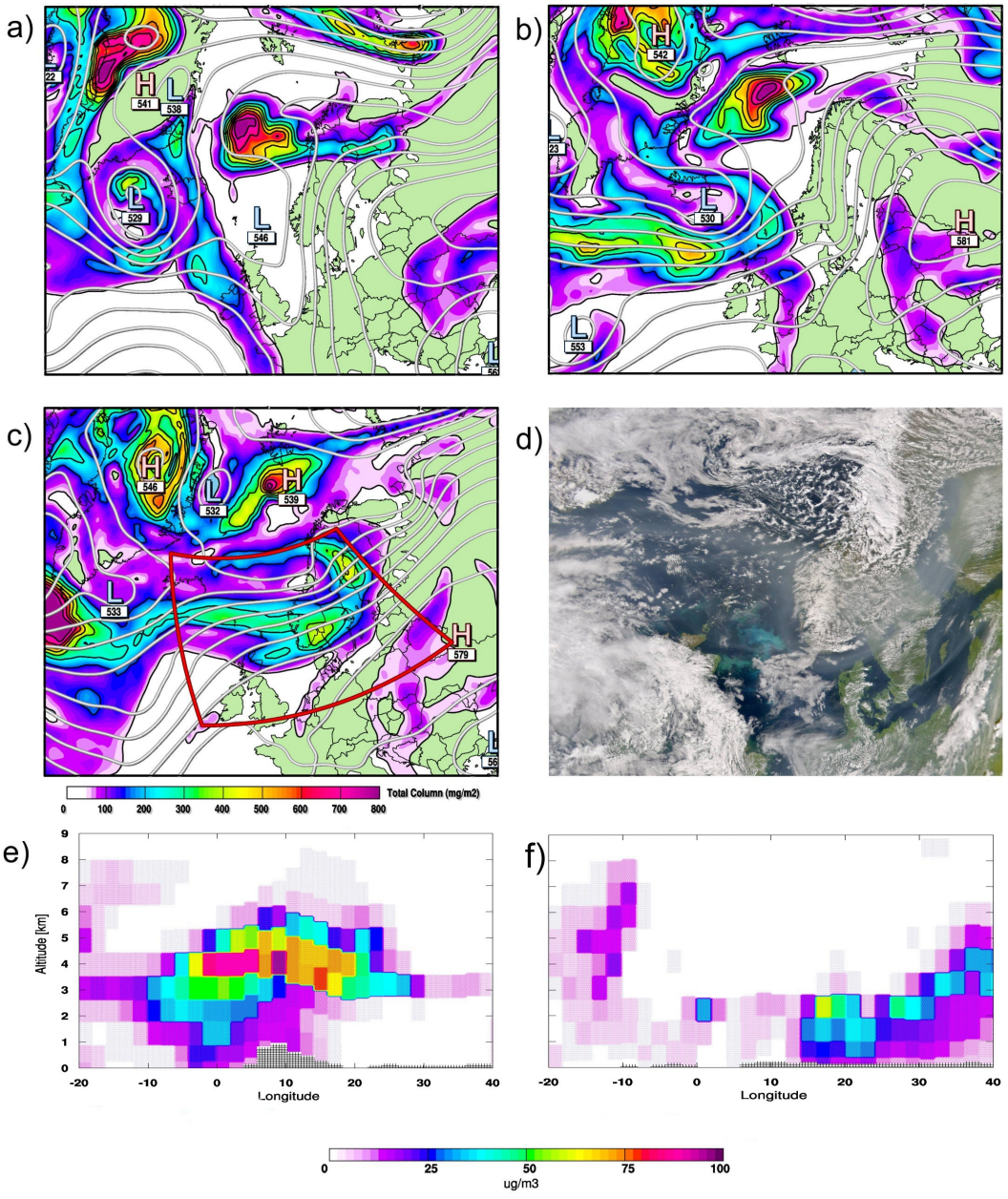

Fig. 5. (a–c) FLEXPART ECMWF CO tracer columns over the north-east Atlantic, Europe and Greenland with superimposed contours of the 500 hPa geopotential surface, based on GFS analyses, contour interval 5 dam, at (a) 25 May 15 UTC, (b) 26 May 15 UTC and (c) 27 May 15 UTC; **(d)** Image of SeaWiFS sensor showing smoke over Scandinavia on 27 May, 2003 at 12:54 UTC. **(e)** and **(f)** vertical section through the FLEXPART CO tracer at 61° latitude on 27 May at 15 UTC and 51° latitude on 29 May at 21 UTC, respectively, using ECMWF data.

maximum over southern Norway corresponds to the component which had been advected over Labrador Sea on 25 May (Fig. 4e) while the maximum over western Finland contains smoke which had been the first to reach the Iceland region on 24 May (Fig. 4d).

The smoke thus arriving over Europe on 27 May had almost completed a loop around the globe and was heading back towards the source region in Russia. It also began inevitably to merge with smoke plumes which had been advected directly from the east out of Russia. The large maximum near Jan Mayen, north-east of Iceland, on 25 May (Fig. 5a) had been advected slowly across northern Scandinavia during the previous days and became stagnant in a region of light mid-tropospheric winds in an anticyclonic ridge. Similarly, the CO tracer plume over Eastern Europe (Fig. 5a–c) was advected slowly from the east in anticyclonic conditions and corresponds well with the observed haze plumes in this region.

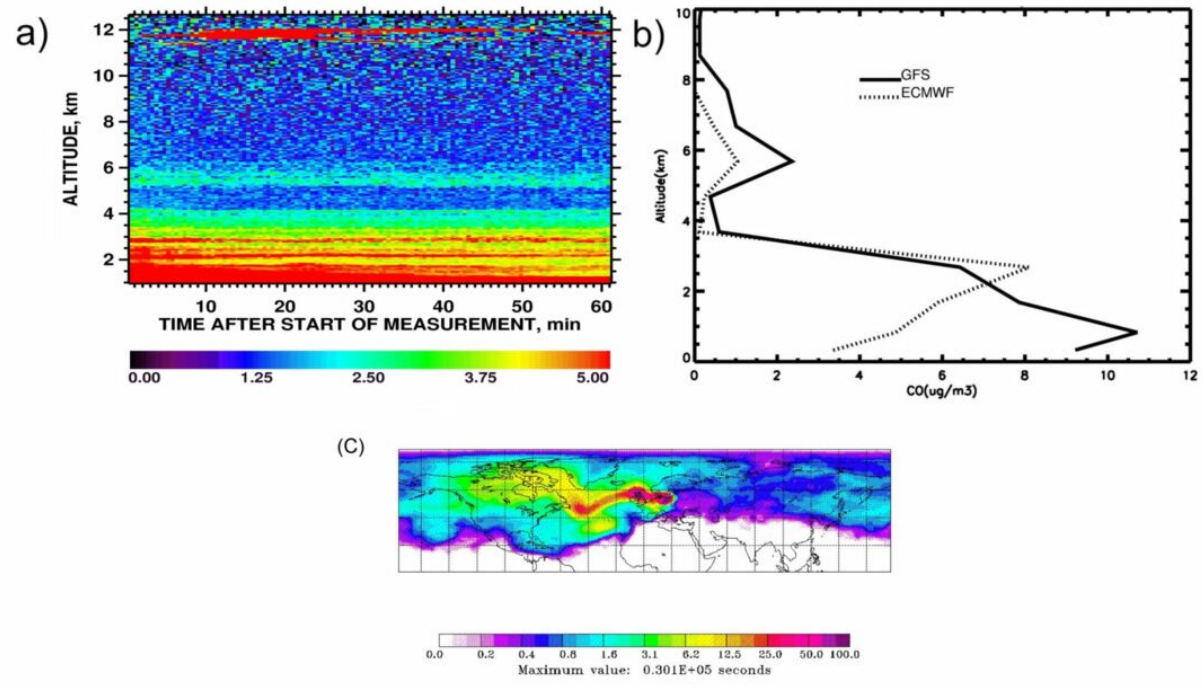

Fig. 6. (a) Lidar time-height plot of particle backscatter ratio at 1064 nm over Leipzig, Germany on 29 May, 2003 from 20 UTC to 21 UTC. The vertical and temporal resolutions are 60 m and 30 s, respectively. **(b)** ECMWF (dotted line) and GFS (solid line) FLEXPART simulation profiles over Leipzig averaged between 18 and 21 UTC of 29 May, 2003. **(c)** Total column residence time of 50 000 particles from a 20 days FLEXPART backward simulation starting at Leipzig on 29 May, 2003 at 21 UTC. The scale is in percentage of the maximum residence time given below the panel.

3.4 Smoke over Germany (16th day)

During the two days following 27 May, the smoke maximum over southern Norway was dissipated by diffluent flow on the edge of a strong ridge building to the south-west. Parts of the plume encroached on eastern Germany and continued to merge with the remnants of the eastern European plume which had been advected directly out of Russia. Observations from the Raman lidar at Leipzig, Germany on 29 May (51.35° N, 12.43° E, 92 m) recorded particle extinction coefficients of 5–30 Mm^{-1} and particle optical depths of 0.03–0.12 at UV and visible wavelengths in the free troposphere from May to July 2003. Such unusually high aerosol levels had never been observed previously since the start of the measurements in 1997 (Mattis et al., 2003) as part of the European Aerosol Research Lidar Network (EARLINET). Lidar measurements from the German aerosol lidar network has been used to observe Canadian forest fire emissions over Germany (Forster et al., 2001). Figure 6a shows a strong lidar backscatter ratio of aerosol at 1064 nm without any separation between the boundary layer and the free tropospheric aerosol layers. Nevertheless, according to radiosonde profiles of potential temperature the boundary layer height was below 2 km (Mattis et al., 2003). One can easily see two maxima, one below 4 km and the other above 5 km. This enhanced aerosol could be observed up to a height of about 6 km.

These lidar results are in good agreement with the FLEXPART forest fire CO simulations with ECMWF (dotted line) and GFS (solid line) data (Fig. 6b), which also show double maxima at similar altitudes over Leipzig between 18–21 UTC on 29 May 2003. Figure 6c shows FLEXPART backward simulation beginning at Leipzig, Germany. It represents the sum of the residence time of the air arriving at the receptor determine on a uniform grid. Further backward calculations suggest that the lower and larger maximum corresponds to parts of the smoke plume which had been over southern Norway two days earlier. The upper and smaller maximum is associated with the remnants of a thin filament which was stretched southwards across Ireland and western France on 25 May (Fig. 5a) and was subsequently advected eastwards, reaching western Germany on 27 May (Fig. 5c). It is also probable that these plumes will have begun to merge by this time with smoke which had been continuing to spread out of Russia directly from the east. The simulated CO tracer concentrations at Leipzig are relatively low but extend over a large altitude range. In the FLEXPART vertical cross section through the latitude at Leipzig (Fig. 5f), Leipzig is close to the edges of the two simulated smoke plumes. The large observed lidar backscatter ratios suggest that in reality Leipzig may have been closer to the center of at least one of the two plumes.

4 Conclusions

In this paper, we investigated the transport of smoke from Russian boreal forest fires from 10 to 31 May, 2003 using the Lagrangian dispersion model, FLEXPART, comparing simulations based on ECMWF and GFS meteorological data.

The transport of the smoke plumes was unique in the sense that, within 17 days, smoke had circumnavigated the globe: perhaps the first time this has been so clearly documented. From the source, smoke crossed the Bering Sea to Alaska, where it was visible in SeaWiFS imagery and then quickly crossed to eastern Canada, where the MODIS Terra satellite witnessed it. It proceeded across the Atlantic to Europe, as captured in a further SeaWiFS image, on its way back to Russia and began to merge over Europe with smoke which had been advected directly out of Russia westwards. By the end of May 2003 the plume had engulfed much of the Northern Hemisphere. The fact that haze plumes from boreal forest fires can circumnavigate the globe and can persist for longer than two weeks has large implications for the radiative heating of the atmosphere (Fiebig et al., 2002). Not accounting for such plumes in climate model simulations or numerical weather predictions may possibly lead to large errors.

FLEXPART simulations based on both ECMWF and GFS data could reproduce much of the fine-scale structure seen in the satellite images with remarkable accuracy, even after the smoke plume had travelled almost around the northern hemisphere. It is not clear from our results which of the two simulations is in better agreement with the observations.

Acknowledgements. We acknowledge ECMWF and the German Weather Service for permitting access to the ECMWF archives and also NCEP for the GFS data. We appreciate the provision of data via the internet by the science teams of MODIS, TOMS and SeaWiFS. This study was funded by the European Commission in the European Research Framework 5 program as part of the PARTS (no. EVK2CT200100112) project and the German Federal Ministry for Education and Research in the Framework of the Atmospheric Research 2000 program as part of the NOXTRAM (07 ATF05) and ATMOFAST (07 ATF08) projects.

Edited by: A. Hofzumahaus

References

Andreae, M. O.: Biomass burning: Its history, use and distribution and its impact on environmental quality and global climate, in Global Biomass Burning: Atmospheric, Climate, and Biospheric Implications, edited by Levine, J. S., pp. 3–21, MIT Press, Cambridge, Mass, 1991.

Andreae, M. O. and Merlet, P.: Emissions of trace gases and aerosols from biomass burning, Global Biogeochem. Cycles, 15, 955–977, 2001.

Beirle, S., Platt, U., Wenig, M., and Wangner, T.: Weekly cycle of NO_2 by GOME measurements: a signature of anthropogenic sources, Atmos. Chem. Phys., 3, 2225–2232, 2003.

Cahoon, D. R., Stocks, B. J, Levine, J. S., Cofer III, W. R., and Pierson, J. M.: Satellite analysis of the severe 1987 forest fires in northern China and southeastern Siberia, J. Geophys. Res., 99, 18 627–18 638, 1994.

Christopher, S., Chou, J., Chang, J., Lin, X., Berendes, T. A., and Welch, R. M.: Shortwave direct radiative forcing of biomass burning aerosols estimated using VIRS and CERES data, Geophys. Res. Lett., 27, 2197–2200, 2000.

Chu, D. A., Kaufman, Y. J., Ichoku, C., Remer, L. A., Tanre, D., and Holben, B. N.: Validation of MODIS aerosols optical depth retrieval over land, Geophys. Res. Lett., 29, 12, doi:10.1029/2001GL013205, 2002.

Cofer, W. R., Winstead, E. L., Stocks, B. J., Goldammer, J. G., and Cahoon, D. R.: Crown fire emissions of CO_2, CO, H_2, CH_4, and TNMHC from dense jack pine boreal forest fire, Geophys. Res. Lett., 25, 3919–3922, 1998.

Conard, S. G. and Ivanova, G. A. : Wildfire in Russian boreal forests – potential impacts of fire regime characteristics on emissions and global carbon estimates, Envir. Pol., 98, 305–313, 1998.

Conard, S. G., Sukhinin, A. I., Stocks, B.J., Cahoon, D. R., Davidenko, E. P., and Ivanova, G. A.: Determining effects of area burned and fire severity on carbon cycling and emissions in Siberia, Climate Change, 55, 197–211, 2002.

Crutzen, P. J.: A discussion of the chemistry of some minor constituents in the stratosphere and troposphere, Pure Appl. Geophys., 106–108, 1385–1399, 1973.

Daniel, J. S. and Solomon, S.: On the climate forcing of carbon monoxide, J. Geophys. Res., 103, 13 249–13 260, 1998.

ECMWF: User Guide to ECMWF Products 2.1, Meteorol. Bull. M3.2, ECMWF, Reading, UK, 1995.

Edwards, D. P., Lamarque, J.-F., Attie, J.-L., Emmons, L. K., Richter, A., Cammas, J.-P., Gille, J. C., Francis, G. L., Deeter, M. N., Warner, J., Ziskin, D. C., Lyjak, L. V., Drummond, J. R., and Burrows, J. P.: Tropospheric ozone over the tropical Atlantic: A satellite perspective, J. Geophys. Res., 108, 4237, doi:10.1029/2002JD002927, 2003.

Emanuel, K. A. and Zivkovic-Rothman, M.: Development and evaluation of a convection scheme for use in climate models, J. Atmos. Sci., 56, 1766–1782, 1999.

Fiebig, M., Petzold, A., Wandinger, U., Wendisch, M., Kiemle, C., Stifter, A., Ebert, M., Rother, T., and Leiterer, U.: Optical closure for an aerosol column: Method, accuracy, and inferable properties applied to a biomass-burning aerosol and its radiative forcing, J. Geophys. Res., 107, 8130, doi:10.1029/2000JD000192, 2002.

Formenti, P., Reiner, T., Wendisch, M., et al.: : STAAARTE-MED 1998 summer airborne measurements over the Aegean Sea, 1, Aerosol particles and trace gases, J. Geophys. Res., 107, 4450, doi:10.1029/2001JD001337, 2002.

Forster, C., Wandinger, U., Wotawa, G., James, P., Mattis, I., Althausen, D., Simmonds, P., O'Doherty, S., Jennings, S., Kleefeld, C., Schnieder, J., Trickl, T., Kreipl, S., Jäger, H., and Stohl, A.: Transport of boreal forest fire emissions from Canada to Europe, J. Geophys. Res., 106, 22 887–22 906, 2001.

Fromm, M., Alfred, J., Hoppel, K., Hornstein, J., Bevilacqua, R., Shettle, E., Servranckx, R., Li, Z., and Stocks, B.: Observations of boreal forest fire smoke in the stratosphere by POAM III, SAGE II, and lidar in 1998, Geophys. Res. Lett., 27, 1407–1410, 2000.

Fromm, M. D. and Servranckx, R.: Transport of forest fire smoke above the tropopause by supercell convection, Geophys. Res. Lett., 30, 1542, doi: 1029/2002GL016820, 2003.

Galanter, M., Levy II, H., and Carmichael, G. R.: Impacts of biomass burning on tropospheric CO, NO_x, and O_3, J. Geophys. Res., 105, 6633–6653, 2000.

Global Fire Monitoring Center (GFMC): Daily/weekly updates of forest fires in the Russian Federation, http://www.fire.uni-freiburg.de/current/globalfire.htm, 2003.

Gordon, H. R. and Wang M.: Retrieval of water-leaving radiance and aerosol optical thickness over the oceans with SeaWiFS: a preliminary algorithm, Appl. Opt., 33, 443–452, 1994.

Hooker, S. B., Mcclain, C. R., and Holmes, A.: Ocean color imaging – Costal Zone Color Scanner (CZCS) to Sea WiFS, Marine Technology Society Journal, 27, 3–15, SPR, 1993.

Hsu, N. C., Herman, J., Gleason, J., Torres, O., and Seftor, C.: Satellite detection of smoke aerosols over a snow/ice surface by TOMS, Geophys. Res. Lett. 26, 1165–1168, 1999.

IPCC: Climate Change, edited by Nebojsa Nakicenovic and Rob Swart, Cambridge Univ. Press, New York, 2001.

Justice, C. O., Kendall, J. D., Dowty, P. R., and Scholes, R.: Satellite remote sensing of fires during the SAFARI campaign using NOAA advanced very high radiometer data, J. Geophys. Res., 101, 23 851–23 863, 1996.

Kasischke, E. S., Stocks, B. J., Oneill, K., French, N. H., and Bourgeau-Chavez, L. L.: Direct effects of fire on the boreal forest carbon budget, in Biomass burning and its Inter – Relationships with the Climate System, edited by Innes, J. L., Beniston, M., and Verstraete, M. M., pp. 51–68, Kluwer Academic Publishers, Dordrecht, Netherlands, 2000.

Kasischke, E. S. and Bruhwiler, L. P.: Emissions of carbon dioxide, carbon monoxide, and methane from boreal forest fires in 1998, J. Geophys. Res., 108, 8146, doi:10.1029/2001JD000461, 2003.

Kaufman, Y. J., Justice, C. O., Flynn, L. P., Kendall, J. D., Prins, E. M., Giglio, L., Ward, D. E., Menzel, W. P., and Setzer, A. W.: Potential global fire monitoring from EOS-MODIS, J. Geophys. Res., 103, 32 215–32 238, 1998.

Kaufman, Y. J., Ichoku, C., Giglio, L., Korontzi, S., Chu, D. A., Hao, W. M., Li, R.-R., and Justice, C. O.: Fire and smoke observed from Earth Observing System MODIS instrument – products, validation, and operational use, Int. J. Remote Sensing, 24, 1765–1781, 2003.

Lavoue, D. C., Liousse, C., Cachier, H., Stocks, B. J., and Goldammer, J. G.: Modelling of carbonaceous particles emitted by boreal and temperate wildfires at northern latitudes, J. Geophys. Res., 105, 26 871–26 890, 2000.

Logan, J. A., Prather, M. J., Wofsy, S. C., and McElroy, M. B.: Tropospheric chemistry: A global perspective, J. Geophys. Res., 86, 7210–7254, 1981.

Mattis, I., Ansmann, A., Wandinger, U., and Müller, D.: Unexpectedly high aerosol load in the free troposphere over Central Europe in spring/summer 2003, Geophys. Res. Lett., 30, 2178, doi:10.1029/2003GL018442, 2003.

Platt, U.: Differential optical absorption spectroscopy (DOAS), in air monitoring by spectroscopic techniques, M. W. Sigrist (Ed.), Chemical Analysis Series vol. 127, John Wiley, New York, 1994.

Remer, L. A., Tanre, D., Kaufman, Y. J., Ichoku, C., Mattoo, S., Levy, R., Chu, D. A., Holben, B. N., Dubovik, O., Ahmad, Z., Smirnov, A., Martins, J. V., and Li, R.-R.: Validation of MODIS aerosol retrieval over ocean. Geophys. Res. Lett. 29, 12, doi:10.1029/2001GL013204, 2002.

Seinfeld, J. H. and Pandis, S. N.: Atmospheric Chemistry and Physics, 1326pp., John Wiley, Inc., New York, 1998.

Shvidenko, A. Z., and Nilsson, S.: Fire and the carbon budget of Russian forest, in Fire, Climate Change, and Carbon Cycling in the Boreal Forest, edited by E. S. Kasischke, Ecol. Stud., 138, 289–311, 2000

Shvidenko, A. and Goldammer, J. G.: Fire situation in Russia, International Forst Fire News, 24, 41–59, 2001.

Soja, A. J., Sukhinin, A. I., Cahoon, D. R., Shugart, H. H., and Stackhouse, P. W.; AVHRR-derived fire frequency, distribution and area burned in Siberia, Int. J. Remote Sensing, 25, 1939–1960, 2004.

Spichtinger, N., Wenig, M., James, P., Wagner, T., Platt, U., and Stohl, A.: Satellite detection of a continental-scale plume of nitrogen oxides from boreal forest fires, Geophys. Res. Lett., 28, 4579–4583, 2001.

Stohl, A., Hittenberger, M., and Wotawa, G.: Validation of the Lagrangian particle dispersion model FLEXPART against large scale tracer experiment data, Atmos. Environ., 24, 4245–4264, 1998.

Stohl, A. and Trickl, T.: A textbook example of long-range transport: Simultaneous observation of ozone maxima of stratospheric and North American origin in the free troposphere over Europe, J. Geophys. Res., 104, 30 445–30 462, 1999.

Stohl, A. and Thomson, D. J.: A density correction for Lagrangian particle dispersion models, Boundary-Layer Meteorol., 90, 155–167, 1999.

Stohl, A.: A one-year Lagrangian climatology of airstreams in the northern hemisphere troposphere and lowermost stratosphere, J. Geophys. Res., 106, 7263–7279, 2001.

Stohl, A., Eckhardt, S., Forster, C., James, P., and Spichtinger, N.: On the pathways and timescales of intercontinental air pollution transport, J. Geophys. Res., 107, 4684, doi:10.1029/2001JD001396, 2002.

Valendick, E. N.: Ecological aspects of forest fires in Siberia, Sib. Ecol. J., 1, 1–8, 1996.

Wandinger, U., Bockmann, C., Mathias, V., et al.: Optical and microphysical characterization of biomass- burning and industrial-pollution aerosols from multiwavelength lidar and aircraft measurements, J. Geophys. Res., 107, 8125, doi:10.1029/2000JD000202, 2002.

Wotawa, G. and Trainer, M.: The influence of Canadian forest fires on pollutant concentrations in the United States, Science, 288, 324–328, 2000.

Yoshizumi, K., Kato, S., Streets, D. G., Tsai, Y. N., Shvidenko, A., Nilsson, S., McCallum, I., Minko, N. P., Abushenko, N., Altyntsev, D., and Khodzer, T. V.: Boreal forest fires in Siberia in 1998: Estimation of area burned and emissions of pollutants by advanced very high resolution radiometer satellite data, J. Geophys. Res., 107, 4745, doi:10.1029/2001JD001078, 2002.

ARTICLE 3

Atmos. Chem. Phys., 4, 1857–1868, 2004
www.atmos-chem-phys.org/acp/4/1857/
SRef-ID: 1680-7324/acp/2004-4-1857

Atmospheric Chemistry and Physics

Boreal forest fires in 1997 and 1998: a seasonal comparison using transport model simulations and measurement data

N. Spichtinger[1], R. Damoah[1], S. Eckhardt[1], C. Forster[1], P. James[1], S. Beirle[2], T. Marbach[2], T. Wagner[2], P.C. Novelli[3], and A. Stohl[4]

[1]Department of Ecology, Technical University of Munich, Germany
[2]Institute for Environmental Physics, University of Heidelberg, Germany
[3]NOAA, Climate Monitoring and Diagnostics Laboratory, Colorado
[4]Cooperative Inst. for Research in Environmental Sciences (CIRES), Univ. of Colorado/NOAA Aeronomy Laboratory, USA

Received: 9 January 2004 – Published in Atmos. Chem. Phys. Discuss.: 18 May 2004
Revised: 16 August 2004 – Accepted: 19 August 2004 – Published: 14 September 2004

Abstract. Forest fire emissions have a strong impact on the concentrations of trace gases and aerosols in the atmosphere. In order to quantify the influence of boreal forest fire emissions on the atmospheric composition, the fire seasons of 1997 and 1998 are compared in this paper. Fire activity in 1998 was very strong, especially over Canada and Eastern Siberia, whereas it was much weaker in 1997. According to burned area estimates the burning in 1998 was more than six times as intense as in 1997. Based on hot spot locations derived from ATSR (Along Track Scanning Radiometer) data and official burned area data, fire emissions were estimated and their transport was simulated with a Lagrangian tracer transport model. Siberian and Canadian forest fire tracers were distinguished to investigate the transport of both separately. The fire emissions were transported even over intercontinental distances. Due to the El Niño induced meteorological situation, transport from Siberia to Canada was enhanced in 1998. Siberian fire emissions were transported towards Canada and contributed concentrations more than twice as high as those due to Canada's own CO emissions by fires. In 1998 both tracers arrive at higher latitudes over Europe, which is due to a higher North Atlantic Oscillation (NAO) index in 1998. The simulated emission plumes are compared to CMDL (Climate Monitoring and Diagnostics Laboratory) CO_2 and CO data, Total Ozone Mapping Spectrometer (TOMS) aerosol index (AI) data and Global Ozone Monitoring Experiment (GOME) tropospheric NO_2 and HCHO columns. All the data show clearly enhanced signals during the burning season of 1998 compared to 1997. The results of the model simulation are in good agreement with ground-based as well as satellite-based measurements.

Correspondence to: N. Spichtinger
(spichtinger@forst.tu-muenchen.de)

1 Introduction

Biomass burning causes large emissions of carbon dioxide (CO_2), carbon monoxide (CO), nitrogen oxides (NO_x), methane (CH_4), aerosols and other trace substances, which influence the concentrations of trace gases and aerosols in the atmosphere and affect the atmosphere in various ways. CO_2 and CH_4 are important greenhouse gases, contributing to global warming. The solar radiation budget is strongly affected by the aerosols emitted by the forest fires, too (Asakuma et al., 2002; Torres et al., 1998, 2002). Finally, forest fires can even be a source of stratospheric aerosols (Fromm and Servranckx, 2003). Tropospheric chemistry is influenced by the emissions of CO and NO_x, precursors of tropospheric ozone (O_3) (Chan et al., 2003) – an effective greenhouse gas itself –, and nitric acid (HNO_3), a product which is part of the nitrogen chemical reaction cycle, leading to acid rain (Jaegle et al., 1998). Boreal fires emit relatively large quantities of NO_x due to high burning temperatures, especially during the appearance of crown fires, which account for most of the areas burned in the boreal fire regime (Kajii et al., 2002; Cofer et al., 1998). Additionally, other trace gases are emitted like methyl bromide and methyl chlorine which are involved in catalytic cycles of stratospheric O_3 destruction.

The input of biomass burning emissions into the atmosphere is often discussed as a phenomenon of the tropical rain forest and savannas (Crutzen and Merlet, 1990; Andreae et al., 2001; Andreae and Merlet, 2001). However, the boreal forest contains one third of the terrestrial carbon storage, boreal burning emits up to 20 percent of the global biomass burning CO (Conard and Ivanova, 1997) and temperature increases are expected as a consequence of climate change (Stocks et al., 1998) in the ecologically sensitive high

Table 1. Areas burned [Mha] in Canada and Siberia during the years 1997 and 1998, according to different sources: [a] UNECE (1999), [b] Conard et al. (2002),[c] Kasischke and Bruhwiler (2003).

Siberia	Canada	Year
Area Burned		
0.98	0.62	1997[a]
5.34	4.71	1998[a]
13.3		1998[b]
boreal region		
17.9		1998[c]

Table 2. Hot spots detected on the basis of ATSR night-time data for the years 1997 to 2001.

	hot spot counts	
year	Canada	Siberia
1997	974	6321
1998	8701	21721
1999	3588	5803
2000	3469	8302
2001	1797	5031

northern latitudes, possibly leading to enhanced fire activity in the future (Flannigan, 1998). Furthermore, the lifetimes of many trace gases and aerosols in the atmosphere are much longer in the boreal region than in the tropics. Because low annual average temperatures and dryness lead to accumulation of ground fuel through slow decomposition processes, boreal fires consume large amounts of fuel, burn with high intensity and spread particularly fast. Furthermore, boreal fires are subjected to a strong interannual variability (Amiro et al., 2001). Finally, boreal forest fires are not only a local disturbance factor but, due to atmospheric transport processes, they affect tropospheric chemistry on regional (Kato et al., 2002; Tanimoto et al., 2000) and even continental and hemispheric scales (Fromm et al., 2000; Wotawa and Trainer, 2000; Forster et al., 2001; Spichtinger et al., 2001; Wotawa et al., 2001).

Boreal forest fires occur mainly from May to October (Lavoue et al., 2000) and are most frequent in Canada and Siberia. The 1998 burning season in the boreal region was much more active than the 1997 one (Table 1). 1998 was one of the worst five years since forest fires are recorded in Canada (Svidenko and Goldammer, 2001), and one of the most severe years during the last 15 years in Siberia (UNECE, 1999).

Strong burning is favoured by drought conditions and high temperatures (Svidenko and Goldammer, 2001; Kajii et al., 2002; French et al., 2003). Cahoon et al. (1994), for instance, described how high temperatures, dryness and strong winds lead to extensive forest fires in China in 1987. During the last three decades the burned area in the boreal region shows a positive trend, a consequence of increasing temperatures. Especially the years with very strong fire activity all coincided with positive temperature anomalies (Kasischke and Bruhwiler, 2003; Stocks et al., 1998; Flannigan, 1998). South East Siberia normally experiences dry anti cyclonic conditions in combination with the monsoon circulation until July and then shifts into a cyclonic humid situation. In 1998 midlatitude cyclones did not reach latitudes higher than 30°–35° N and it remained dry and hot east of the Okhotsk Sea longer than normal (Efremov and Sheshukov, 2000). Fig. 1 shows maps of the temperature anomalies from June to August for the years 1997 and 1998, calculated using NCAR/NCEP reanalysis data. In 1998 most of the northern hemisphere features positive temperature anomalies. Regions with extremely high values, up to 4.5 K, are found in the boreal burning regions in northern and central Canada and eastern Siberia, respectively. In 1998 in most parts of these regions high temperatures are combined with less than normal precipitation (Fig. 2). Thus, fire-favouring meteorological conditions prevailed in 1998 presumably due to the strong El Niño/Southern Oscillation event of 1997/1998 (Kita et al., 2000; Novelli et al., 2003; Duncan et al., 2003). In contrast, no large anomalies are found for 1997.

This paper compares measurement data from various sources (surface measurements of CO and CO_2 from a flask sampling network, aerosol index values and columns of tropospheric NO_2 and HCHO from satellite remote sensing) and transport model simulations for the years 1997 and 1998. In the next section, estimates for the areas burnt and the respective trace gas emissions in 1997 and 1998 are made. In Sect. 3, the measurement data and model simulations are described. In Sect. 4, results from the transport model simulations are shown, and in Sect. 5 analyses of the measurement data are presented. Finally, conclusions are drawn in Sect. 6.

2 Areas burned and emissions

Data on the areas burned and emissions from fires are the basis and at the same time the limiting factor for the quality of quantitative transport modelling of biomass burning plumes. Different estimates of total areas burned in Canada and Siberia are shown in Table 1. According to official data, more than 10 million ha were burned in both regions in 1998 (UNECE, 1999), which is more than six times the area burned in 1997. However, it is known that the Russian official data strongly underestimate the burned areas in Siberia (Conard and Ivanova, 1997; Conard et al., 2002), where a large number of forest fires remain undetected (Cahoon et al., 1994). Using remote sensing data, Kasischke and Bruhwiler (2003) estimated that 17.9 million ha forest burned in the boreal region in 1998, the largest area burned of the decade. For comparison, in 1997 an area of just 1.6 million ha has burned

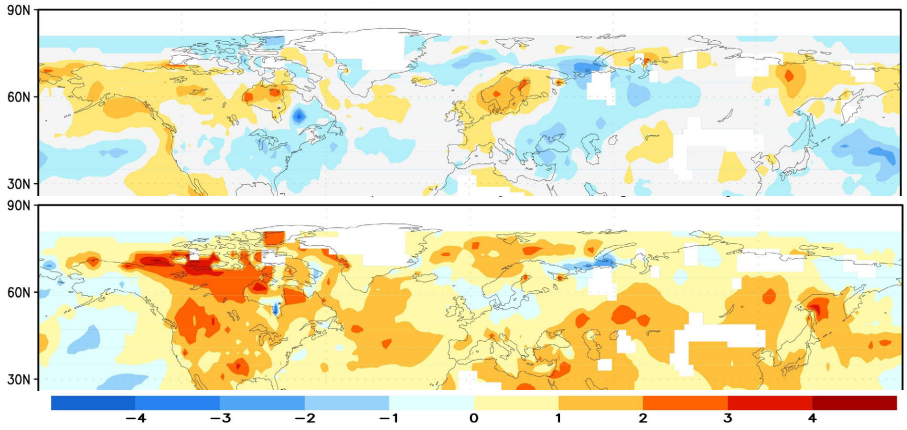

Fig. 1. Climatological surface temperature anomaly [K] from June to August of 1997 (top) and 1998 (bottom), according to NCEP reanalysis data.

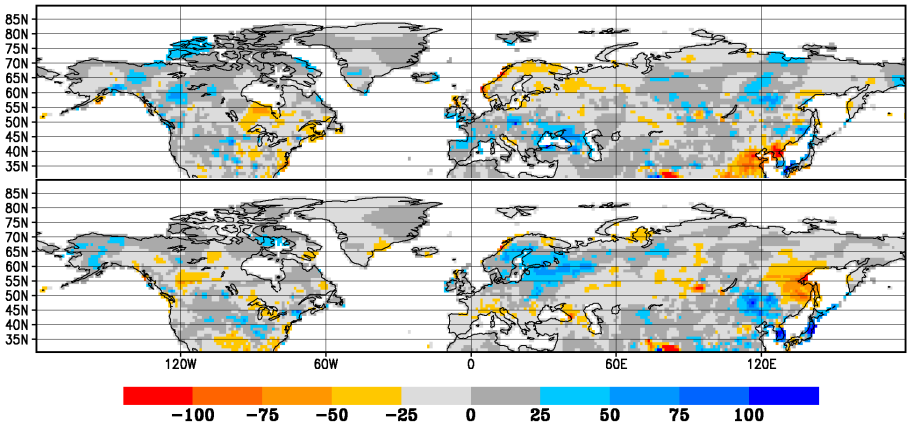

Fig. 2. Precipitation anomaly [mm/month] from June to August of 1997 (top) and 1998 (bottom), according to GPCC (Global Precipitation Climatology Centre) data.

(UNECE, 1999) (Table 1). Official data from UNECE (1999) suggest similarly large areas burned in Canada and Siberia in 1998 (Table 1). But Kasischke and Bruhwiler (2003) estimated that 29 % of the total area was burned in Canada and 71% in Siberia. Unfortunately, more detailed fire inventories are not available, especially not for Siberia.

Therefore, night-time fire hot spots, based on data from the ATSR instrument flying on the ERS-2 platform (see http://shark1.esrin.esa.it/ionia/FIRE/), were used for characterizing the spatial distribution of the fires. Coordinates of hot spot locations are available on a daily basis for the period 1997 to 2001 and their total numbers are shown in Table 2. There is a high variation of the number of hot spots detected during the different years. 1997 has a below-average occurrence of hot spots, especially in Canada, whereas 1998 stands out as the year with most hot spot detections both in Canada and Siberia. In 1997 (Fig. 3 top), hot spots were detected mainly in the United States of America, Europe and Southern Asia, but in 1998 (Fig. 3 bottom) regions with high density of fire hot spots can be seen in Canada and Eastern Siberia. A distinct maximum of hot spot occurrence was located over the Russian Far East, whereas the rest of Russia experienced a moderate fire season (Conard et al., 2002). The Russian Far East always has a very high fire danger because of the recurrence of drought conditions, the regional meteorological and topographical situation and the abundance of combustible material (Efremov and Sheshukov, 2000). However, in 1998 the situation was extreme, due to the strong drought caused by the El Niño/Southern Oscillation (Generoso et al., 2003; Novelli et al., 2003).

The hot spot data cannot directly be used to estimate the areas burned, and therefore we have to use other sources for this information. The ratio between Siberian and Canadian ATSR hot spot counts in 1998 is around 2.5 (see Table 2) in good agreement with the burned area estimation of Kasischke and Bruhwiler (2003). In order to obtain the same ratio

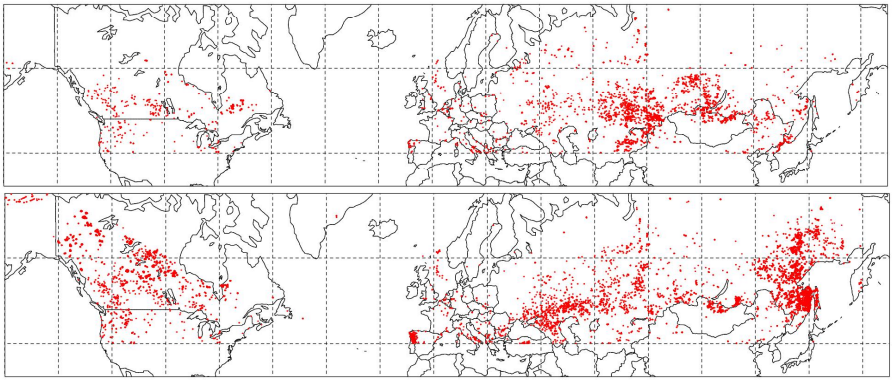

Fig. 3. ATSR hot spots summed from May to October of 1997 (top) and 1998 (bottom).

Table 3. Emitted masses of CO [Tg] derived from the FLEXPART model setup.

	Siberia		Canada	
	1997	1998	1997	1998
May	2.45	3.37	0.25	2.07
June	1.31	2.85	1.27	1.12
July	0.79	13.28	0.26	7.01
Aug	1.04	21.51	0.34	8.77
Sep	1.55	11.10	0.29	1.96
Oct	2.52	1.21	0.37	0.52
total	9.68	53.68	2.78	21.45

between Canadian and Siberian burned areas the official estimate (UNECE, 1999) for the total burned area in Canada was multiplied by a factor of 2.5. Therefore for the simulation of the burning period of 1998 4.7 Mha and 11.7 Mha burned area were assumed for Canada and Siberia, respectively. Using the estimates of total area burned and the number of hot spots detected in 1997 and 1998, we estimate that, on average, a hot spot covered an area of 380 ha in 1997 and 540 ha in 1998. Although the actual areas burned may vary considerably from hot spot to hot spot, assuming that they all burned equal areas, we can use the hot spot data to determine the temporal and spatial variation of the burning, which were needed for the emission estimates. Because of the biases of satellite detection due to, e.g. cloud cover and smoke (Kasischke et al., 2003), the burned areas we use are rough assumptions.

In our model simulations we used a CO tracer to study the prevailing transport patterns and thus needed an estimate for the CO emissions. Emission factors for CO are normally based on the amount of biomass burned. For instance, Andreae et al. (2001) estimate 107 g CO/kg biomass burned. In order to apply this emission factor, we need to know the amount of biomass burned. Cofer et al. (1998) report fuel consumption rates for boreal forest fires of 4.27 kg/m^2. Using this rate together with our previous estimates of the areas burned, we can determine the emission rates of trace gases. Table 3 shows the monthly variation of the estimated CO emissions for both Siberia and Canada in 1997 and 1998 based on this algorithm. Total CO emissions of Canada and Siberia were estimated as around 75 Tg in 1998 and about 12 Tg in 1997. Compared to Canada's anthropogenic CO emissions of 52.7 Tg/y (see EDGAR emission inventory (1995), http://arch.rivm.nl/env/int/coredata/edgar/) Siberian CO emissions by fires in 1998 are around equal.

Our estimates of the CO emissions (see Table 3) are in good agreement with those of Kasischke and Bruhwiler (2003) and Duncan et al. (2003) who estimated that 88–102 Tg and 70 Tg, respectively, of CO were emitted in the boreal region in the year 1998, and with the values given by Kajii et al. (2002), who calculated that 50 Tg CO were emitted in Siberia, in 1998. Finally, Novelli et al. (2003) calculated emissions of 300 Tg CO by all fires (including fires in the tropics) that burned during the El Niño in 1997/1998. Thus, based on our assumption of 75 Tg CO the boreal region contributed a substantial fraction, 25%, to the total fire emissions in 1997/1998. Compared to the averaged global CO emissions by biomass burning of 748 Tg/a estimated by Holloway et al. (2000) and Galanter et al. (2000), the boreal region accounted for about 10% in 1998 and 1.6% in 1997.

3 Data and Methodology

The transport of forest fire emissions was simulated with the Lagrangian particle dispersion model FLEXPART (version 5.1) (Stohl et al. 1998,http://www.forst.tu-muenchen.de/EXT/LST/METEO/stohl/) for the burning seasons of 1997 and 1998 from May to October. For this study, FLEXPART was used with northern hemispheric data from the European Centre for Medium-Range Weather Forecasts (ECMWF, 1995) with a horizontal resolution of 1×1 degree, 31 vertical levels and a time resolution of 3 h (analyses at 0, 6, 12,

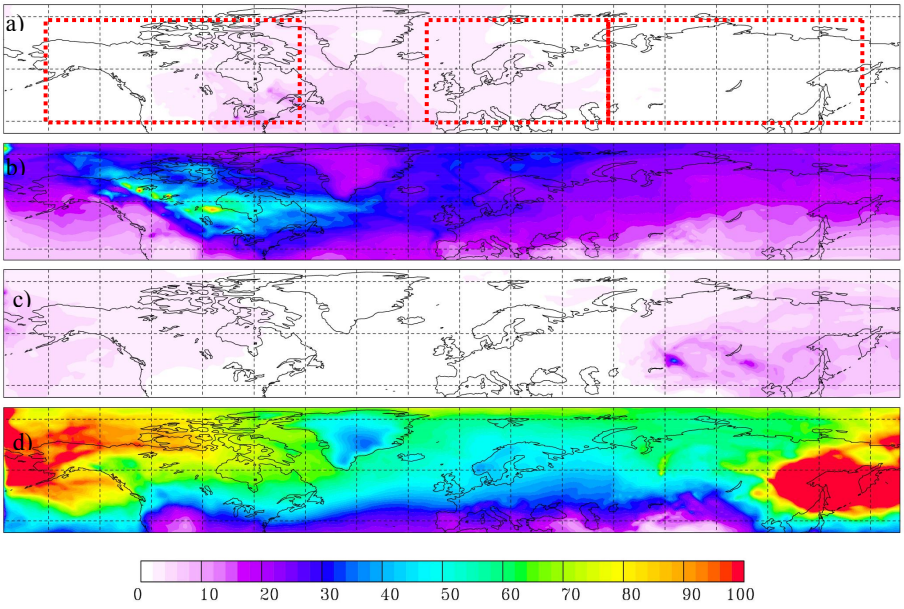

Fig. 4. Total columns of FLEXPART CO tracers [mg/m^2] averaged from May to October: **(a)** Canadian CO tracer (1997), **(b)** Canadian CO tracer (1998), **(c)** Siberian CO tracer (1997) and **(d)** Siberian CO tracer (1998). The red boxes in panel (a) show the regions used for calculating source-receptor-relationships (see text for more details).

18 UTC; 3-hour forecasts at 3, 9, 15, 21 UTC). FLEXPART calculates the trajectories of a multitude of particles to simulate the transport of passive tracers. We simulated tracers for CO emitted by boreal forest fires, which were released according to our emission estimates (see Sect. 2), but for which deposition and chemical processes were considered only by applying a constant chemical lifetime of 60 days for the CO tracers. The lifetime of the CO tracer is assumed as a mean of the global lifetime of CO which is given by Seinfeld and Pandis (1998) within the range of 30 to 90 days. Independent CO tracers were used for Canadian and Siberian forest fires (according to Canadian and Siberian box shown in Fig. 4a) , in order to distinguish between these two sources. CO emissions were put into the lowest 3 km of the model atmosphere. In order to see whether the simulated forest fire plumes appear also in observations, NOAA CMDL flask data, TOMS aerosol index data and GOME tropospheric NO_2 and HCHO columns were inspected.

The NOAA CMDL Carbon Cycle Greenhouse Gases group makes measurements of CO_2 and CO. These measurements form a global network of background sites for carbon cycle monitoring (Novelli et al., 2003; Randerson et al., 1999), which measure continuously since the end of the 1970s. CO_2 data are available since 1982 and CO data since 1990.

The TOMS instrument on board the Earth Probe satellite (for further details, see http://toms.gsfc.nasa.gov/) provides data on UV-absorbing tropospheric aerosols, including dust, volcanic ash and smoke from biomass burning. Absorbing particles are determined by a differencing method, which is more sensitive for UV-absorbing aerosols than for non-absorbing aerosols like clouds and sulfur particles (Hsu et al., 1996). Forest fires, desert dust, volcanic ash and anthropogenic sources all create absorbing particles, but in high-latitude regions forest fires are the main source of these particles in summer.

GOME tropospheric NO_2 column densities are used to see whether boreal forest fires are a significant source of NO_x. Spichtinger et al. (2001) have found strong enhancements of NO_2 above a fire burning in Canada in 1998, but it is important to clarify whether boreal forest fires can also create NO_2 anomalies on a seasonal basis. The tropospheric NO_2 columns are supplemented by tropospheric HCHO columns, because HCHO is a primary emission product from biomass burning (Carlier et al., 1986; Lipari et al., 1984). Maps of tropospheric NO_2 columns and tropospheric HCHO columns were derived from spectroscopic data from the GOME instrument on board the ERS-2 satellite, which was launched into a polar sun-synchronous orbit in April 1995. Raw spectral data undergo several processing steps, as described in Beirle et al. (2003), to obtain tropospheric NO_2 columns. Basically, differential optical absorption spectroscopy (DOAS) is used to produce total vertical NO_2 column densities, from which an estimate of the stratospheric portion is subtracted. HCHO slant columns are also determined from GOME spectra by using algorithms developed at the IUP Heidelberg, with basically the same DOAS retrieval method as used for the HCHO ground measurements (Wagner et al., 2004). In contrast to NO_2, the stratospheric HCHO can be neglected. Thus, the retrieved slant columns directly represent

Table 4. Source-receptor relationships for boreal forest fire emissions.

Source	Receptor	Avg. column dens. [mg/m^2(%)[1]]	Avg. surface mix. ratio [ppb]
	1997	CO	
Russia	Canada	2.7 (18)	0.3
Russia	Russia	6.2 (37)	0.5
Canada	Europe	2.1 (11)	0.1
Canada	Canada	2.3 (28)	0.2
	1998	CO	
Russia	Canada	69 (26)	6.8
Russia	Russia	91 (22)	7.4
Canada	Europe	24 (13)	2.3
Canada	Canada	29 (32)	2.4

Percentage of FLEXPART total emitted mass [1].

the tropospheric HCHO. However, we applied an offset correction to account for GOME degradation effects for each latitude: the slant column densities over oceans, supposed to be zero, have been subtracted to normalize the HCHO slant columns. With a ground pixel size of $40\times320\,\mathrm{km}^2$ GOME data have a global coverage at the equator every 3 days, but better time resolution in polar regions.

4 Transport Modelling

In order to evaluate the dominating transport patterns of boreal forest fire emissions on a seasonal basis, the FLEXPART model results for the Siberian and Canadian CO tracers were averaged over the burning seasons of 1997 and 1998. Figure 4 shows the total columns of the CO tracers for the Canadian and Siberian tracers during the burning seasons of the two years. Due to the fewer fires in 1997 simulated CO columns are lower than in 1998. In both years the largest CO tracer columns are found directly over the source regions, but significant transport to downwind regions occurs. The Canadian fire plume moves eastward across the Atlantic ocean towards Europe. Siberian fire emissions take a pathway eastwards across the Northern Pacific towards Canada. Taking this pathway, the fire plume also travels over northern Japan, where in 1998 Japanese surface CO measurements showed a maximum difference of about 30 ppb between air masses which have and those which have not passed the 1998 Siberian fires according to trajectory analyses (Kato et al., 2002). Additionally, Tanimoto et al. (2000) found baseline enhancements and episodic high concentrations of CO at the measurement site of Rishiri, Japan, during the boreal burning season of 1998. To estimate the extent of intercontinental transport of the forest fire emissions, the relative CO tracer amounts remaining close to the source and reaching another continent were calculated by defining three boxes for the latitude band 40°–80° N: Canada (160°–60° W), Europe (10° W–60° E) and Siberia (60°–140° E) (see Fig. 4a). As shown in Table 4, a larger fraction of the Russian forest fire emissions was transported to Canada in 1998 than in 1997. This is due to the special meteorological situation during the burning season of 1998, when the abnormally persistent high pressure system east of Siberia (Efremov and Sheshukov, 2000) channeled pollution across the northern Pacific. In 1998, the average column densities of the Siberian tracer are more than twice as high as the Canadian tracer columns in the Canadian receptor box. At the surface in the Canadian receptor box the Siberian tracer mixing ratio is 6.8 ppb on average (see Table 4 and Fig. 6). Especially at the Canadian west coast, transport from Siberia provided the dominant fraction of the CO tracer (Fig. 4d).

The Canadian CO tracer was transported to similar fractions in both years. But, at the surface the Canadian tracer plume is shifted to the south compared to the total columns (Figs. 6 and 4b), due to the prevailing low-level flows in subtropical latitudes, as compared to the frontal lifting that typically accompanies poleward transport (Stohl, 2001). Canadian forest fire emissions contributed 2.3 ppb of CO to the average European CO surface mixing ratios in 1998. These intercontinental transport processes are documented in more detail in Fig. 5. Meridionally oriented vertical cross sections of zonal means of the forest fire CO tracers for each of the above defined boxes are shown for 1997 and 1998. In all receptor boxes the maxima of all tracers appear at an altitude range from about 2 to 6 km. The highest concentrations of the Siberian tracer over the source region are found at latitudes up to 70° N in both years. Over Canada the Siberian plume is, on average, found at higher altitudes than over the Siberian source region. The Canadian tracer extends to higher latitudes over the source, in 1998 it reached 80° N. Significant differences in the plume positions over Europe are found between the two years. Both tracers arrive at higher latitudes in 1998 than in 1997, which is due to a higher NAO index in 1998 than in 1997, which shifts the North Atlantic stormtrack and, thus, the dominant transport pathway to the north (Eckhardt et al., 2003). In general, drought conditions in parts of the boreal region, which were likely induced by ENSO, caused extensive burning in 1998 with a maximum in the far east of Siberia near the coast of the Okhotsk Sea. From there the emissions are directly subjected to the westerly flow. This is in contrast to 1997, when the hot spots were situated much more westerly in continental regions of Siberia. Furthermore, transport pathways are shifted northwards according to the positive phase of NAO. This produces a shift of the tracer distribution towards higher latitudes in 1998 compared to 1997.

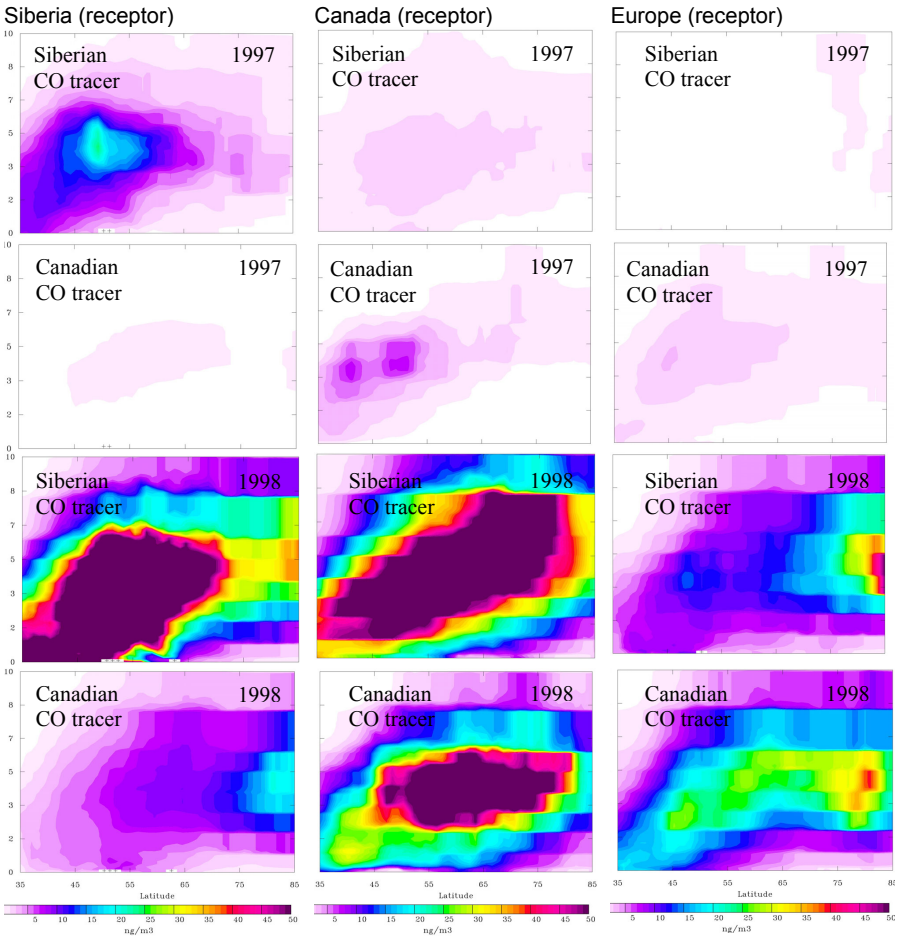

Fig. 5. Vertical cross sections of zonal means of the averaged CO tracer concentrations for the three receptor regions (see Fig.4). Siberia (left column), Canada (middle column) and Europe (right column). The rows from top to bottom show the Siberian CO tracer in 1997, the Canadian CO tracer in 1997, the Siberian CO tracer in 1998 and the Canadian CO tracer in 1998 against altitude [km].

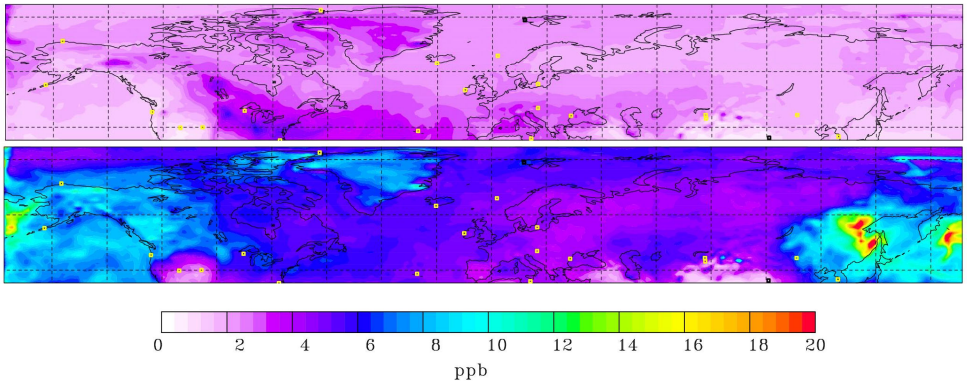

Fig. 6. FLEXPART mixing ratios at the lowest model layer in 1998; Canadian CO tracer (top), Siberian CO tracer (bottom); CMDL stations are marked as yellow squares

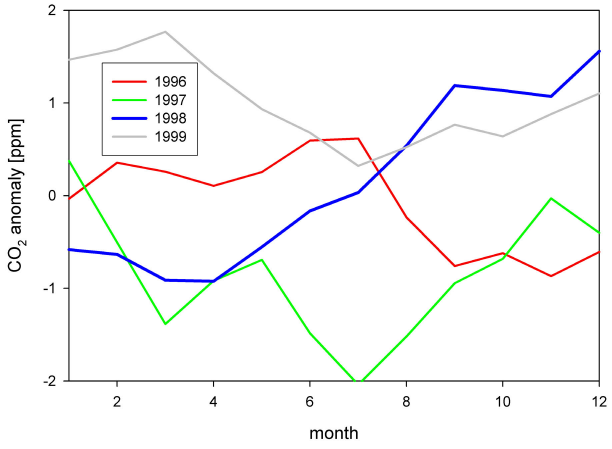

Fig. 7. Seasonal variation of the detrended anomalies [ppm] of CO_2 averaged over all CMDL stations north of 35° N.

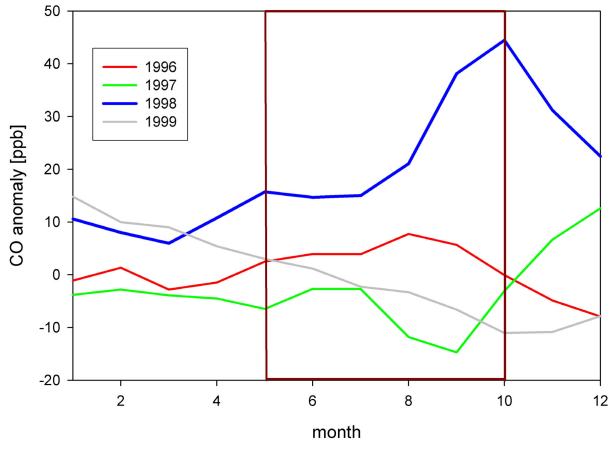

Fig. 8. Seasonal variation of the detrended anomalies (ppb) of CO averaged over all CMDL stations north of 35° N; the dark red rectangle reflects the burning season from May to October, which is shown in Fig. 9

5 Ground Based Measurements and Satellite Remote Sensing Results for the Burning Seasons 1997 and 1998

Around 90% of carbonaceous emissions from forest fires are CO_2. Ground based measurements of CO_2 and CO are available continuously since 1982 and 1990, respectively, from the CMDL flask network. To find a signal from the boreal forest fires in these data, monthly means were calculated for all stations located north of 35° N. CO_2 concentrations are increasing due to continuing anthropogenic CO_2 emissions, whereas CO concentrations are decreasing, because of reduced anthropogenic CO emissions (Wotawa et al., 2001; Novelli et al., 2003). In order to remove these trends, the monthly mean CO_2 and CO data were detrended using a linear regression function. Monthly anomalies of the detrended

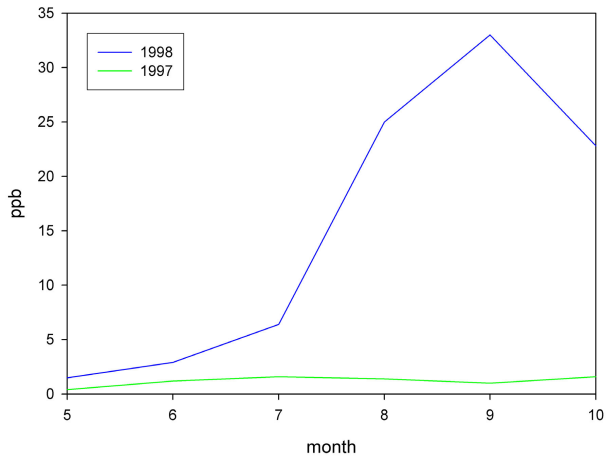

Fig. 9. Monthly mean FLEXPART CO tracer mixing ratios averaged for the positions of the CMDL stations.

CMDL data for both species for the years 1996 to 1999 are shown in Fig. 7 and 8. In 1997 the CO_2 anomalies were negative during most of the year, indicating less than normal fire activity. In contrast, in 1998 they increased rapidly from May on, when the burning season started. The CO_2 anomaly peaked at 1.2 ppm in September, after the strongest burning was over. But because of the long lifetime (much longer than 1 year (Seinfeld and Pandis, 1998)) of CO_2, the CO_2 anomalies remained elevated until April 1999, when the CO_2 pulse from the fires was sufficiently diluted by mixing into the tropics and the southern hemisphere. Furthermore, because of increased soil temperatures the flux of CO_2 and other trace gases out of the soils may persist even after the fires are extinguished (Kim and Tanaka, 2003).

Because of the shorter lifetime of CO (30 to 90 days) compared to CO_2, monthly CO anomalies for 1998 give a slightly different picture (Fig. 8), tracking the temporal variations of the burning more closely. There is a first peak in the CO anomalies in May 1998, followed by a slight decrease in June and July burned, and a sharp increase into September and October, caused by the strong boreal burning from the middle of July until October. After negative CO anomalies during most of the 1997 burning season, CO started increasing in September 1997 when strong burning in Southeast Asia occurred. The positive CO anomaly in May 1998, was likely to be caused by northward transport of emissions from the subtropics. For instance, Van der Werf et al. (2004) assume a contribution of tropical fires to boreal CO amounts of around 26%. In October, the CO anomaly was 44 ppb, a substantial fraction of the detrended CO value of around 115 ppb for that month. This indicates that forest fires were a major contributor to the CO budget in the summer of 1998, in agreement with previous studies (Wotawa et al., 2001; Novelli et al., 2003). In contrast, CO anomalies for the summer of 1997 were all negative, most strongly at the end of the burning season in September.

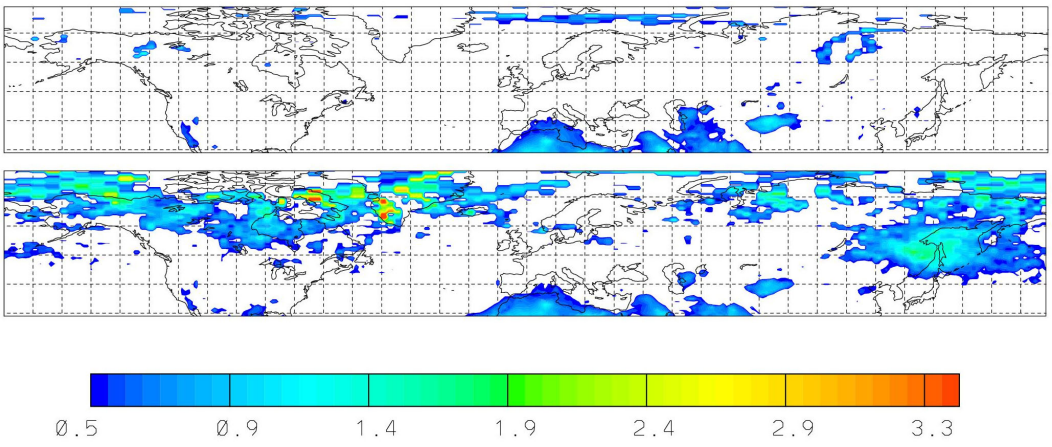

Fig. 10. TOMS aerosol index averaged from May to October 1997 (top) and 1998 (bottom).

To compare the model results with the CO measurements, modelled monthly mean surface layer CO mixing ratios were averaged for the locations of the CMDL stations marked in Fig. 6. The sum of the surface CO tracers for both sources, Canada and Siberia are shown in Fig. 9 (the simulation was started with the estimated emissions shown in Table 3). FLEXPART CO tracers give a similar picture as the CMDL CO measurements (Fig. 8), with a strong increase starting in July 1998 and extremely low CO mixing ratios in 1997. The FLEXPART simulation shows the maximum CO enhancement of 33 ppb (above the background) already in September 1998, one month earlier than the measurements. This may be due to the rather short 60-day lifetime we have assumed in our simulations. The maximum would be delayed by using a longer lifetime or a seasonally increasing lifetime. Furthermore, as mentioned previously, CO emissions may persist even after the above-ground fires are extinguished and no hot spots are detected anymore. Such continuing emissions are not accounted for in our simulations. However, the comparison between Fig. 8 and 9 shows that the assumed emissions and their seasonal variation is in good general agreement. The underestimation of the CO measurement data by the FLEXPART model simulation amounts around 25%, which is comparable to the contribution of tropical fire emissions to boreal CO concentrations, mentioned by Van der Werf et al. (2004). Figure 10 shows the average TOMS AI for the burning seasons of 1997 and 1998, respectively. In both years the enhancements due to Saharan dust can be seen at low latitudes. During 1997 there are relatively few enhancements of the AI over the boreal region. In contrast, in 1998 a large maximum over Canada and the neighbouring oceanic regions and a further maximum over eastern Siberia and the bordering Pacific are found. The maxima over Canada and Siberia are in magnitude comparable to the extended biomass burning regions of Central Africa. The areas of enhanced AI spread in a wavely band over Canada, are more concentrated over eastern Siberia and join over the northern Pacific region. On the one hand TOMS measurements show the broad region affected by the aerosols emitted from the fires of 1998 and on the other hand aerosols detected over the oceans give a clear proof for atmospheric transport of fire emissions. The general patterns confirm the model simulations (Fig. 4).

Figure 11 shows maps of tropospheric NO_2 and HCHO columns derived from GOME, (averaged from July to August) for 1997 and 1998. Beside the high values over the industrial regions of USA, Europe, Middle East and Asia, relatively large enhancements can be seen over Southeast Siberia in 1998 compared to 1997, when the burning was most intense (see circle in Fig. 11). The enhanced biomass burning over southeast Siberia in 1998 can also be well identified and correlated with a high HCHO plume. The high HCHO columns over eastern USA are due to biogenic isoprene emissions (Chance et al., 2000). In consideration of the variance of forest fire emissions in contrast to the continuity of anthropogenic NO_2 emissions, the GOME signal over Eastern Siberia reveals the strength of this emission source in 1998. Although NO_2 enhancements over fires are occasionally also seen over Canada (compare Spichtinger et al., 2001), on a seasonal basis the enhancements are far less pronounced than over Siberia. This is probably due to the smaller areas burned and the more widespread distribution of fires in Canada (see Fig. 3).

6 Summary and conclusions

In this study we compared the boreal burning seasons of 1997 and 1998. According to burned area statistics fire activity was relatively low and atmospheric effects were moderate in 1997 compared to 1998. In 1998 the boreal region, particularly in Canada and southeastern Siberia, suffered from a severe drought and high temperatures, both of which favoured the occurrence of forest fires. Temperature anomalies up to 4.5 K above the climatological average were found in the regions where most of the burning occurred.

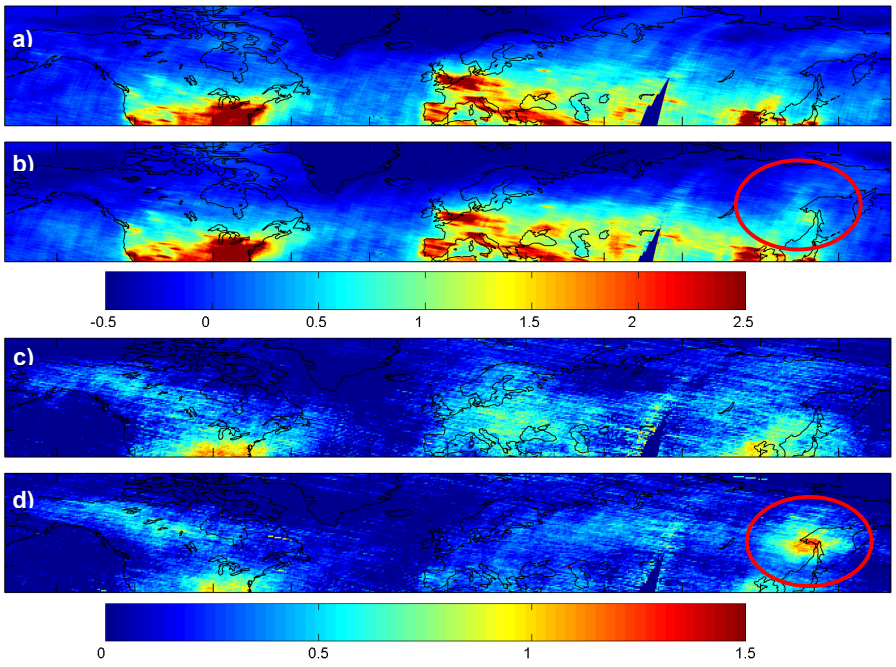

Fig. 11. GOME tropospheric NO_2 [10^{15}molecules/cm^2] and HCHO [10^{16}molecules/cm^2] columns averaged from July to August 1997 (**a** for NO_2 and **c** for HCHO) and 1998 (**b** for NO_2 and **d** for HCHO). The red circle marks enhanced NO_2 and HCHO columns over eastern Siberia where the strongest fire activity occurred in 1998.

These anomalies were likely a consequence of the strong ENSO event of 1997/1998. We simulated the atmospheric transport of the emissions from the burning during the fire seasons of 1997 and 1998 with a Lagrangian transport model using CO as a tracer. Forest fire emissions were released at the ATSR hot spot locations. To quantify the transport of the forest fire emissions the modelled fire plumes were split into a Canadian, a European and a Siberian sector. FLEXPART results were compared to measurement data of CO_2 and CO. The influence of burning on these two species can be seen in surface measurements of the CMDL flask sampling network. Strong positive anomalies of both species in 1998 are in contrast to negative anomalies in 1997. Forest fires emit large amounts of aerosols which are detected by TOMS AI. The signal of the GOME instrument measuring tropospheric NO_2 and HCHO columns is not as clear as the TOMS one, but there is enhanced NO_2 and HCHO over the strongest burning region of Southeast Siberia.

The main conclusions of this study are:

- The transport simulation shows intercontinental transport of CO emitted by forest fires. Likely induced by ENSO, in 1998 a larger fraction of forest fire CO was transported from Siberia towards Canada, contributing more than twice as high concentrations as Canada's own biomass burning CO. In 1998 both tracers arrived at higher latitudes over Europe than in 1997, consistent with a higher NAO index in 1998.
- The interannual variability of fire activity in the boreal region could clearly be seen in ground based measurements of CO and CO_2 as well as in satellite data of the TOMS and the GOME instruments.
- Monthly variations of CMDL CO data are reproduced by the FLEXPART model simulation. The maximum anomaly of the CO measurements was 44 ppb in October 1998, the maximum CO mixing ratio calculated with FLEXPART for the lowest model layer was 33 ppb in September 1998. The delay of the maximum is attributed to the relatively short lifetime of CO (60 days) which was used for the FLEXPART setup.
- TOMS data show expanded maxima over Eastern Siberia and Canada. The aerosol clouds swap from the source regions across the oceans to the neighbouring continents, what reflects transport processes of aerosols, which look very similar than tracer plumes simulated by FLEXPART.
- GOME data show relatively large NO_2 and HCHO enhancements over the burning regions of eastern Siberia in 1998, but no distinct maximum over the Canadian fire regions which were dispersed over a wider latitude range.
- Model simulations and measurement data revealed a strong impact of boreal forest fire emissions on the atmospheric composition of the northern higher latitudes in 1998.

Acknowledgements. This study was funded by the German Ministry for Education and Research as part of the NOXTRAM project (Atmospheric Research 2000) and the PARTS Project. We thank the Deutscher Wetterdienst for kindly providing access to ECMWF and GPCC data. We appreciate the provision of data via the internet by NASA/GSFC and ATSR World Fire Atlas.

Edited by: D. Grainger

References

Amiro, B. D., Todd, J. B., Wotton, B. M., Logan, K. A., Flannigan, M. D., Stocks, B. J., Mason, J. A., Martell, D. L., and Hirsch, K. G.: Direct carbon emissions from Canadian forest fires, 1959–1999, Can. J. Forest Res., 31, 512–525, 2001.

Andreae, M. O., Artaxo, P., Fischer, H., Freitas, S. R., Grégoire, J.-M., Hansel, A., Hoor, P., Kormann, R., Krejci, R., Lange, L., Lelieveld, J., Lindinger, W., Longo, K., Peters, W., de Reus, M., Scheeren, B., Silva Dias, M. A. F., Ström, J., van Velthoven, P. F. J., and Williams, J.: Transport of biomass burning smoke to the upper troposphere by deep convection in the equatorial region, Geophys. Res. Lett., 28, 951–954, 2001.

Andreae, M. O. and Merlet, P.: Emission of trace gases and aerosols from biomass burning, Global Biogeochem. Cyc., 15, 955–966, 2001.

Asakuma, K., Kuze, H., Takeuchi, N., and Yahagi, T.: Detection of biomass burning smoke in satellite images using texture analysis, Atmos. Env., 36, 1531–1542, 2002.

Beirle, S., Platt, U., Wenig, M., and Wagner, T.: Weekly cycle of NO2 by GOME measurements: a signature of anthropogenic sources, Atmos. Chem. Phys., 3, 2225–2232, 2003

Cahoon Jr., D. R., Stocks, B. J., Levine, J. S., Cofer III, W. R., and Pierson, J.: Satellite analysis of the severe 1987 forest fires in northern China and southeastern Siberia, J. Geophys. Res., 99, 18 627–18 638, 1994.

Carlier, P., Hannachi, H., and Mouvier, G.: The chemistry of carbonyl compounds in the atmosphere, Atmos. Env., 20, 2079–2099, 1986.

Chance, K., Palmer, P. I., Spurr, R. J. D., Martin, R. V., Kurosu, T. P., and Jacob, D. J.: Satellite observations of formaldehyde over North America from GOM, Geophys. Res. Lett., 27, 3461–3464, 2000.

Chan, C. Y., Chan, L. Y., Harris, J. M., Oltmans, S. J., Blake, D. R., Qin, Y., Zheng, Y. G., and Zheng, X. D.: Characteristics of biomass burning emission sources, transport, and chemical speciation in enhanced springtime tropospheric ozone profile over Hong Kong, J. Geophys. Res., 108, 4015, doi:10.1029/2001JD001555, 2003.

Cofer III, W. R., Winstead, E. L., Stocks, B. J., Goldammer, J. G., and Cahoon, D. R.: Crown fire emissions of CO_2, CO, H_2, CH_4, and TNMHC from a dense jack pine boreal forest fire, Geophys. Res. Lett., 25, 3919–3922, 1998.

Conard, S. G. and Ivanova, G. A.: Wildfire in Russian boreal forests–potential impacts on fire regime characteristics on emissions and global carbon balance estimates, Env. Pollut., 98, 305–313, 1997.

Conard, S. G., Sukhinin, A. I., Stocks, B. J., Cahoon, D. R., Davidenko, E. P., and Ivanova, G. A.: Determining effects of area burned and fire severity on carbon cycling and emissions in Siberia, Clim. Cange, 55, 197–211, 2002.

Crutzen, P. J. and Merlet, A.: Biomass burning in the Tropics: Impact on atmospheric chemistry and biogeochemical cycles, Science, 250, 1669–1678, 1990.

Duncan, B. N., Randall, M. V., Staudt, A. C., Yevich, R., and Logan, J. A.: Interannual and seasonal variability of biomass burning emissions constrained by satellite observations, J. Geophys. Res., 108, 4100, doi:10.1029/2002JD002378 2003.

Eckhardt, S., Stohl, A., Beirle, S., Spichtinger, N., James, P., Forster, C., Junker, C., Wagner, T., Platt, U., and Jennings, S. G.: The North Atlantic Oscillation controls air pollution transport to the Arctic, Atmos. Chem. Phys., 3, 1769–1778, 2003.

Efremov, D. F. and Sheshukov, M. A.: Ecological and economic evaluation of the consequences of catastrophic fires in the Russian Far East: The Khabarovsk Territory Example of 1998, IFFN, 22, 53–62, 2000.

ECMWF: User Guide to ECMWF Products 2.1, Meteorological Bulletin M3.2, ECMWF, Reading, UK, 1995.

Flannigan, M. D., Bergeron, Y., Engelmark, O., and Wotton, B. M.: Future wildfire in circumboreal forests in relation to global warming, J. Vegetation Sci., 9, 469–476, 1998

Forster, C., Wandinger, U., Wotawa, G., James, P., Mattis, I., Althausen, D., Simmonds, P., O'Doherty, S., Jennings, S. G., Kleefeld, C., Schneider, J., Trickl, T., Kreipl, S., Jäger, H., and Stohl, A.: Transport of boreal forest fire emissions from Canada to Europe, J. Geophys. Res., 106, 22 887–22 906, 2001.

French, N. H. F., Kasischke, E. S., and Williams, D. G.: Variability in the emission of carbon-based trace gases from wildfire in the Alaskan boreal forest, J. Geophys. Res., 108, 8151, doi:10.1029/2001JD000480, 2003.

Fromm, M., Alfred, J., Hoppel, K., Hornstein, J., Bevilacqua, R., Shettle, E., Servranckx, R., Li, Z., and Stocks, B.: Observations of boreal forest fire smoke in the stratosphere by POAM III, SAGE II, and lidar in 1998, Geophys. Res. Lett., 27, 1407–1410, 2000.

Fromm, M. and Servranckx, R.: Transport of forest fire smoke above the tropopause by supercell convection, Geophys. Res. Lett, 1542, doi:10.1029/2002GL016820, 2003.

Galanter, M., Levy II, H., and Carmichael, G. R.: Impacts of biomass burning on tropospheric CO,NO_x,and O_3, J. Geophys. Res., 105, 6633–6653, 2000.

Generoso, S., Breon, F.-M., Balkanski, Y., Boucher, O., and Schulz, M.: Improving the seasonal cycle and interannual variations of biomass burning aerosol sources, Atmos. Chem. Phys., 3, 1211–1222, 2003.

Guzzi, R., Ballista, G., Di Nicolantonio, W., and Carboni, E.: Aerosol maps from GOME data, Atmos. Env., 35, 5079–5091, 2001.

Holloway, T., Levy II, H., and Kasibhatla, P.: Global distribution of carbon monoxide, J. Geophys. Res., 105, 12 123–12 147, 2000.

Hsu, N. C., Herman, J. R., Bhartia, P. K., Seftor, C. J., Torres, O., Thompson, A. M., Gleason, J. F., Eck, T. F., and Holben, B. N.: Detection of biomass burning smoke from TOMS measurements, Geophys. Res. Lett., 23, 745–748, 1996.

Jaegle, L., Jacob, D. J., Wang, Y., Weinheimer, A. J., Ridley, B. A., Campos, T. L., Sachse, G. W., and Hagen, D. E.: Sources and chemistry of NO_x in the upper troposphere over the United States, Geophys. Res. Lett., 25, 1709–1712, 1998.

Kajii, Y., Kato, S., Streets, D. G., Tsai, N. Y., Shvidenko, A., Nilsson, S., McCallum, I., Minko, N. P., Abushenko, N., Altyntsev, D., and Khodzer, T. V.: Boreal forest fires in Siberia in 1998: Estimation of area burned and emissions of pollutants by advanced very high resolution radiometer satellite data, J. Geophys. Res., 107, 4745,doi:10.1029/2001JD001078, 2002.

Kasischke, E. S. and Bruhwiler, L. P.: Emissions of carbon dioxide, carbon monoxide, and methane from boreal forest fires in 1998, J. Geophys. Res., 108, 8146, doi:10.1029/2001JD000461, 2003.

Kasischke, E. S., Hewson, J. H., Stocks, B., Van der Werf, G., and Randerson, J.: The use of ATSR active fire counts for estimating relative patterns of biomass burning – a study from the boreal forest region, Geophys. Res. Lett., 30, 1969, doi:10.1029/2003GL017859, 2003.

Kato, S., Pochanart, P., Hirokawa, J., Kajii, Y., Akimoto, H., Ozaki, Y., Obi, K., Katsuno, T., Streets, D. G., and Minko, N. P.: The influence of Siberian forest fires on carbon monoxide concentrations at Happo, Japan, Atmos. Env., 36, 385–390, 2002.

Kim, Y. and Tanaka, N.: Effect of forest fire on the fluxes of CO_2, CH_4 and N_2O in boreal forest soils, interior Alaska, J. Geophys. Res., 108, 8164, doi:10.1029/2001JD000663, 2003.

Kita, K. , Fujiwara, M., and Kawakami, S.: Total ozone increases associated with forest fires over the Indonesian region and its relation to the El Niño-Southern oscillation, Atmos. Env., 34, 2681–2690, 2000.

Lavoue, D. C., Liousse, C., Cachier, H., Stocks, B. J., and Goldammer, J. G.: Modelling of carbonaceous particles emitted by boreal and temperate wildfires at northern latitudes, J. Geophys. Res., 105, 26 871–26 890, 2000.

Lipari, F., Dasch, J. M., Scuggs, W. F.: Aldehyde emissions from wood-burning fireplaces, Env. Sci. Techn., 18, 326–330, 1984.

Novelli, P. C., Masarie, K. A., Lang, P. M., Hall, B. D., Myers, R. C., and Elkins, J. W.: Reanalysis of tropospheric CO trends: Effects of the 1997–1998 wildfires, J. Geophys. Res., 108, 4464, doi:10.1029/2002JD003031, 2003.

Randerson, J. T., Field, C. B., Fung, I. Y., and Tans, P. P.: Increases in early season ecosystem uptake explain recent changes in the seasonal cycle of atmospheric CO_2 at high northern latitudes, Geophys. Res. Lett., 26, 2765–2768, 1999.

Seinfeld, J. H. and Pandis, S. N.: Atmospheric chemistry and physics, John Wiley and Sons, Inc., New York, 1998.

Spichtinger, N., Wenig, M., James, P., Wagner, T., Platt, U., and Stohl, A.: Satellite detection of a continental-scale plume of nitrogen oxides from boreal forest fires, Geophys. Res. Lett., 28, 4579–4582, 2001.

Stocks, B. J., Fosberg, M. A., Lynham, T. J., Mearns, L., Wotton, B. M., Yang, Q., Jin, J.-Z., Lawrence, K., Hartley, G. R., Mason, J. A., and McKenney, D. W.: Climate change and forest fire potential in Russian and Canadian boreal forests, Clim. Change, 38, 1–13, 1998.

Stohl, A.: A one-year Lagrangian "climatology" of airstreams in the northern hemisphere troposphere and lowermost stratosphere, J. Geophys. Res., 106, 7263–7279, 2001.

Stohl, A., Hittenberger, M., and Wotawa, G.: Validation of the Lagrangian particle dispersion model FLEXPART against large scale tracer experiment data, Atmos. Env., 32, 4245–4264, 1998.

Svidenko, A. and Goldammer, J. G.: Fire situation in Russia, IFFN, 24, 41–59, 2001.

United Nations Economic Commission for Europe: Timber Bulletin, Forest fire statistics 1996–1998, 52, 1999.

Tanimoto, H., Kajii, Y., Hirokawa, J., Akimoto, H., and Minko, N. P.: The atmospheric impact of boreal forest fires in far eastern Siberia on the seasonal variation of carbon monoxide: observations at Rishiri, a northern remote island in Japan, Geophys. Res. Lett., 27, 4073–4076, 2000.

Torres, O., Bhartia, P. K., Herman, J. R., Sinyuk, A., Ginoux, P., and Holben, B.: A long-term record of aerosol optical depth from TOMS observations and Comparison to AERONET measurements, J. Atmos. Sci., 59, 398–413, 2002.

Torres, O., Bhartia, P. K., Herman, J. R., Ahmad, Z., and Gleason, J.: Derivation of aerosol properties from satellite measurements of backscattered ultraviolet radiation: theoretical basis, J. Geophys. Res., 103, 17 099–17 110, 1998.

Van der Werf, G., Randerson, J. T., Collatz, G. J., Giglio, L., Kasibhatla, P. S., Arellano, A. F., Olsen, S. C., and Kasischke, E. S.: Continental-scale partitioning of fire emissions during 1997 to 2001 El Niño/La Niña period: Science, 303, 73–76, 2004.

Wagner, T., Dix, B., Friedeburg, C. V., Frieß, U., Sanghavi, S., Sinreich, R., and Platt, U.: MAX-DOAS O4 measurements - a new technique to derive information on atmospheric aerosols, (I) Principles and information content, J. Geophys. Res., accepted, 2004.

Wotawa, G. and Trainer, M.: The influence of Canadian forest fires on pollutant concentrations in the United States, Science, 288, 324–328, 2000.

Wotawa, G., Novelli, P. C., Trainer, M., and Granier, C.: Interannual variability of summertime CO concentrations in the Northern Hemisphere explained by boreal forest fires in North America and Russia, Geophys. Res. Lett., 28, 4575–4578, 2001.